Technical Report

TR-01-13

Groundwater degassing and two-phase flow in fractured rock:

Summary of results and conclusions achieved during the period 1994–2000

Jerker Jarsjö, Georgia Destouni
Water Resources Engineering
Royal Institute of Technology, Stockholm

John Gale
Fracflow Consultants Inc., Canada

June 2001

Svensk Kärnbränslehantering AB
Swedish Nuclear Fuel
and Waste Management Co
Box 5864
SE-102 40 Stockholm Sweden
Tel 08-459 84 00
+46 8 459 84 00
Fax 08-661 57 19
+46 8 661 57 19

Groundwater degassing and two-phase flow in fractured rock:

Summary of results and conclusions achieved during the period 1994–2000

Jerker Jarsjö, Georgia Destouni
Water Resources Engineering
Royal Institute of Technology, Stockholm

John Gale
Fracflow Consultants Inc., Canada

June 2001

Keywords: Degassing, Two-phase flow, Gas content, Gas saturation, Bubble trapping, Transmissivity, Characteristic relations, Fractured rock, Fracture aperture, Hydraulic testing.

Abstract

Although water saturated conditions generally prevail several hundreds of metres below the ground water table, two-phase flow conditions, i.e. a mixed flow of gas and water, may develop in the vicinity of a repository situated in a regionally saturated rock mass. Deep groundwater naturally contains dissolved gases that may come out of solution if the water pressure is reduced to atmospheric pressure in the vicinity of boreholes and drifts, for instance, during hydraulic and tracer testing. Under certain conditions, this may lead to development of an unsaturated zone, affecting the local hydrology. Other possible sources of two-phase flow conditions in the vicinity of a deep repository include air entry in connection with tunnel ventilation and gas generation in the repository due to corrosion or biological processes. Quantitative two-phase flow models are needed in order to investigate the potential effects of all the above processes. However, traditional constitutive relations for two-phase/unsaturated flow were developed for porous media and are based on parameters that can be readily estimated in soil, but are difficult or impossible to determine independently in fractured rock. Despite the parameter estimation difficulties, several studies have indicated that these relations can be calibrated to reproduce observed unsaturated fracture flow behaviour. In this report, we show that a novel, fractured rock relation is at least equally capable of calibrated reproduction of unsaturated fracture flow as the widely used van Genuchten relation for porous media. Moreover, due to the fact that the novel relation is based on parameters that are physically relevant for (and independently measurable in) rock fractures in the field, it has the potential of independent prediction capabilities, which is not the case for the van Genuchten relation.

We furthermore consider in detail the effects of groundwater degassing on measurements of hydraulic properties in boreholes and drifts, by summarising and systematically interpreting all available laboratory and field investigations that have been conducted within the SKB degassing and two-phase flow programme. Data from various sites in Sweden show that the volumetric percent gas coming out of solution as the pressure of deep groundwater is lowered down to atmospheric pressure is generally less than 5%. Laboratory experiments and an analytical expression showed that conditions often are favourable for trapping and accumulation of gas bubbles in the fracture pore space (once bubbles are formed), implying that local fracture gas saturation degrees may become considerable, even though the evolved percent gas per unit volume flowing water is relatively low. For instance, a saturation degree of 40% was observed in a laboratory fracture for 7% evolved gas. However, degassing effects such as inflow reductions to boreholes and drifts will not be considerable unless the potential degassing zone (where the water pressure is lower than the gas bubble pressure) is sufficiently large in relation to the total length of the fracture. A series of borehole test conducted at Äspö HRL between 300 and 450 meters depth indicated that degassing only causes considerable flow reductions for gas contents that are well above the normal ones in Swedish granitic bedrock. This field result was reproduced by a predictive degassing model, developed considering independent degassing observations in the laboratory. Since the model predictions were shown to be robust with regard to plausible variable ranges for rock fractures intersecting boreholes at depths between 20 and 600 metres, we conclude more generally that groundwater degassing will not cause considerable

inflow reductions in fractures intersecting open boreholes under conditions normal for Swedish granitic bedrock.

We also considered the relatively large drift inflow reductions observed in the Stripa simulated drift experiment. These reductions were hypothesised to be a result of groundwater degassing, although there are also alternative explanations. We show that the only possible degassing-based explanation for the reductions is that gas re-dissolution is relatively slow at this larger scale, as compared with the laboratory and borehole scales. Whereas observational data is sparse on the drift scale, the large number of groundwater degassing observations in the laboratory and in boreholes, in conjunction with consistent model predictions, imply that the processes at these relatively small scales are well understood and that the corresponding conclusions are empirically well founded.

Foreword

This report summarises results and conclusions achieved during the period 1994–2000 within the project *groundwater degassing and two-phase flow*. During the project period, detailed results have continuously been reported in the following publications:

Gale J, 1994. Assessment of the coupled effects of degassing and excavation induced fracture deformation on drift inflows – feasibility study and preliminary experiments – single fractures. SKB Progress Report 25-94-29.

Geller J T, and Jarsjö J, 1995. Groundwater degassing and two-phase flow: Pilot hole test report. SKB International Cooperation Report 95-03.

Jarsjö J, and Geller J T, 1996. Groundwater degassing: Laboratory experiments in rock fracture replicas with radial flow. SKB Progress Report HRL-96-12.

Jarsjö, J. and Destouni, G., 1997a. Groundwater degassing: Pilot injection – withdrawal field tests with gas saturated water. SKB Progress Report HRL-97-02.

Jarsjö J. and Destouni G, 1997b. Conditions for fracture transmissivity reduction due to degassing of groundwater: analytical expressions, numerical simulations and analysis of laboratory and field data. SKB Progress Report HRL-97-03.

Geller J T, 1998. Laboratory studies of groundwater degassing in replicas of natural fractured rock for linear flow geometry. SKB Progress Report HRL-98-18.

Jarsjö J and Destouni G, 1998. Groundwater degassing in fractured rock: Modelling and data comparison. SKB Technical Report TR-98-17.

Gale J, 1999. Impact of flow geometry, flow regime, two-phase flow and degassing on the transmissivity of rough fractures. SKB International Progress Report IPR-99-08.

Jarsjö J and Destouni G, 2000. Degassing of deep groundwater in fractured rock around boreholes and drifts, Water Resources Research, 36(9), 2477–2492.

These publications provide an important basis for this summarising report; we use the developed degassing models to make a consistent interpretation of these available observations of groundwater degassing. We hereby also consider observations on inflow reductions made in the Stripa simulated drift experiment, previously reported in:

Olsson O (Editor), 1992. Site characterisation and validation – Final Report. SKB Stripa Project Technical Report 92-22.

Contents

1 Introduction

1.1 Background

The concept for the storage of high-level radioactive waste preferred by the Swedish Nuclear Waste Management Company (SKB) involves the construction of a final repository in granite bedrock at 400–500 metres depth. For research and demonstration purposes, a full-scale underground research laboratory (the Äspö Hard Rock Laboratory, HRL), has been constructed in the bedrock in south-eastern Sweden /see Banwart et al., 1997/. Through both modelling and experimental studies conducted at the Äspö HRL and other sites in deep bedrock, such as Grimsel and Wellenberg in Switzerland and Yucca mountain in Nevada, the hydraulic and transport properties of the (fractured) bedrock have been investigated under a range of conditions. Phenomena and processes that may affect these properties around deep repositories have hereby been addressed, for instance evaporation and thermal loading effects /Finsterle and Pruess, 1995; Walton, 1994; Pruess et al., 1990/, microbial activity /Pedersen, 1997; Kotelnikova and Pedersen, 1997/, and excavation effects /Emsley et al., 1997/.

The hydraulic and transport properties of fractured rock may change considerably in the presence of a second, separate phase (e.g., gas) in the fracture pore space, as compared with a single-phase system. Although water saturated conditions generally prevail several hundreds of metres below the ground water table, two-phase flow conditions, i.e. a mixed flow of gas and water, may develop in the vicinity of a repository situated in a regionally saturated rock mass. The main sources of two-phase flow conditions are 1) gas generation in the repository due to corrosion or biological processes, 2) exsolution of gas (bubble generation) due to pressure decrease, and 3) entry of gas (air) into the rock mass from ventilated tunnels. The presence of a gas phase in the repository before and after closure must be understood in relation to its effect on repository performance.

In particular, deep groundwater naturally contains dissolved gases that may come out of solution as the water pressures are lowered down to atmospheric pressure. Hence, degassing and bubble generation may occur in the vicinity of open boreholes and drifts; at Äspö HRL, for instance, the drift is subject to the atmospheric pressure, and many boreholes used for characterisation purposes intersect the open drift. This implies that groundwater degassing may influence the hydraulic conditions that are examined through hydraulic and tracer experiments in boreholes and drifts. It is further conceivable that groundwater degassing can arise as a direct result of water pressure lowerings occurring in connection with such testing. If degassing of deep groundwater is a significant factor in controlling the hydrology around boreholes and/or drifts, it is essential to know this when experiments are planned, executed and evaluated.

Regarding implications for fracture transmissivity and borehole/drift inflow, Olsson /1992/ and Birgersson et al. /1993/ concluded that groundwater degassing provided a possible explanation for inflow reductions observed at 385 metres depth during the Stripa Simulated Drift Experiment, although alternative explanations could not be ruled out. Without providing any conclusive answers, the Stripa observations thus raised important questions about whether or not and to what extent groundwater degassing may be expected to affect hydraulic property values that are estimated on basis of drift

or borehole inflow measurements. Furthermore, a transient change in hydraulic properties due to two-phase flow conditions around drifts and deposition holes may affect conditions during emplacement of the engineered barriers. A reduction in hydraulic conductivity due to two-phase flow conditions may simplify emplacement of buffer material in deposition holes but may also delay saturation and swelling of the buffer mass. Other examples where degassing may affect flow to various degrees include the recovery of oil from deep geological formations and artificial groundwater recharge. A resent study furthermore showed that degassing provides a potential explanation to the observed behaviour of the core at WAC Bennet Dam /Billsten and Svensson, 2000/.

As previously mentioned, possible sources of two-phase flow conditions in the vicinity of a deep repository, besides groundwater degassing, include air entry in connection with tunnel ventilation and gas generation in the repository due to corrosion or biological processes. Whereas groundwater degassing is primarily expected to occur relatively close to open boreholes and drifts, where detailed information on fracture aperture properties in principle can be obtained, other multiphase processes that can potentially affect the performance of deep repositories may take place at much larger scales. For instance, for the scenario of gas generation in the repository and subsequent transport through the fractured rock, the relevant scale can be on the order of a kilometre. On this scale, the hydrologic conditions cannot be known in detail throughout the domain. Rather, detailed information will be available in a finite number of sampling locations. This point information then needs to be interpreted in some way that is relevant for the large-scale problem.

In order to address all the above-mentioned two-phase flow problems in fractured rock, quantitative models are needed. However, traditional constitutive relations for unsaturated flow in porous media /e.g., Brooks and Corey, 1964; and van Genuchten, 1980/ are based on parameters that can readily be estimated in soil, but are difficult or impossible to determine independently in fractured rock. As a consequence, the predictive capability of such typical soil constitutive relations is limited for rock fractures under field conditions, although several studies have indicated that they can be calibrated to reproduce observed unsaturated fracture flow behaviour. Therefore, a novel relation for two-phase flow was developed considering fractured rock /Jarsjö and Destouni, 1998, using similar assumptions as Pruess and Tsang, 1990/. This relation is based on properties (the mean aperture and the aperture standard deviation), for which undisturbed field estimates can be obtained through the resin injection technique.

1.2 Objectives and scope

In this study, we compare traditional, characteristic curves for relative permeability with novel relations developed for fractured rock. The overall aim is to identify and investigate the applicability of relations and model approaches that can be used for predictive modelling of two-phase flow in fractured rock. This is expected to be of importance in the addressing of the various two-phase flow processes that are plausible in the vicinity of a deep repository during operating and construction stages (see the background section for further details).

Furthermore, we specifically address groundwater degassing processes and their implications for the hydraulic properties of deep bedrock. The main objective for the groundwater degassing investigations is to show if, or under what conditions, degassing of groundwater at low pressures has significant effects on measurements of hydraulic properties in boreholes and drifts. Conditions expected to be of importance are gas content, chemical composition of groundwater, fracture characteristics (aperture distribution and transmissivities), and flow conditions.

The objectives are addressed in this report by systematically summarising and interpreting the achievements within the SKB degassing and two-phase flow programme (see the foreword for a list of previous publications). The achievements include laboratory studies, field studies, model development and interpretation, briefly explained in the following paragraphs.

In an early stage of the SKB degassing project, the focus of an experimental field programme was directed towards borehole tests, because they are easier to control and may be conducted at much lower costs than drift experiments. The main objective was to investigate whether the lowering of pressures down to atmospheric pressures in a borehole intersecting a water bearing fracture would lead to degassing, unsaturated zone formation and, as a consequence, changes in the fracture hydraulic properties. Four different borehole degassing tests at both natural and elevated gas contents were conducted within the field programme /Geller and Jarsjö, 1995; Jarsjö and Destouni, 1997a/. Through a first series of laboratory experiments /Jarsjö and Geller, 1996, degassing effects were further observed in two different rock fracture replicas under radial flow conditions (relevant also for inflow to boreholes and drifts in the field). The main objective for these experiments was to investigate the effect of different gas contents (of similar range as previously observed in the field) and boundary pressures on the flow reduction due to degassing.

In a previous technical report SKB TR-98-17 /Jarsjö and Destouni, 1998/, methods were developed for the for estimation of the steady-state degree of fracture gas saturation and transmissivity reduction due to groundwater degassing in fractured rock, using a statistical description of the fracture aperture. The model predictions were then compared with the borehole field experiments and these first laboratory experiments. More recently, additional experimental investigations addressed the effects of groundwater degassing under a wider range of conditions. These conditions included linear flow experiments in transparent rock fracture replicas /Geller, 1998/, linear flow experiments in actual rock fractures, and linear and radial flow visualisation experiments in artificial fractures /Gale, 1999/.

In this report, we use this extended data set as a basis for testing underlying assumptions and applicability of the relations developed by Jarsjö and Destouni /1998/. We also use these relations for performing a more detailed interpretation of the field experiments /Geller and Jarsjö, 1995; Jarsjö and Destouni, 1997a/, including the Stripa SDE /Olsson, 1992/. Based on these experimental and model results, we then draw conclusions regarding the occurrence and magnitude of groundwater degassing effects.

2 Physical concepts

2.1 Groundwater degassing

2.1.1 Basic relations

The extent of the zone around a borehole, or a drift, where groundwater degassing may occur is limited to the region where the water pressure p_w is lower than the bubble pressure p_b:

$$p_w < p_b \qquad \textbf{(}2\text{-}1\textbf{)}$$

In the following, we will refer to the zone around a borehole or drift, where (2-1) is satisfied under water saturated (single-phase) conditions as the low-pressure zone. The extent of the low-pressure zone, X_{low}, is then a measure of the size of the region where groundwater degassing can possibly occur. In addition, differences in properties between different gases imply that the volumetric amount of gas that will be released for a specific water pressure lowering (below p_b) is gas specific.

Provided that equilibrium prevails between a gas phase and a liquid phase, the relation between the partial pressure of the gas, p_g, and the concentration of the gas dissolved in the liquid, C_g, follows Henry's law:

$$p_g = HC_g \qquad (2\text{-}2)$$

where p_g is the absolute gas partial pressure in kPa, H is Henry's law constant for the gas in the liquid in kPa·m^3·mol^{-1} and C_g is the molar concentration of the gas dissolved in the liquid. The decrease in dissolved gas concentration ΔC due to a water pressure lowering to $p_w<p_b$ then becomes $\Delta C = (p_b - p_w) / H$. This decrease in dissolved gas concentration can be related to a corresponding evolved volumetric gas content $\Delta\theta_g = \Delta V_g/V_w$ (gas volume coming out of solution per total water volume) through the ideal gas law as:

$$\Delta\theta_g = \frac{p_b - p_w}{H}\frac{RT_{abs}}{p_w} \qquad (2\text{-}3)$$

where R is the gas constant and T_{abs} is the absolute temperature. Thus, the bubble pressure p_b can be estimated from Equation (2-3) by measuring the evolved gas volume, ΔV_g, from a total water volume, V_w, when the water pressure is lowered down to p_w.

For radial inflow to both boreholes and drifts, the low-pressure zone is situated in the nearest vicinity of the borehole/drift (hereafter referred to as the well), due to steep gradients caused by the converging flow. Given that the hydraulic head $\phi=H_0$ at the outer boundary (dashed circle in Figure 2-1) at distance r_0 from the well centre and $\phi=H_w$ at the well boundary (distance r_w in Figure 2-1), the steady-state hydraulic head profile around the well is /Bear, 1979/:

$$\phi(r) = H_w + (H_0 - H_w)\frac{\ln(r/r_w)}{\ln(r_0/r_w)} \tag{2-4}$$

where (H_0-H_w) is the drawdown at the well, r is the radial distance from the well centre, r_w is the well radius and r_0 is referred to as the radius of influence (Figure 2-1). The water pressures in a fracture plane at an angle of Θ degrees from the horizontal plane is given by $p_w(x,z) = \rho g(\phi(x,z) - z \cdot \sin(\Theta))$, where ρ is the water density, g is the mass gravity and x and z extend in the plane of the fracture; the co-ordinate system is shown in Figure 2-1 with the x-axis being horizontal. Equation (2-4) can be transformed to Cartesian co-ordinates in order to express the pressure profile around a borehole intersecting the fracture plane according to:

$$p_w(x,z) = \rho g\left(H_w + (H_0 - H_w)\frac{\ln\left(\sqrt{x^2+z^2}/r_w\right)}{\ln(r_0/r_w)} - z \cdot \sin(\Theta) \right)$$

$$\text{for } r_w \le \sqrt{x^2+z^2} \le r_0 \tag{2-5}$$

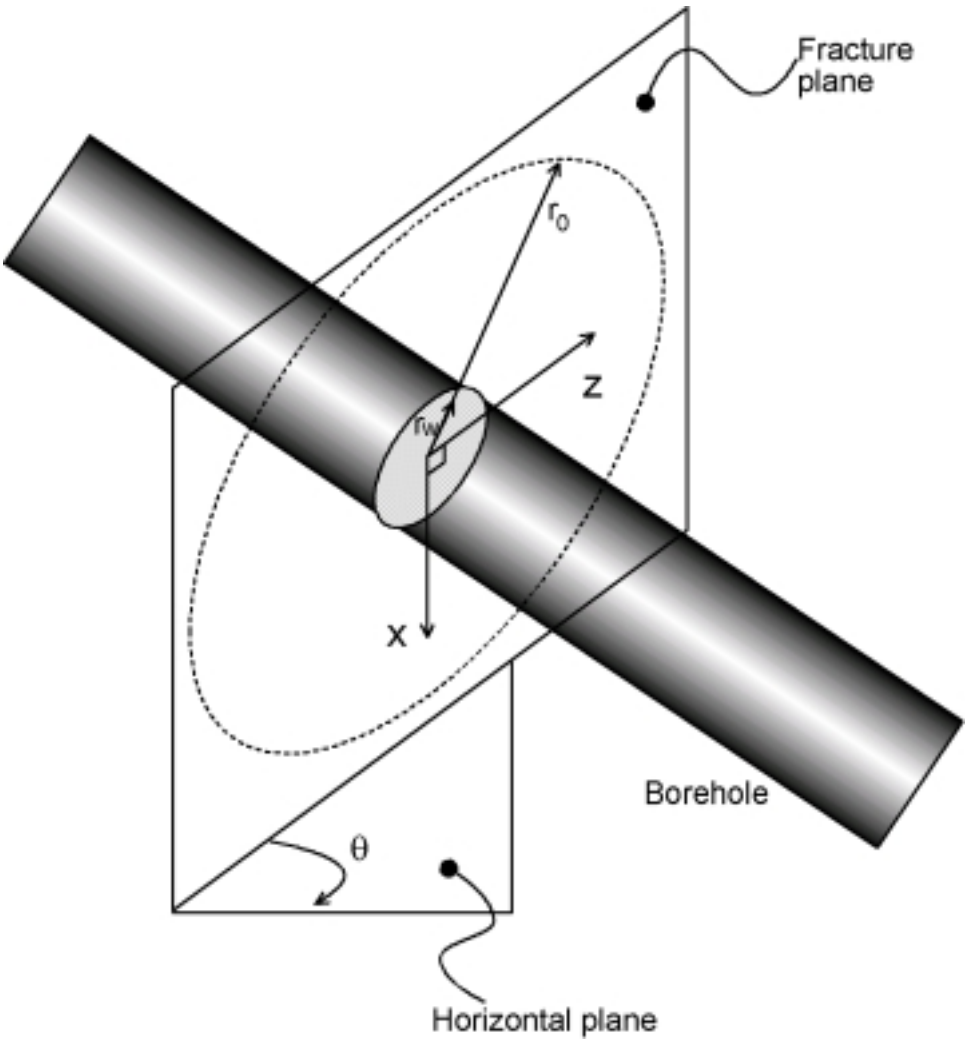

Figure 2-1. *Schematic view of a borehole intersecting a fracture.*

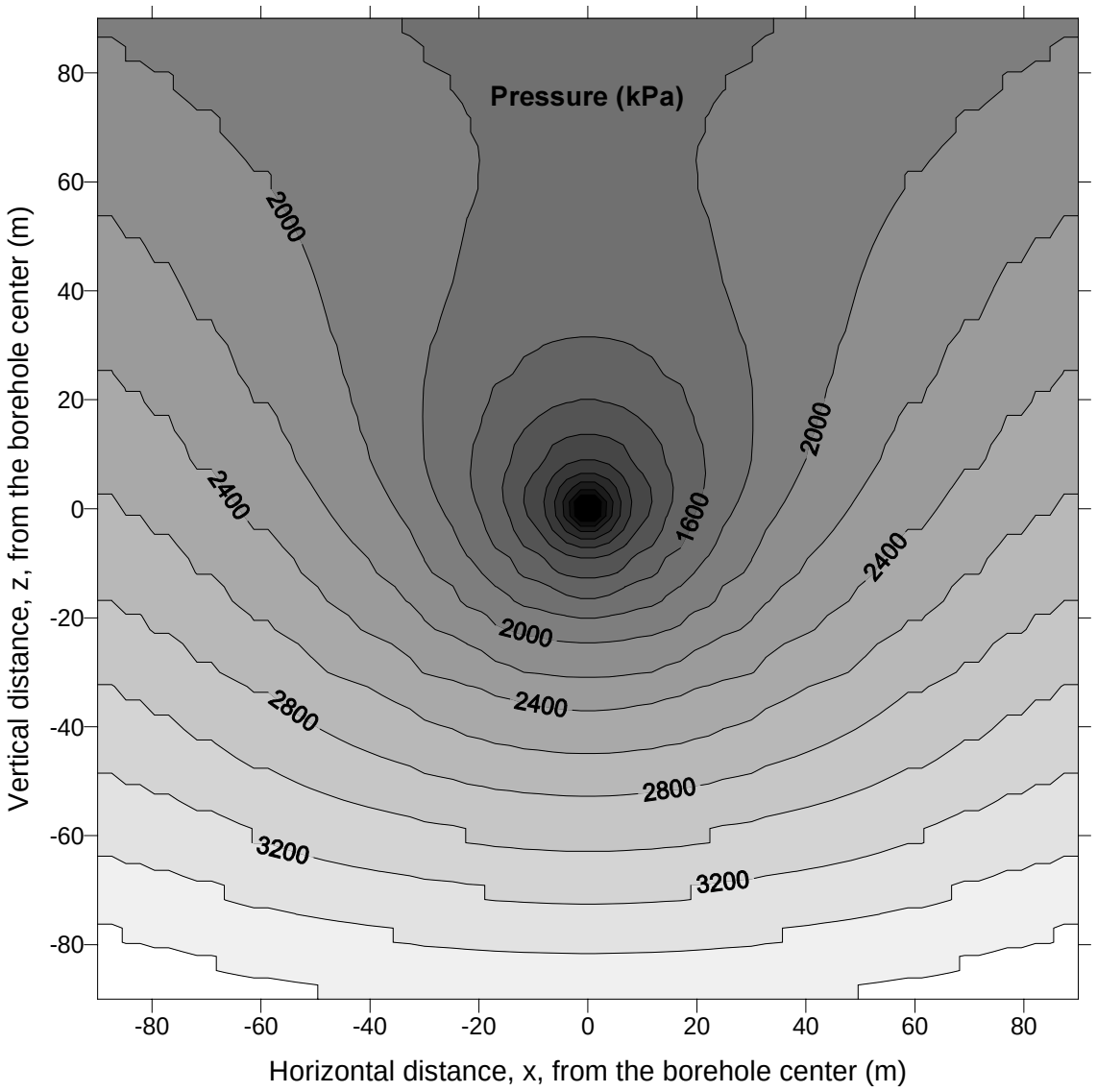

Figure 2-2. *Radial inflow to a horizontal tunnel (equation 2-5). Parameter values: r_w=2m, r_0=150m, H_w=0m, H_0=300m, Θ=90°.*

Equation (2-5) implies that in immediate vicinity of the well, within one metre's radial distance from the well bore, the hydrostatic pressure differences are negligible in comparison to the pressure differences caused by the converging flow, regardless of the value of Θ; at 300 metres depth (assuming well radii between 0.03 to 3 metres and a radius of influence of 150 metres), the hydrostatic pressure difference is 5% or less of the pressure difference caused by the drawdown. The nearly circular pressure-lines close to the centre of Figure 2-2 illustrate these relatively small differences in the pressures (kPa) at the same radial distances in the vicinity of a horizontal tunnel (located at (0,0); tunnel radius r_w=2m). Thus, fracture orientation is not expected to influence the occurrence of degassing to any measurable degree, and will therefore not be further considered.

2.1.2 Implications for the occurrence and effects of degassing

The implications of Equations (2-1), (2-3) and (2-5) for the case of degassing of deep groundwater around boreholes and drifts are illustrated in Figure 2-3, which shows a comparison of the estimated pressure field (Equation (2-5) with Θ=0) around a borehole (solid line) and a drift (dashed line) at 300 metres depth, assuming borehole and drift radii of 0.03 and 3 metres, respectively. Figure 2-3 illustrates that the pressures around the drift are significantly lower than those around the borehole at the same radial distances. If one assumes that water releases 1.5 volumetric % nitrogen gas as the water pressure is lowered to atmospheric pressure (which corresponds to a nitrogen bubble pressure of 100 kPa of water according to Equation (2-3)), the radial extent of the low-pressure zone (where the water pressure is lower than the bubble pressure) is X_{low}=0.4 metres for the drift, whereas X_{low} is only 0.01 metres for the borehole (Figure 2-3). Figure 2-3 also shows that the extent of the low-pressure zone, X_{low}, around a borehole is increased by about 50 times to 0.5 metres when increasing the bubble pressure 10 times, to 1000 kPa, which corresponds to 15% evolved N_2. The corresponding area of the low-pressure zone ($A_{low}=\pi(X_{low}+r_w)^2-\pi r_w^2$) is then enlarged by 350 times. This calculation example illustrates that similarly favourable degassing conditions, in terms of the size of the low-pressure zone, may be obtained around drifts at lower gas contents as around boreholes at high gas contents. The results illustrated in Figure 2-3 are relatively insensitive to the assumed value of the radius of influence r_0 (of 150 metres), due to the logarithmic relation in Equations (2-4) and (2-5); see Jarsjö and Destouni (1997b) for further details.

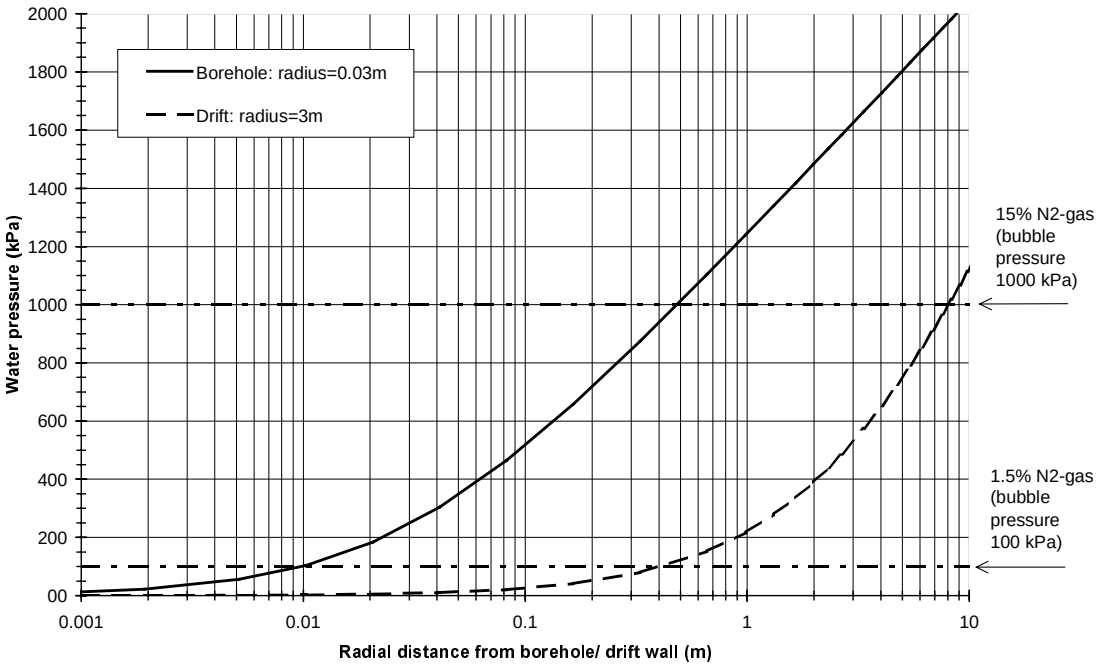

Figure 2-3. *The water pressures in the vicinity of an open borehole in comparison with a drift.*

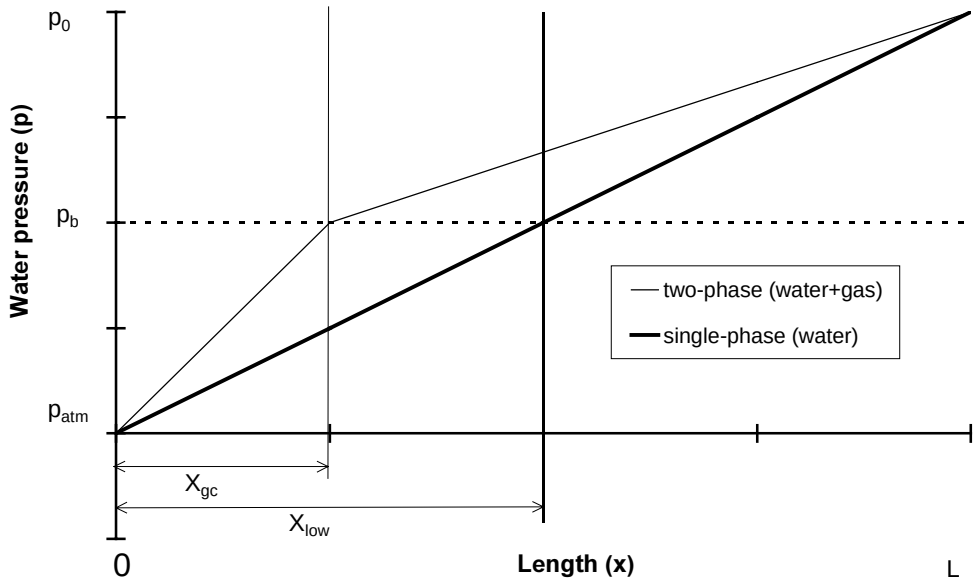

Figure 2-4. *Illustration of the expected effect of a local gas-containing zone X_{gc} on the pressure distribution for linear flow conditions: a comparison between single-phase and two-phase conditions.*

The actual extent of a developed gas-containing zone X_{gc} may in fact be smaller than the full low-pressure zone X_{low}, due to the kinetics of the bubble nucleation process /see, e.g. Parlar and Yortsos, 1989/. Furthermore, the evolution of a separate gas phase is expected to increase water pressure gradients in the vicinity of the borehole relative to the single-phase case, which would also reduce the actual, steady-state, gas-containing zone X_{gc} relative to the full low-pressure zone X_{low}. This expected change in local water pressures under degassing conditions is illustrated schematically in Figure 2-4 for linear flow conditions. The thick line in Figure 2-4 illustrates the expected single-phase pressure distribution under water saturated conditions between the fracture outlet (x=0), where the water pressure equals the atmospheric pressure p_{atm}, and the outer boundary (x=L), where the water pressure equals p_0. The bubble pressure p_b is illustrated by the dashed line, and the low-pressure zone extent at saturated conditions X_{low} extends from x=0 to the intersection between the bubble pressure line and the single-phase water pressure line. The thin pressure line in Figure 2-4 illustrates the water pressure distribution that is expected as a result of a gas phase development within the low-pressure zone, and a local decrease in fracture transmissivity due to unsaturated water flow within this zone. Local transmissivity reduction implies steeper pressure gradient in the vicinity of the fracture outlet, causing the gas-containing zone under two-phase conditions X_{gc} to be smaller than the low-pressure zone under water saturated conditions (X_{low}; see Figure 2-4). Since the overall decrease in fracture transmissivity is depending on the extent of the zone where the transmissivities are decreased in relation to the full fracture extent (L in Figure 2-4), we expect that the probability for degassing-related flow reductions increases as the ratios X_{low}/L and X_{gc}/L increase.

2.1.3 Influence of heterogeneity in rock fracture properties

Field experiments in the Stripa mine involving solute transport in a single fracture showed that fluid flow was unevenly distributed along the fracture plane /Olsson, 1992; Birgersson et al., 1993/. Large areas did not carry water, implying the existence of preferential flow paths. There is also strong evidence for localised, preferential pathways in the unsaturated, fractured rock at Yucca Mountain in Nevada, the U.S. potential repository for high-level nuclear waste /Pruess et al., 1999/. Furthermore, differences in fracture properties and differences in connectivity between individual fractures in fracture networks can give rise to considerable heterogeneity effects at a larger scale /see, e.g., review by Smith and Schwartz, 1993/.

As shown by for instance Hakami /1995/, the aperture of natural rock fractures is often log-normally distributed, rather than of constant width. Figure 2-5 shows an example of the hydraulic head distribution in a single fracture with log-normally distributed aperture. The fracture is an epoxy replica of an actual rock fracture, sampled at the Äspö Hard Rock Laboratory. The aperture distribution of the epoxy replica was measured by Jarsjö and Geller /1996/ and the hydraulic head values of Figure 2-5 was calculated using MODFLOW /McDonald and Harbaugh, 1988/, on basis of the measured aperture values. The irregular and sometimes oval-shaped hydraulic head iso-lines (solid lines in Figure 2-5 show that in contrast to the homogeneous case, the local hydraulic head values may differ at the same radial distances from the simulated borehole in the centre of the Figure 2-5. The distance to an adjacent iso-line also varies along each line, which implies differences in hydraulic head gradients and local flow velocities (being proportional to the local hydraulic head gradients).

Fracture heterogeneities, such as those illustrated in Figure 2-5, and the resulting differences in local flow velocities may give raise to flow channeling, with considerably higher flowrates in the least resistive paths or channels. The effect of flow channeling on the transport of solutes in water saturated fractures and strongly heterogeneous media has been investigated by, e.g., Moreno and Tsang /1991; 1994/. For multiphase flow conditions, Birkholzer and Tsang /1997/ showed in numerical simulations that the degree of channeling, the location of channels and the hydraulic properties along the channels are very much a function on the saturation in the domain, which in turn, is depending on the local fracture aperture characteristics and capillary pressures. One important reason for the dependence on saturation is that high permeability zones for saturated conditions are characterised by wider apertures, which drain faster than the tighter apertures. As a consequence, the high permeability zones become low permeability zones for unsaturated flow. Furthermore, pore scale aperture variability as that illustrated in Figure 2-5 is expected to be of great importance for the fate of gas bubbles in individual fractures, both in terms of gas bubble trapping and gas dissolution into the water phase. Therefore, we use an aperture-related description of unsaturated flow (Section 2.3.2) in combination with the basic degassing relations (described in Section 2.1.1), as a basis in the development of more detailed, predictive, degassing models (Section 3.1).

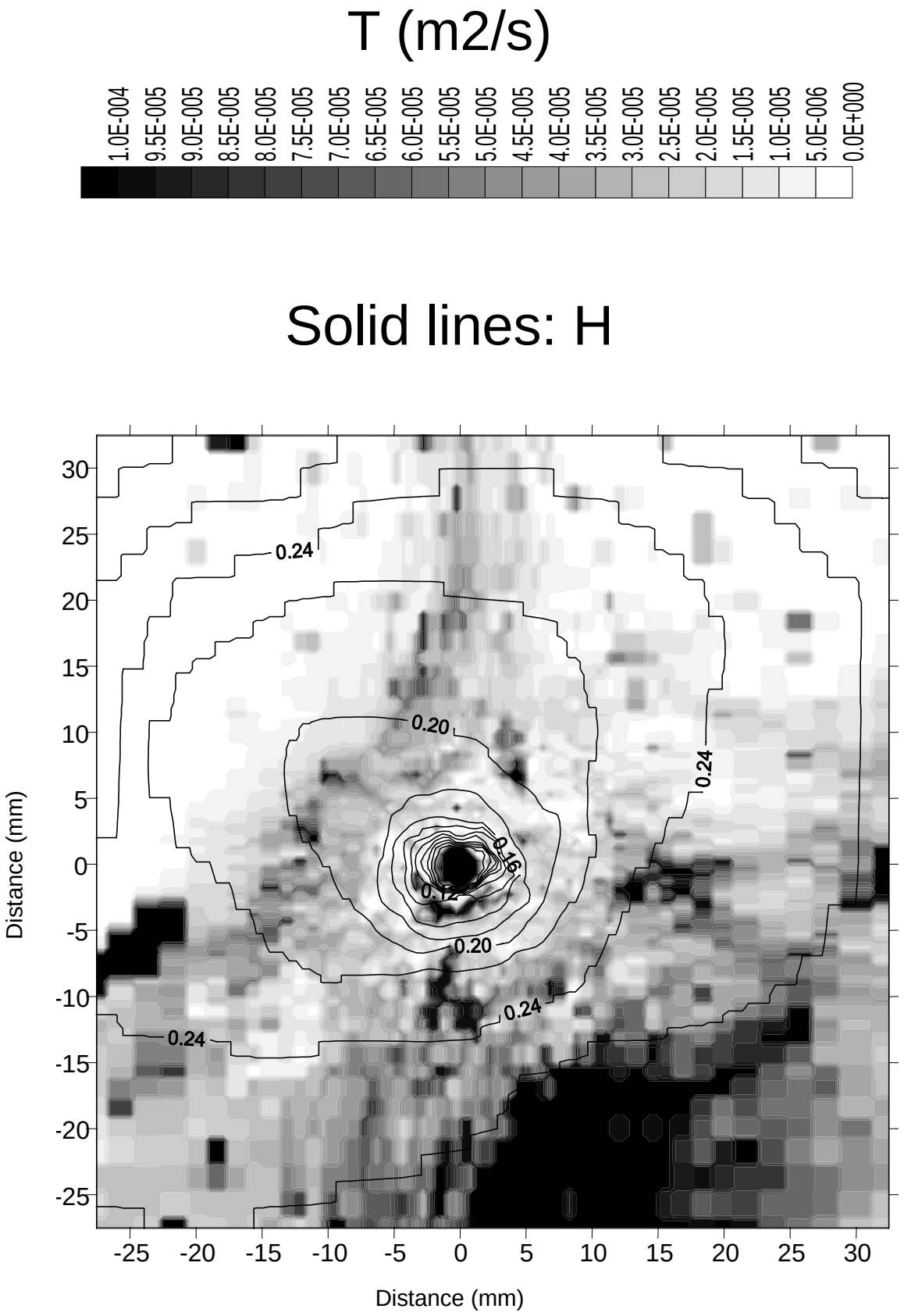

Figure 2-5. *Hydraulic heads under radial flow conditions in a variable aperture fracture.*

2.2 Saturated fracture flow

For the simplified case of two-dimensional, laminar flow between parallel plates, the saturated hydraulic conductivity K_s can be related to the separation distance (or the aperture) a between the plates according to /see, e.g., Witherspoon et al., 1980/:

$$K_S = \frac{\rho g}{12\mu} a^2 \tag{2-6}$$

where μ is the fluid viscosity, ρ is the fluid density and g is the gravitational constant. Equation (2-6) has also been proven useful as an approximate expression for local hydraulic conductivity values in variable aperture fractures, in which the local aperture value a varies in space.

The hydraulic properties of fractured media are often expressed in terms of transmissivity T, defined as $T=K \cdot a$, rather than in terms of hydraulic conductivity K. One main reason for this use of transmissivity is that this quantity can be directly related to fracture flow, as it is commonly being measured and interpreted in borehole tests in fractured rock (see also Section 2.3.2). Provided that (2-6) is approximately true for the local hydraulic conductivity value in a variable aperture fracture, the corresponding local fracture transmissivity value is:

$$T = \frac{\rho g}{12\mu} a^3 \tag{2-7}$$

This relation is referred to as the cubic law, and has in many cases proven to be a useful approximation for the relation between local fracture transmissivity and local aperture value /see, e.g., Murphy and Thomson, 1993/. Discussing properties of variable aperture fractures, many authors use the term *hydraulic aperture* a_h. This is simply an equivalent aperture associated with the transmissivity T under the assumption that the cubic law (2-7) holds:

$$a_h = \sqrt[3]{\frac{12\mu T}{\rho g}} \tag{2-8}$$

Since the cubic law is only approximately true for variable aperture fractures, the value of a_h may differ from the mean aperture value $\bar{a}$. Hakami /1995/ compiled data from several different fractures, and found that the ratio $\bar{a}/a_h$ ranged from 1.1 to 1.7. These fractures had mean values of ln a ranging between –2.3 and 0.2 (with a given in mm), and standard deviation values of ln a ranging between 0.2 and 1.2.

2.3 Quantification of unsaturated flow

When two or more liquid phases, or a liquid and a gas phase, are present in the subsurface, interfacial tensions and curved interfaces result in pressure differences over the liquid-liquid, or gas-liquid interface; this pressure difference is commonly denoted the capillary pressure, p_c. In a two-phase system, p_c is defined as $p_c=p_g-p_w$, where p_g is the

non-wetting phase (e.g., gas or oil) pressure and p_w is the wetting phase (e.g., water) pressure immediately adjacent to the interface. The relation between the capillary pressure and the radius r of a cylindrical pore is:

$$p_c = \frac{2\sigma}{r}\cos\theta \tag{2-9}$$

where σ is the interfacial tension between the fluids occupying the pore and θ is the contact angle between the fluid interface and the wall of the pore. For water – air systems, $\cos\theta$ is usually assumed to equal unity. In quantitative models for unsaturated flow, the effective wetting phase saturation S_e is commonly expressed as a function of either the capillary pressure, or a corresponding pressure head h, defined as $-p_c/(\rho g)$. Furthermore, the conductivity with respect to each phase may be expressed as a function of either the phase saturation or the capillary pressure; these functional relations, originally developed for porous media, are described below.

2.3.1 Porous medium relations

Constitutive relations between capillary pressure p_c saturation S and relative conductivity K_{rel} (or relative transmissivity T_{rel}) provide an important basis for quantitative multiphase flow models. For porous medium applications, there are a number of developed and widely employed p_c -S - K_{rel} functional relations /e.g, Brooks and Corey, 1964; Mualem, 1976; van Genuchten, 1980/. In some cases, these relations have also been applied in the modelling of multiphase flow in fractured media /e.g., Reitsma and Kueper, 1994; Finsterle and Pruess 1995; Fisher et al., 1998; Birkholzer et al., 1999/. In this section, we will briefly present the Brooks-Corey and van Genuchten models, and discuss their applicability for fractured rock applications.

In the Brooks and Corey /1964/ model, the relation between the wetting phase effective saturation S_e and the pressure head h (being related to the capillary pressure p_c as $h=-p_c/\rho g$) is:

$$\begin{aligned} S_e &= \left(\frac{h_b}{h}\right)^{\lambda} && \text{for } h<h_b \\ S_e &= 1 && \text{for } h>h_b \end{aligned} \tag{2-10}$$

where h_b represents the bubble pressure head (or air entry pressure head) and λ is a soil pore size distribution related parameter. In the van Genuchten /1980/ model, the corresponding relation is:

$$\begin{aligned} S_e &= \left(\frac{1}{1+(\delta|h|)^n}\right)^{1-1/n} && \text{for } h<0 \\ S_e &= 1 && \text{for } h\geq 0 \end{aligned} \tag{2-11}$$

where δ and n are soil parameters which are related to (the inverse of) the bubble pressure head value and the width of the soil pore size distribution, respectively.

In both the models of Brooks-Corey (BC) and van Genuchten (vG), the effective saturation is defined as:

$$S_e = \frac{S_w - S_{w,r}}{n_m - S_{w,r}} \tag{2-12}$$

where S_w is the volumetric water saturation (volume of water per total pore volume) $S_{w,r}$ is the residual, or irreducible, water saturation and n_m is the porosity of the medium. Usually, the BC parameters h_b, and λ and the vG parameters δ and n are determined by matching the above functional relations with drainage curves, which are obtained from laboratory experiments on soil samples.

In the BC and vG relations, the hydraulic conductivity K is expressed either as a function of S_e or h. We will in the following use the relation between K and h, which for the BC-model is:

$$\begin{aligned} K(h) &= K_s\left(\frac{h_b}{h}\right)^{3\lambda+2} && \text{for } h<h_b \\ K(h) &= K_s && \text{for } h\geq h_b \end{aligned} \tag{2-13}$$

and the corresponding expression for the vG relation is:

$$\begin{aligned} K(h) &= K_s \frac{\left(1-\left(\delta|h|\right)^{n-1}\left(1+\left(\delta|h|\right)^{n}\right)^{-(1-1/n)}\right)^2}{\left(1+\left(\delta|h|\right)^{n}\right)^{m(1-1/n)}} && \text{for } h<0 \\ K(h) &= K_s && \text{for } h\geq 0 \end{aligned} \tag{2-14}$$

In Equations (2-13) and (2-14), the parameters λ, h_b, δ and n are the same as in Equations (2-10) and (2-11). The parameter m is an additional fitting parameter. Mualem /1976/ and van Genuchten /1980/ found that the value of m=0.5 provided the best match with a set of experimental data from 45 soils.

Usually, the BC parameters h_b and λ, and the vG parameters δ and n, are determined by matching the above functional relations with drainage curves, which are obtained from laboratory experiments on soil samples. Whereas these measurements can be performed in relatively undisturbed soil samples, it is extremely hard to sample a rock fracture and re-assemble it in the laboratory, in such a way that the hydraulic conditions relevant for that specific field situation are reproduced in the laboratory /see, e.g., review by Jouanna, 1993/. Further, the measurement of such relations are more difficult to perform in fractured media than in porous media, since the total pore volume generally is much smaller in fractures /see Pruess and Tsang, 1990/. In fractured rock applications, the use of these porous medium relations have therefore been restricted to the following two cases:

(1) to reproduce the conditions in specific laboratory experiments /e.g., Reitsma and Kueper, 1994; Persoff and Pruess, 1995/,

(2) to reproduce the field system responses by use of optimisation schemes, where observations on the field response are used as a basis for the determination of an optimum set of several unknown model parameters /so-called inverse modelling, see e.g., Finsterle and Pruess, 1995; Bandurraga and Bodvarsson, 1999/.

2.3.2 Alternative relations for fractured media

For fractured rock, an alternative approach to the common porous medium characteristic curves is to use a statistical description of the fracture aperture and relate the conductive properties of the (unsaturated) fracture to aperture distribution related parameters. The advantage is that robust techniques have indeed been developed for the measurement of the aperture distribution of rock fractures, both in the field /through resin injection, see Gale et al., 1990; Hakami and Stephansson, 1993; Hakami, 1995/, and the laboratory /see for instance Hakami, 1995; Jarsjö, 1998; and Lanaro, 1999/. Models that are based on such a statistical description of the fracture aperture are hence promising in the sense that they are based on properties that can be directly measured in the field (and not only in the laboratory), which considerably reduces the number of uncertain model parameters. In fact, the simplest possible aperture distribution based $S(p_c)$ model does not contain a single fitting parameter. A disadvantage is that phase accessibility related effects may need to be considered, and they may vary with the system under study.

Pruess and Tsang /1990/ used a statistic description of fracture aperture. They defined a critical cut-off aperture a_c, corresponding to a capillary pressure of

$$p_c = 2\sigma_w / a_c \tag{2-15}$$

(where σ_w is the air-water interfacial tension; see also Equation (2-9)) and occupied all apertures smaller than a_c with the wetting (water) phase and all larger apertures with the non-wetting (gas or oil) phase. This cut-off aperture assumption can now be combined with a statistical description of the fracture aperture, in order to obtain an expression for the saturation degree in the fracture. Specifically, we will consider fractures with a log-normal fracture aperture probability density function (pdf) defined by

$$f_{\ln}(a;\mu_{\ln a},\sigma_{\ln a}) = \frac{1}{a\sigma_{\ln a}\sqrt{2\pi}} \exp\left(-\frac{1}{2\sigma^2}(\ln a - \mu_{\ln a})^2 \right) \tag{2-16}$$

where a is the log-normally distributed random variable (here the fracture aperture), $\mu_{\ln a}$ is the mean value of ln a and $\sigma_{\ln a}$ is the standard deviation of ln a. Based on this pdf for a and the cut-off aperture assumption, the degree of fracture water saturation (S_w) can be estimated as the volume of fracture filled with water V_w divided by the total fracture volume V_{total}:

$$S_w(a_c;\mu_{\ln a},\sigma_{\ln a}) = V_w / V_{total} = \int_0^{a_c} a f_{\ln}(a;\mu_{\ln a},\sigma_{\ln a})da \Big/ \int_0^{\infty} a f_{\ln}(a;\mu_{\ln a},\sigma_{\ln a})da \tag{2-17}$$

The water saturation S_w can now be expressed as a function of the capillary pressure by combining Equation (2-15) and (2-17):

$$S_w(p_c;\mu_{\ln a},\sigma_{\ln a}) = \int_0^{2\sigma_w / p_c} a f_{\ln}(a;\mu_{\ln a},\sigma_{\ln a})da \Big/ \int_0^{\infty} a f_{\ln}(a;\mu_{\ln a},\sigma_{\ln a})da \tag{2-18}$$

The fracture gas saturation S_g is equal to (1- S_w). Further, by introducing the cubic law and arithmetic averaging, the following expression between the fracture transmissivity (for water) T_w and capillary pressure is obtained:

$$T_w(p_c;\mu_{\ln a},\sigma_{\ln a}) = T_s \int_0^{2\sigma_w/p_c} a^3 f_{\ln}(a;\mu_{\ln a},\sigma_{\ln a})da \Big/ \int_0^{\infty} a^3 f_{\ln}(a;\mu_{\ln a},\sigma_{\ln a})da \qquad (2\text{-}19)$$

where T_s is the transmissivity at water saturated conditions.

2.3.3 Comparison between porous medium and fractured medium relations

Whereas it has been shown that the porous medium relations for unsaturated flow can be fitted to reproduce the unsaturated fracture flow behaviour in rock fractures (see Section 2.3.1), the alternative relations for fractured media (Section 2.3.2) have not been compared with observational data. In this section, we compare the porous media and fractured rock relations, in order to see if they are capable of reproducing similar relations between the permeability of the medium and the capillary pressure, although they are based on different parameters. Specifically, we compare the characteristics of Equation (2-19) for the relative fracture transmissivity with the characteristics of the widely used porous medium van Genuchten (vG) relation, Equation (2-14). If a similarity is found, this shows that the fractured rock relations are equally capable of reproducing unsaturated flow conditions as the well-established porous medium relations are, which further implies that they can reproduce the actual observations made in various fractures equally well. Such a similarity would hence imply that there is no basis for assuming that one of the two methods would be less capable of *reproducin*g unsaturated flow observations. Since the fractured rock relations are based on parameters that are potentially quantifiable in rock fractures, they may provide additional, *predictive* capabilities in fractured rock, which cannot be obtained by applying porous medium relations in fractured rock.

The transmissive properties of a fracture can be evaluated from measured flowrates Q and hydraulic head gradients ($\mathrm{d}\phi/\mathrm{d}x$), through Darcy's law: $T=(Q/w)/(\mathrm{d}\phi/\mathrm{d}x)$, where w is the width of the fracture (more specifically, the length dimension perpendicular to the flow direction). In contrast, the fracture conductivity cannot be evaluated unless the aperture value a is known, since $K=T/a=(Q/(aw))/(\mathrm{d}\phi/\mathrm{d}x)$. If, on the other hand, the aperture is known, then both the conductivity and the transmissivity can be estimated on basis of this aperture value, see equations (2-6) and (2-7). However, the conductivity estimation is redundant since the flow (per fracture width w) can be fully determined through the transmissivity value and the hydraulic head gradient in Darcy's law. This implies that the flow in fractures is characterised by transmissivities rather than conductivities, see also the discussion in Persoff and Pruess /1995/. Furthermore, the use of the parallel plate approximation for the estimation of flow in variable aperture fractures implies that flow through a fracture may be viewed as analogous to two-dimensional flow through an aquifer. However, recall that the flow in porous aquifers of varying thickness is characterised by conductivities, since there are no relations between conductivity and aquifer thickness, i.e., there are no analogous relations to the above-discussed relation between fracture aperture and conductivity.

On basis of the above discussion, we will in the following characterise the unsaturated flow in porous media by consideration of its conductivity, whereas we for fractured media consider its transmissivity. More specifically, we will for comparative purposes use relative conductivities K_{rel} and transmissivities T_{rel}, which express the unsaturated conductivity/ transmissivity normalised by the saturated conductivity/ transmissivity.

Specifically, they are calculated as $K_{rel}(p_c)=K(p_c=-\rho gh)/K_s$ (with K as in (2-14)) and $T_{rel}(p_c)=T_w(p_c)/T_s$ (with T_w as in (2-19). Hence, both T_{rel} and K_{rel} are dimensionless and take on values between 0 and 1.

We will predict the relative water transmissivity for a wide range of hypothetical fracture aperture distributions, characterised by different mean aperture values $\mu_{\ln a}$, and standard deviation values $\sigma_{\ln a}$, and compare the shape of these curves with correspondingly matched the vG-relations. As a basis for the comparison, we use $\mu_{\ln a}$ and $\sigma_{\ln a}$ values that are consistent with the range that was observed in 19 different fractures /Hakami, 1988; Gentier, 1990; Hakami and Stephansson, 1993; Iwano and Einstein, 1993; Hakami, 1995/. The range of mean apertures in these fractures was $-2.3 \le \mu_{\ln a} \le 0.2$, where a is given in mm. This corresponds to 0.1 mm $< a^G=\exp(\mu_{\ln a}) <$ 1.2 mm, where a^G is the geometric mean aperture. Furthermore, the range of standard deviation of ln$a$ was $0.2 \le \sigma_{\ln a} \le 1.2$.

The solid curves of Figure 2-6 show fracture aperture based relative transmissivities T_{rel} as functions of p_c (using Equation (2-19)). The thinnest, solid curve in Figure 2-6 shows $T_{rel}(p_c)$ for a mean aperture value $\mu_{\ln a}$ of –1 (corresponding to a geometric mean aperture a^G of 0.37mm) and the thickest solid curve shows $T_{rel}(p_c)$ for a considerably smaller mean aperture value of –4 (corresponding to a geometric mean aperture of 0.018 mm). For all three solid curves, the standard deviation $\sigma_{\ln a}$ was kept constant at the value 0.8.

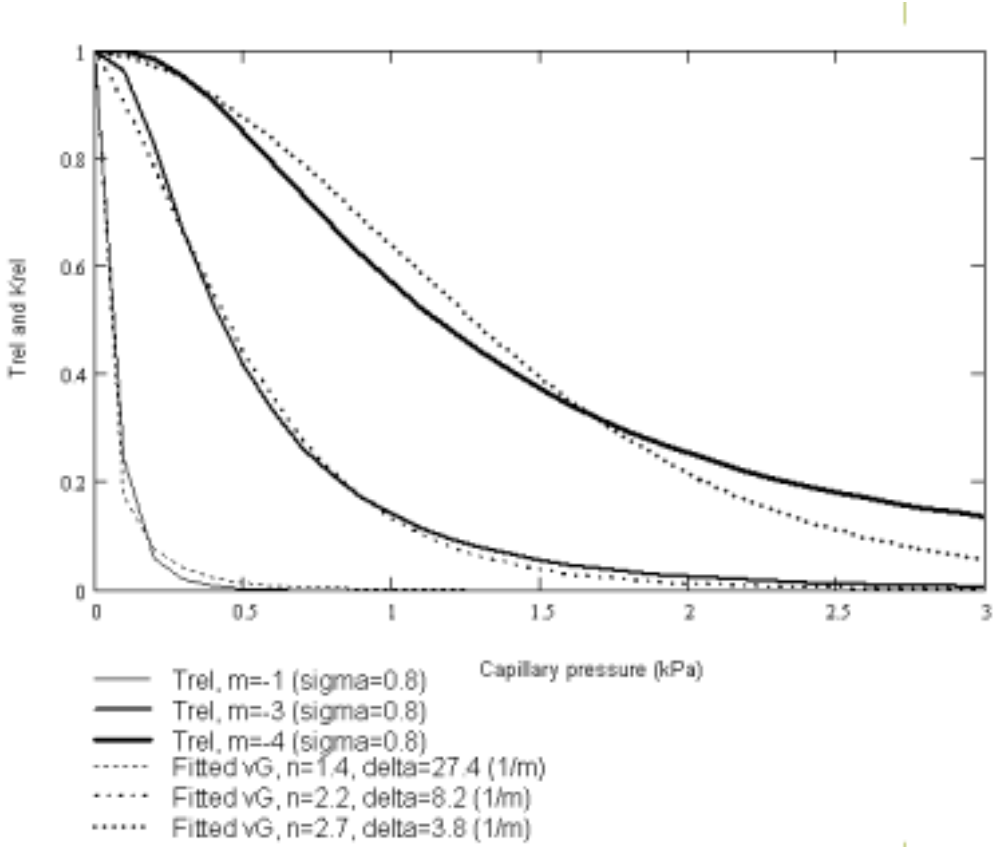

Figure 2-6. *Comparison between the fractured rock characteristic relation (Equation 2-19 with different mean aperture values $\mu_{\ln a}$) and the fitted vG-relation (Equation 2-14).*

As expected, relation (2-19) predicts that the widest fracture (thinnest, solid line) is drained at considerably lower capillary pressures than the other two fractures.

Figure 2-6 also shows that similar curves (dotted) are obtained when fitting the vG-relation (2-14) for relative conductivity, $K_{rel}(p_c)$, to the fractured rock relation, $T_{rel}(p_c)$. The fitted vG-parameter δ ranged between 3.1 and 27 m^{-1} and the parameter n ranged between 1.4 and 2.7 for the curves of Figure 2-6 (m was held constant at a value of 0.5). Data on vG-parameter values for an extensive set of soils (ranging in pore sizes from clay soils to sandy soils) compiled from the studies of Demond and Roberts /1993/; Durner /1994/; Reitsma and Kueper /1994/; Khaleel and Relyea /1995/ and Rajaram et al. /1997/ show that the range of δ was between 0.06 and 50 m^{-1} and the range of n was between 1.1 and 8. Hence, the range of parameter values for the vG-curves of Figure 2-6 is within the wider range of vG-parameters that previously have been reported for various soils in the literature.

In Figure 2-7, a comparison similar to that of Figure 2-6 is made between the fractured rock characteristic relation (Equation 2-19) and the vG-relation (Equation 2-14). However, in contrast to Figure 2-6, the mean aperture value μ_{lna} is in Figure 2-7 held constant

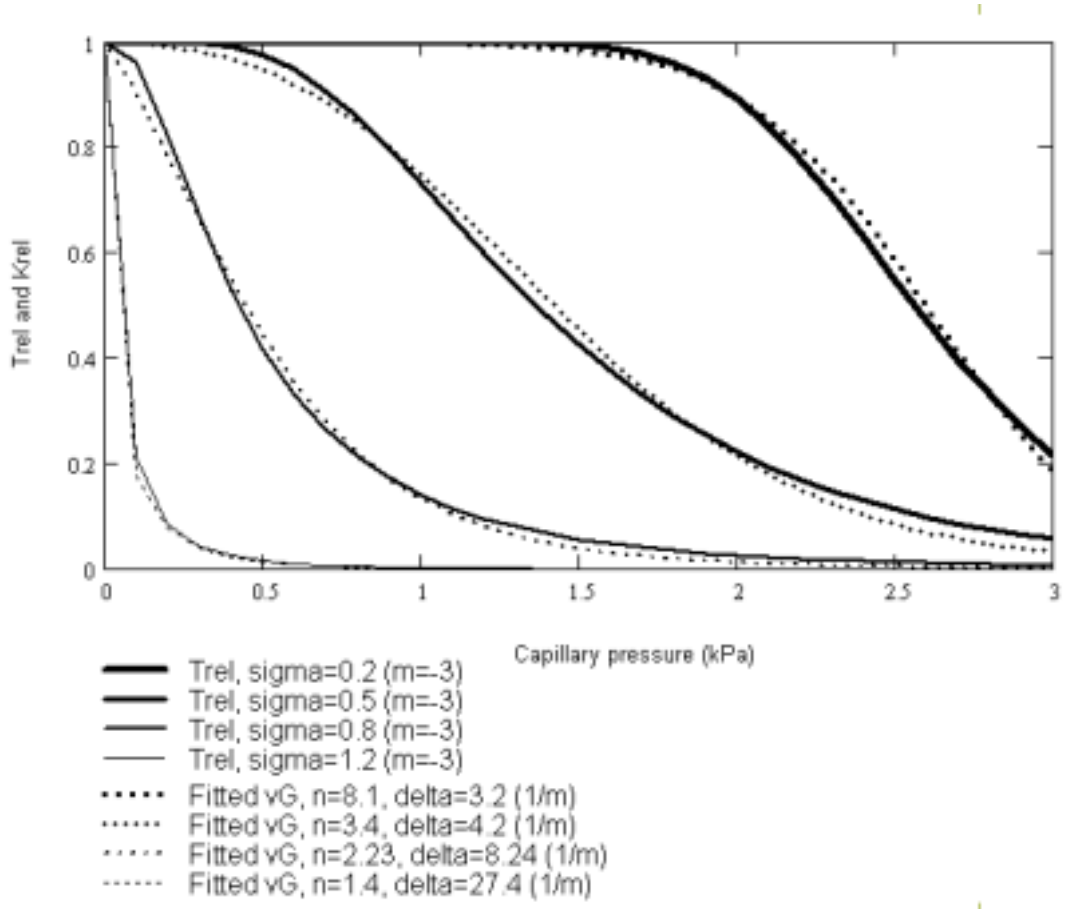

Figure 2-7. *Comparison between the fractured rock characteristic relation (Equation 2-19 with different aperture standard deviation values σ_{lna}) and the fitted vG-relation (Equation 2-14).*

at the value –3, and instead the different solid curves represent different aperture standard deviation values σ_{lna} (ranging from 0.2 to 1.2). Figure 2-7 shows that the vG-relation matches well with the fractured rock characteristic relation also in this case. Furthermore, the range of vG parameter values shown in Figure 2-7 again falls within the larger range of parameter values previously reported for various soils.

Hence, the comparison shows that the fractured rock relation for T_{rel} (2-19) is consistent with the for soils widely used vG relation (2-14), for a wide range of μ_{lna} and $\sigma_{lna.}$ This implies that both relations can reproduce the same kind of unsaturated flow behaviour although they are based on completely different sets of parameters. With relation (2-19), there are additional possibilities of performing predictive modelling for fractured rock, using parameters that are relevant for site-specific field conditions. One should note that the fractured rock relation is based on simplifying assumptions regarding both gas and water phase distribution and interference; the general relevance of these assumptions have as of now not been thoroughly addressed in experimental investigations. However, for the special case of groundwater degassing, we develop the relations further Chapter 3, and compare the developed relations with the actual outcome of both laboratory and field experiments in Chapter 6.

2.3.4 Scaling of unsaturated flow relations in fractured rock

Groundwater degassing is primarily expected to occur relatively close to open boreholes and drifts, see Section 2.1. On this scale, the rather detailed hydraulic and/ or fracture aperture properties that are needed to address the degassing problem can, in principle, be obtained through in situ borehole tests and/ or laboratory experiments. However, other multiphase processes that can potentially affect the performance of deep repositories may take place at much larger scales. For instance, for the scenario of gas generation in the repository and subsequent transport through the fractured rock, the relevant scale can be on the order of a kilometre. On this scale, the hydrologic conditions cannot be known in detail throughout the domain. Rather, detailed information will be available in a finite number of sampling locations. This point information then needs to be interpreted in some way that is relevant for the large-scale problem.

The relative conductivity/ transmissivity relations (the so-called characteristic curves), described in Sections 2.3.1 and 2.3.2, provide an important basis for the quantification of unsaturated (water/gas) flow. They are relevant on the scale at which their parameters (μ_{lna} and σ_{lna}) can be measured, i.e., up to a few meters. Models considering larger scales may hence need to account for the possible variability in these parameters over the domain. In the following, we consider a numerical model set-up in which the size of the individual cells are such that the unsaturated flow within each cell are well represented by the characteristic curve (2-19), although the actual shape of the curve varies from cell to cell. We will now investigate if and how this variability can be accounted for, considering the typical case that detailed ("cell-by-cell") information of the shape of the curve is unavailable. More specifically, we will investigate the relevance of scaling the characteristic curves measured in one subregion (or cell), based on "soft" data (some information on the prevailing fracture transmissivity) for another subregion, in order to obtain relevant characteristic curves for the latter subregion. We expect that this question is principally important for the interpretation of the gas injection tests that were performed at Äspö HRL by the German organisation BGR, because data on mean

apertures and aperture standard deviations were not available throughout the test domain.

Our starting point for this investigation will be the Leverett-scaling procedure /see p. 446 in Bear, 1972/, which was developed for porous media. We will now modify it considering the conditions prevailing in fractured media, and test the relevance and applicability of the modified relation.

The following site-specific information is needed in order to apply the scaling procedure:

(i) More detailed statistics on the physical fracture aperture for one subregion (corresponding to a "cell" in the numerical model).

(ii) Some information/ statistics on either the mean aperture width, or the saturated transmissivity value, for the other subregions/ cells.

We further assume that the fracture apertures within each subregion/ cell are log-normally distributed (see equation 2-16).

The Leverett scaling relation may be expressed as /Bear, 1972/:

$$p_c(S_w)_2 = p_c(S_w)_1\sqrt{k_1/k_2} \tag{2-20}$$

where subscripts 1 and 2 refer to the two different media. Hence the (unknown) capillary pressure p_c at a particular water saturation S_w in medium number 2 can be estimated on basis of the corresponding (known) capillary pressure at the same water saturation in medium number 1, and the permeability ratio k_1/k_2 between the media.

However, the most relevant measure of the hydraulic properties in fractured media is transmissivity (T), rather than permeability (k), see further Section 2.3.3. With the aim to obtain a scaling relation based on fracture transmissivities, we therefore recall the following relation between permeability and transmissivity (originally developed for flow between parallel plates):

$$k = \frac{\mu T}{\rho g a_h} \tag{2-21}$$

where μ is the liquid viscosity, ρ is the liquid density, g is the gravitational constant and a_h is the hydraulic fracture aperture. Then, one can use the corresponding relation between a_h and k, $a_h = \sqrt{12k}$, to eliminate a_h from the above expression and obtain

$$k = \sqrt[3]{12}\left(\frac{\mu T}{\rho g}\right)^{2/3} \tag{2-22}$$

which, when inserted in relation (2-20) results in the following scaling relation:

$$p_c(S_w)_2 = p_c(S_w)_1\sqrt[3]{T_1/T_2} \tag{2-23}$$

In order to compare the proposed scaling procedure of the characteristic curves, through (2-23), with direct estimates of the characteristic curves, through Equation (2-19), we used the following steps:

(a) Consider two different fractures F1 and F2, characterised by $f_{\ln}(a_{F1};\ \mu_{\ln aF1},\sigma_{\ln aF1})$ and $f_{\ln}(a_{F2};\ \mu_{\ln aF2},\sigma_{\ln aF2})$, respectively.

(b) Calculate the characteristic curves (for T_{rel}) for fracture F1 and F2 through Equation (2-19).

(c) Estimate the saturated transmissivity ratio between these fractures through the expression

$$T_1 / T_2 = \int_0^{\infty} a_{F1}{}^3 f_{\ln}(a_1;\mu_{\ln aF1},\sigma_{\ln aF1})da_{F1} \Big/ \int_0^{\infty} a_{F2}{}^3 f_{\ln}(a_{F2};\mu_{\ln aF2},\sigma_{\ln aF2})da_{F2} \quad (2\text{-}24)$$

which is consistent with Equation (2-19).

(d) Use Equation (2-24) and the modified Leverett function (2-23) to scale the characteristic curve obtained for fracture F1 (see step (b) above) to yield the characteristic curve for fracture F2. Compare with the curve for fracture F2, directly obtained in step (b) above.

First, we conducted steps (a) to (d) for two fractures F1 and F2, differing by their mean aperture values $\mu_{\ln a}$, but having the same standard deviation value $\sigma_{\ln a}$. Fracture F1 was characterised by $f_{\ln}(a_{F1};\ \mu_{\ln aF1}$=-4, $\sigma_{\ln aF1}$=0.8) and fracture F2 was characterised by $f_{\ln}(a_{F2};\ \mu_{\ln aF2}$=-3, $\sigma_{\ln aF2}=\sigma_{\ln aF1}$=0.8). Figure 2-8 shows that for this case, the scaled curve for fracture F2 (crosses in Figure 2-8), based on the curve for fracture F1 (thick solid line), coincides with the curve for fracture F2 estimated directly from aperture statistics (thin solid line).

Then, we conducted steps (a) to (d) for two fractures F3 and F4, differing by their standard deviation values $\sigma_{\ln a}$, but having the same mean aperture value $\mu_{\ln a}$. Fracture F3 was characterised by $f_{\ln}(a_{F3};\ \mu_{\ln aF3}$=-3, $\sigma_{\ln aF3}$=0.2) and fracture F4 was characterised by $f_{\ln}(a_{F4};\ \mu_{\ln aF4}=\mu_{\ln aF3}$=-3, $\sigma_{\ln aF4}$=0.5). Figure 2-9 shows that in this case, the scaled curve for fracture F4 (crosses), based on the curve for fracture F3 (thick, solid line) differs from the curve for fracture F4 estimated directly from aperture statistics (thin, solid line).

Figure 2-8 and Figure 2-9 hence indicate that the errors associated with scaling using equation (2-23) are small for fractures of different mean apertures, as long as the aperture standard deviations are similar. The method is exact for fractures with different mean apertures and the same aperture standard deviation, as shown by the coinciding scaled and directly estimated characteristic curves in Figure 2-8.

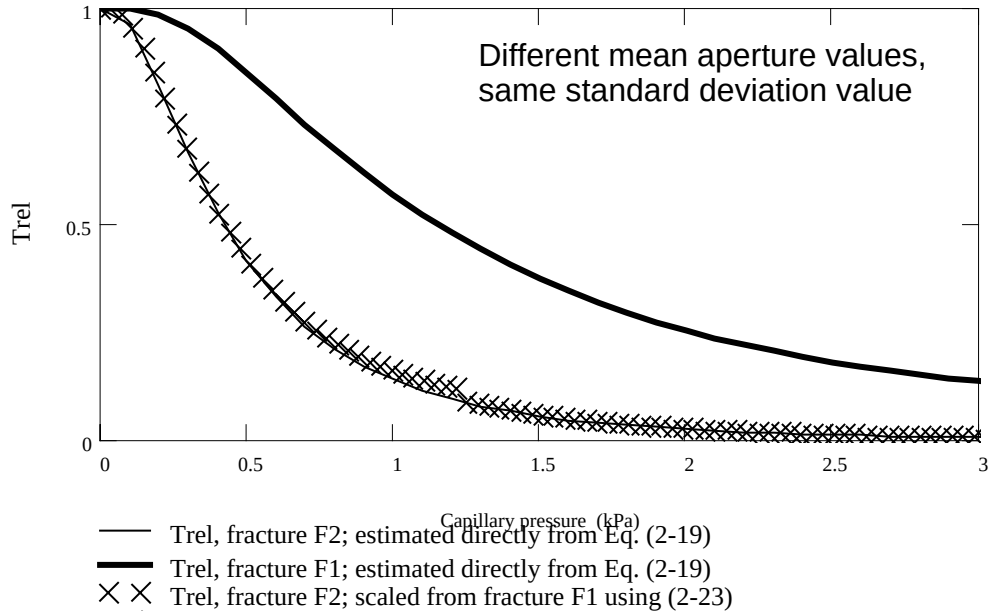

Figure 2-8. *Scaled characteristic curve for fracture F2 (crosses), based on the characteristic curve for fracture F1 (thick, solid line), compared with the directly estimated characteristic curve for fracture F2 (thin, solid line), for the case of different mean aperture values* μ_{lna}*, but the same standard deviation value* $\sigma_{lna.}$

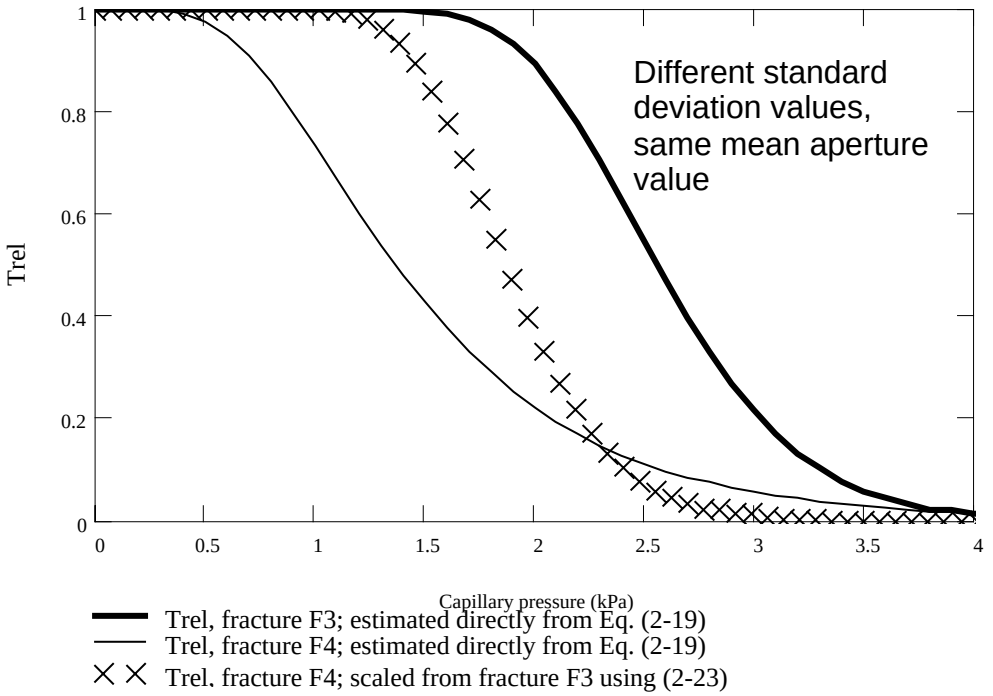

Figure 2-9. *Scaled characteristic curve for fracture F4 (crosses), based on the characteristic curve for fracture F3 (thick, solid line), compared with the directly estimated characteristic curve for fracture F4 (thin, solid line), for the case of different standard deviation values* $\sigma_{lna.}$ *but the same mean aperture value* $\mu_{lna.}$

3 Degassing models and alternative explanations for inflow reduction

3.1 Degassing models

3.1.1 Parameters

There are at least two factors that may contribute to a considerable hydraulic conductivity reduction due to degassing. Firstly, the occurrence of bubble trapping implies that gas may accumulate in the fracture, such that that the local degree of fracture gas saturation (i.e., gas volume per total fracture volume) is considerably greater than the evolving volumetric gas content $\Delta\theta_g$ /see Gardescu, 1956, for a detailed description of the behaviour of gas bubbles in capillary spaces/. Secondly, the non-linear relative hydraulic conductivity functions for unsaturated fractured media imply that hydraulic conductivity decreases considerably with increasing degree of gas saturation /e.g., Pruess and Tsang, 1990; Fourar et al., 1993 and Persoff and Pruess, 1995/. However, none of these two factors can possibly contribute to hydraulic conductivity reduction unless a separate gas phase forms within the fracture pore space. Further, the size of the fracture zone where gas forms and the local hydraulic conductivity changes needs to be sufficiently large in relation to the total fracture size; otherwise, if the developed gas phase occupies only a very small part of the water-bearing fracture, the effective hydraulic conductivity of the entire fracture will remain essentially unchanged.

Since the size of the low-pressure zone X_{low} (see Figure 2-4), provides an upper limit for the actual size of the developed gas-containing zone X_{gc} (Figure 2-4), it is reasonable to hypothesise that the low-pressure zone extent in relation to the total fracture length, X_{low}/L, must exceed some critical length measure in order to make the conditions for gas phase development favourable, and the hydraulic effects of groundwater degassing significant. However, besides groundwater degassing, there are other conceivable explanations for field observations of hydraulic conductivity reductions. Such alternative explanations include fracture deformation due to water pressure lowering during the experiment and/ or turbulence effects (see Section 3.2). Importantly, none of these explanations would result in the hypothesised correlation between the X_{low}/L ratio and the experimental outcome in terms of the occurrence/ absence of hydraulic conductivity reductions. The X_{low}/L ratio has relevance only for the degassing explanation (see Figure 2-4) and is meaningless for all other explanations, implying that if a correlation is found, it constitutes a clear support for the degassing explanation. In the interpretation chapter of this report (Section 6.1), we will therefore investigate whether there is such a correlation between the estimated value of X_{low}/L and the actual outcome field and laboratory experiments in terms of whether or not hydraulic conductivity reduction has been observed in each experiment.

Through the above-mentioned X_{low}/L-estimation and comparison, we address the question whether or not degassing is likely to affect flowrates under different conditions. However, a more detailed understanding of processes is needed for quantitative predictions of groundwater degassing effects. In the following sections, we therefore outline models that have been developed to investigate the probability for gas bubble trapping

and gas accumulation under different conditions (Section 3.1.2, and the effects of a gas phase on the fracture transmissivity, provided that this gas phase is trapped in the fracture (Section 3.1.3). Further, in the interpretation chapter, the model predictions are compared with experimental observations (Sections 6.2 and 6.3).

3.1.2 Bubble trapping /Jarsjö and Destouni, 1998/

Gas bubbles in variable aperture fractures may be trapped, such that they no longer follow the flowing water, due to differences in the aperture width over the bubble length. The occurrence of such bubble trapping depends, for instance, on the aperture variation and spatial correlation, and the local hydraulic gradients. Jarsjö and Destouni /1998/ estimated the occurrence of bubble trapping by calculating a bubble trapping probability, which was related to both physical fracture aperture characteristics and local hydraulic conditions.

The starting point was the equilibrium relation stating that the difference in capillary pressure upstream and downstream of a trapped bubble (Δp_c) equals the corresponding difference in water pressure (Δp_w; caused by the hydraulic gradient over the fracture). Then, for a local pressure gradient of (dp/dl) along the mean flow direction, the difference in water pressure over the bubble is $\Delta p_w=p_1-p_2=L_b(dp/dl)$ (using the notation of Figure 3-1), where L_b is the bubble length along the mean flow direction l. Furthermore, the difference in capillary pressure over the bubble is $\Delta p_c=2\sigma_w(1/a_2-1/a_1)$, where σ_w is the surface tension of water and a_1 and a_2 are the apertures upstream and downstream the bubble, respectively.

Using the above-mentioned equality between Δp_c and Δp_w that is required for bubble trapping, the length L_b of a trapped bubble was expressed as a function of the apertures a_1 and a_2:

$$L_b = 2\sigma_w\left(\frac{dp}{dl}\right)^{-1}\left(\frac{1}{a_2}-\frac{1}{a_1}\right) \qquad (3\text{-}1)$$

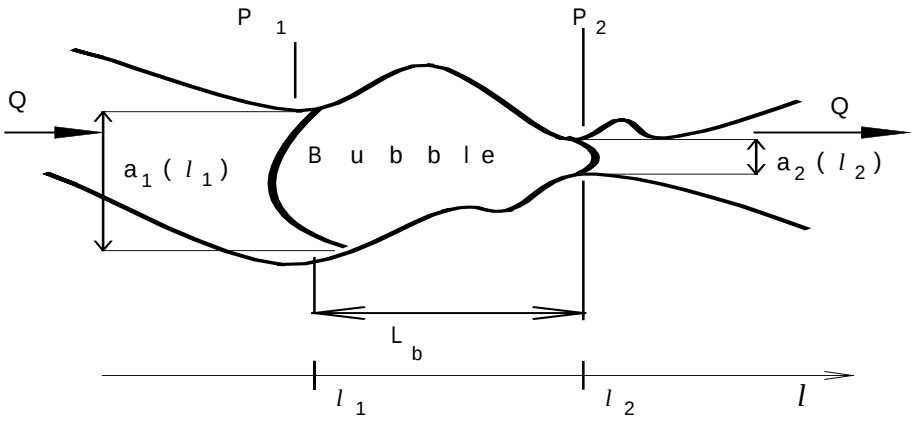

Figure 3-1. *Trapped gas bubble in a variable aperture fracture.*

Now consider a variable aperture fracture for which the aperture a_i at location $l=l_i$ along the mean flow direction can be described statistically with a log-normal pdf (Equation (2-16)), characterised by the mean value $\mu_{\ln a}$ and standard deviation $\sigma_{\ln a}$. The probability for a bubble of length L_b, extending from $l=l_1$ to $l=l_2$, to be trapped is the probability that equality (3-1) is true. In (3-1), the apertures a_1 at l_1 and a_2 at l_2 are random variables, and it is therefore uncertain whether or not an aperture combination $a_1(l_1)$ and $a_2(l_2)$ can be found such that the distance l_2-l_1=L_b, as it must be for the equality (3-1) to be true. Jarsjö and Destouni /1998/ estimated the probability for such an aperture combination to occur through the following probability density function (pdf) for L_b, which was derived on basis of the pdf's $f_{\ln}(a_1;\mu_{\ln a},\sigma_{\ln a})$ and $f_{\ln}(a_2;\mu_{\ln a},\sigma_{\ln a})$ for a_1 and a_2, respectively (note that both these pdf's are identical, i.e., characterised by the same mean aperture value and standard deviation value, since we consider statistically stationary and uncorrelated aperture values):

$$f(L_b) = \frac{(dp/dl)}{2\sigma_w} \int_{-\infty}^{0} f_{\ln}(-\xi;-\mu_{\ln a},\sigma_{\ln a}) \cdot f_{\ln}\left(\frac{L_b(dp/dl)}{2\sigma_w} - \xi;-\mu_{\ln a},\sigma_{\ln a} \right) d\xi \qquad (3\text{-}2)$$

where the pdf $f_{\ln}$ is defined through Equation (2-16) and ξ is a dummy integration variable.

The above pdf $f(L_b)$ can be used to quantify the probability for a bubble of the specific length L_b to occur in the fracture due to capillary trapping under the given gradient (dp/dl). However, the pdf is mathematically defined throughout the range $(-\infty \le L_b \le \infty)$ and some of these mathematically possible L_b-values, such as for instance negative values, are physically not meaningful as lengths of trapped bubbles. By formulating relevant physical constraints for the bubble lengths that can possibly be trapped in a given fracture, we may estimate the probability for this range of possible bubbles to occur as the area below the pdf $f(L_b)$ between the limits given by the maximum and minimum possible L_b-values.

One constraint for the physically possible lengths of trapped bubbles (Figure 3-1) is that the length L_b must be greater than the local aperture value. Spherical bubbles, for instance, would otherwise be too small to connect both opposite fracture surfaces. Assuming that the fluctuations of a are small (small perturbation assumption) one may formulate this constraint as $L_b \ge \overline{a}$ (with the minimum bubble length then becoming $L_{b,min} = \overline{a}$), where $\overline{a}$ is the mean aperture. At this stage, the pdf $f(L_b)$ and the above expression for $L_{b,min}$ is not only valid for degassing applications, but is generally relevant for gas bubble trapping between two rough surfaces. For degassing applications, we can add the constraint that $L_b \le X_{low}$ (with the maximum bubble length then becoming $L_{b,max}=X_{low}$), where X_{low} is the extent of the low-pressure zone (read: the extent of the zone where pressures are lower than the bubble pressure under water saturated conditions and where degassing can possibly occur).

Equation (3-2) was derived under the assumption that a_1 and a_2 are spatially uncorrelated, i.e., that the correlation length λ of the variable aperture fracture is much smaller than L_b. For the case that there is a correlation between the aperture values $a_1(l_1)$ and $a_2(l_2)$, Jarsjö and Destouni derived a corresponding pdf for L_b (see Equation 10 of Jarsjö and Destouni, 1998). This expression may be further simplified and expressed as:

$$f(L_b;h)=\frac{(dp/dl)}{2\sigma_w}\int_{-\infty}^{0} f_j\left(-\xi,\frac{L_b(dp/dl)}{2\sigma_w}-\xi;-\mu_{\ln a},\sigma_{\ln a},h\right)d\xi \qquad (3\text{-}3)$$

where f_j is a joint two-variable log-normal pdf that is consistent with the marginal one-variable log-normal pdf (2-16), and is given by:

$$f_j(x_1,x_2;\mu_{\ln x},\sigma_{\ln x},h)=\frac{1}{2\pi x_1 x_2\sqrt{\sigma_{\ln x}^4-C^2}}\cdot$$
$$\cdot\exp\left(-\frac{\sigma_{\ln x}^2(\ln x_1-\mu_{\ln x})^2-2C(\ln x_1-\mu_{\ln x})(\ln x_2-\mu_{\ln x})+\sigma_{\ln x}^2(\ln x_2-\mu_{\ln x})^2}{2(\sigma_{\ln x}^4-C^2)}\right) \qquad (3\text{-}4)$$

where x_1 and x_2 are the spatially correlated, random, variables at positions l_1 and l_2, respectively, being separated by a distance $h=l_2-l_1$ (along the mean flow direction; Figure 3-1). In (3-4), $C=\sigma_{\ln x}^2\cdot\exp(-\lambda/h)$ is an assumed exponential and isotropic auto-correlation function for the random variable x, which is assumed stationary, having the same mean value $\mu_{\ln x}$ and the same standard deviation $\sigma_{\ln x}$ at all locations, l. See Jarsjö and Destouni /1998/ for a more extensive discussion of the use of Equation (3-4) and a comparison with Equation (3-2).

3.1.3 Transmissivity reduction due to groundwater degassing /Jarsjö and Destouni, 1998/

Jarsjö and Destouni /1998/ used a statistical description of the fracture aperture and derived expressions for the relative transmissivity (i.e., the ratio between the unsaturated transmissivity and the saturated transmissivity) under degassing conditions. These expressions were obtained for different underlying assumptions regarding the water and gas phase occupancy in different regions of the variable fracture aperture at steady-state. The best agreement between modelled transmissivity reduction and experimentally observed transmissivity reduction for a fracture with a log-normally distributed aperture was obtained using the phase occupancy assumption illustrated in Figure 3-2. In analogy with the cut-off aperture assumption of Pruess and Tsang /1990/, all apertures tighter than the critical cut-off aperture a_c is assumed to be completely filled with water. However, in contrast to the Pruess and Tsang /1990/ assumption, both gas and water are allowed to co-exist in the wide aperture region, where $a>a_c$ (Figure 3-2). The factor α quantifies the fraction of water occupancy in the wide aperture region. This assumption is consistent with direct observations of the gas phase distribution during degassing experiments in transparent rock fracture replicas (see Figure 5-1, Section 5.1).

In order to obtain degassing-based relations between the dissolved gas content C_g in the water on the one hand, and the steady-state gas/water saturation and relative transmissivity on the other hand, there is a need to relate C_g to the cut-off aperture a_c. In the following, we will consider water with a certain amount of dissolved gas, and use the term bubble pressure p_b for the critical water pressure below which a separate gas phase forms. For steady-state conditions, Henry's law (2-2) then implies the following relation between C_g and p_b:

$$p_b=HC_g \qquad (3\text{-}5)$$

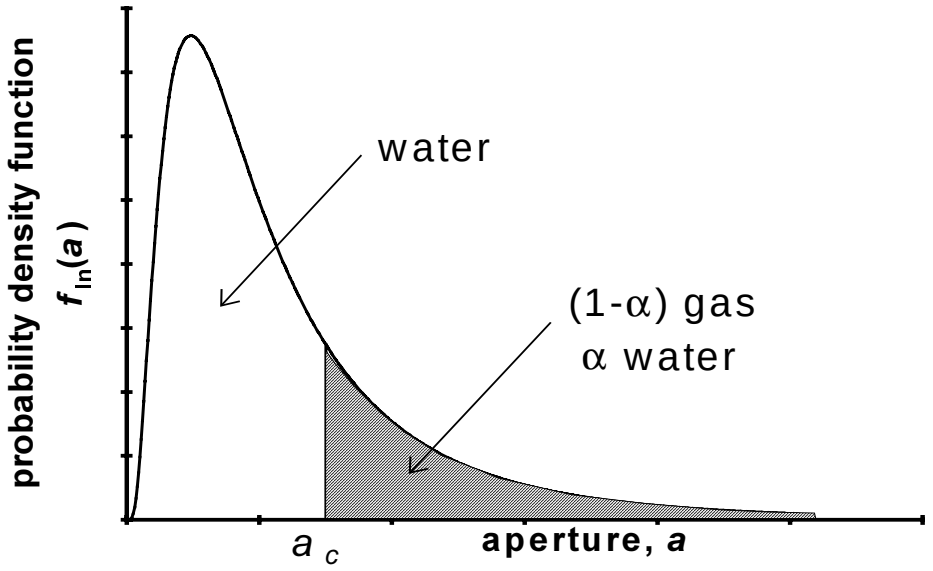

Figure 3-2. *Assumed water and gas phase occupancy in a fracture with a log-normally distributed aperture.*

in which p_b is the bubble pressure in kPa (abs), H is Henry's law constant for the gas in the liquid in kPa·m^3·mol^{-1}, and C_g is the molar concentration of gas dissolved in the liquid. Jarsjö and Destouni /1998/ then related p_b with a_c through relation (2-15), using the fact that p_c is defined as p_g-p_w in conjunction with the fact that the gas phase pressure p_g equals p_b when the gas starts to form under equilibrium conditions. Then, the relation between a_c and p_b becomes:

$$a_c = \frac{2\sigma_w}{p_b - p_w} \tag{3-6}$$

where σ_w is the surface tension of water.

Based on Equation (2-17), with a_c as in (3-6) and using the phase occupancy assumption of Figure 2-1, Jarsjö and Destouni /1998/ obtained the following degassing-based relations between p_b and water saturation S_w:

$$S_w(p_b;\mu_{\ln a},\sigma_{\ln a},\alpha) = \frac{\int_0^{\frac{2\sigma_w}{p_b-p_w}} a f_{\ln}(a;\mu_{\ln a},\sigma_{\ln a})da + \alpha \int_{\frac{2\sigma_w}{p_b-p_w}}^{\infty} a f_{\ln}(a;\mu_{\ln a},\sigma_{\ln a})da}{\int_0^{\infty} a f_{\ln}(a;\mu_{\ln a},\sigma_{\ln a})da} \tag{3-7}$$

The corresponding expression for the relation between the p_b and water transmissivity T_w is:

$$T_w(p_b;\mu_{\ln a},\sigma_{\ln a},\alpha) = T_s \frac{\int_0^{\frac{2\sigma_w}{p_b-p_w}} a^3 f_{\ln}(a;\mu_{\ln a},\sigma_{\ln a})da + \alpha \int_{\frac{2\sigma_w}{p_b-p_w}}^{\infty} a^3 f_{\ln}(a;\mu_{\ln a},\sigma_{\ln a})da}{\int_0^{\infty} a^3 f_{\ln}(a;\mu_{\ln a},\sigma_{\ln a})da} \quad (3\text{-}8)$$

3.2 Alternative explanations

The occurrence of turbulence can imply non-linear relations between water pressure gradient and flowrate. Groundwater degassing effects are expected to occur only at relatively low water pressures (see Figure 2-3 and Figure 2-4), implying high pressure gradients and relatively high flowrates. Hence, the possible onset of turbulence at these relatively high flowrates may provide an alternative explanation to observations of non-linear relations between water pressure and flowrate, in addition to explanations provided by groundwater degassing (see the above paragraph). We will therefore in the interpretation (Section 6.4.1) compare the conditions prevailing during degassing tests with studies specifically addressing turbulence in fractures. The basis of this comparison is provided by the Reynolds number (Re), defined as:

$$\mathrm{Re} = \frac{Dv}{\upsilon} \quad (3\text{-}9)$$

where D is the hydraulic diameter, v is the pore water velocity and υ is the kinematic viscosity. In analogy with Fourar et al. /1993/ we use the relation $D=2a_h$, where a_h is the hydraulic fracture aperture. Further, we estimate v as $Q/(2\pi r a_h)$ where Q is the volumetric rate of borehole/ well inflow and r is the radial distance to the borehole/ well centre. As indicated by the resulting expression $\mathrm{Re}=Q/(\pi r \upsilon)$, Re increases with decreasing values of r. The highest value $\mathrm{Re}=\mathrm{Re}_{max}$ occurs at the wall of the borehole/ well, i.e., at $r=r_w$.

The critical Re value for which turbulence effects start to evolve differs from medium to medium. In porous media, it is commonly assumed that turbulence causes considerable effects for Reynolds numbers greater than 100, whereas it is assumed that no turbulence effects will occur for Reynolds numbers less than some value between 1 and 10. Further, for flow in pipes the critical value of Re between laminar and turbulent flow is around 2000. For fractured rock, experimental results reviewed by Romm /1966/ showed an onset of turbulence for Re values between 10 and 100 in rougher fractures, and between 100 and 2000 in smoother fractures. Another phenomenon that may in principle lead to measurable hydraulic conductivity reductions is stress-induced fracture deformation caused by increased effective stresses when lowering the borehole pressure to atmospheric pressure. This is addressed in Section 6.4.2.

4 Field observations of gas contents and degassing effects

4.1 Gas content measurements

The evolved volumetric gas content, i.e., the evolved volume of gas at atmospheric pressure conditions per total water volume, ranged between 2 and 4% at 385 meters depth during the Stripa Simulated Drift Experiment (see Section 4.2 below). Measurements at various sites in Sweden have shown results that are similar to those of the Stripa mine; at the Äspö HRL (at 350–450 metres depth) the gas contents at atmospheric pressure conditions ranged between 0.1% and 5% /Geller and Jarsjö, 1995; Nilsson, 1997; Pedersen, 1997/ and the gas contents at Laxemar (located about one kilometre from Äspö HRL) at 800–1000 metres depth ranged between 2% and 5% /Pedersen, 1997/. Further, the data show that there is a considerable spatial variability in gas contents within each site. The groundwater gas content in two different fractures some twenty metres apart may for instance differ by a factor two. At all the above-referenced sites, nitrogen is the dominating gas, occupying approximately 80% of the total gas volume. Some of the nitrogen may have atmospheric origin. However, in most cases the observed gas contents exceed the solubility limit at atmospheric pressure, which implies that more nitrogen is added at some depth, possibly through microbial processes /Pedersen, 1997/.

At the Wellenberg site in Switzerland, a change in gas composition and content with depth has been observed, with the more shallow groundwater being dominated by nitrogen and the deeper groundwater being dominated by methane /NAGRA, 1997/. At 300–400 metres depth, the formation water is generally close to fully saturated with methane at formation pressure /with local existences of a free gas phase; NAGRA, 1997/, implying even higher volumetric gas contents at atmospheric pressure conditions than for corresponding depths at the Swedish sites.

4.2 The Stripa observations /Olsson, 1992/

During a hydraulic test series in the Stripa mine in Sweden at 385 metres depth, Olsson /1992/ and Birgersson et al. /1993/ observed that the inflow to a drift was a factor eight smaller than the inflow measured at the same location before the drift excavation, in six boreholes forming a ring. Olsson /1992/ and Birgersson et al. /1993/ suggested that the reduced inflow was possibly caused by the development of an unsaturated zone around the drift, due to degassing of groundwater in the low-pressure zone near the atmospheric pressure boundary at the drift wall. As opposed to the drift case, water pressures around the boreholes were considerably above atmospheric pressure due to borehole pressure regulation, thus preventing degassing to occur around the boreholes.

The potential occurrence and impact of degassing, relative to other phenomena that may have contributed to the observed inflow reduction in Stripa (such as changes in the rock stress conditions), could not be quantified based on available data. Without providing conclusive answers, the Stripa observations thus raised important questions about

whether or not and to what extent groundwater degassing may be expected to affect hydraulic property values that are determined from drift inflow measurements at large depths below the groundwater table, or from hydraulic tests in boreholes.

4.3 Borehole observations at Äspö HRL

Four field degassing tests have been conducted at the Äspö HRL. Three of these tests were conducted at the pilot resin site in boreholes KXTP2, KXTP4 and KXTP8 (abbreviated P2, P4 and P8, respectively) at approximately 450 metres depth below the water table (see Figure 4-1). A pilot hole test was also conducted in borehole KA2512A at approximately 300 metres depth below the water table (not shown in Figure 4-1). The main objective with the testing was to investigate whether the lowering of pressures down to atmospheric pressures in a borehole intersecting a water bearing fracture would lead to degassing and formation of an unsaturated zone in the vicinity of the borehole. Furthermore, the possible effect of this unsaturated zone on the fracture conductive properties was to be quantified.

Table 4-1 shows that three of the tests were conducted in fractures with transmissivity values on the order of 10^{-9} m^2/s, whereas one test (the pilot hole test) was conducted in a fracture with a considerably higher transmissivity of $8 \cdot 10^{-7}$ m^2/s. Table 4-1 also shows the evolved gas content during the testing and the ratio of the transmissivity before the degassing test and during/ after the degassing test ($T_{rel,obs}$), see Sections 4.3.1 and 4.3.2 for further details.

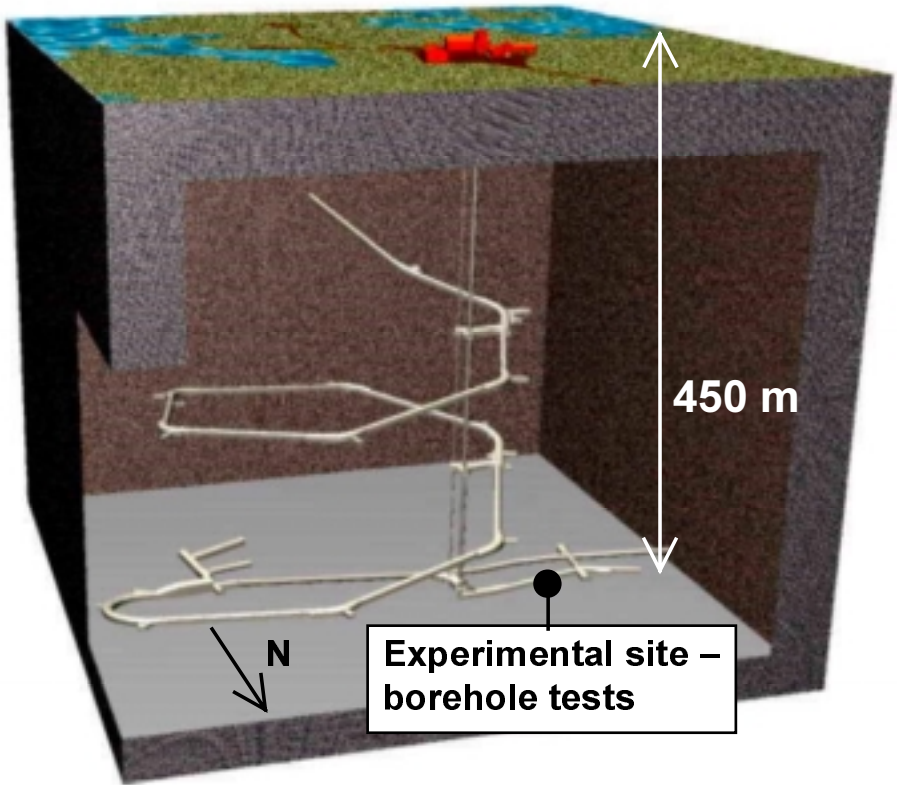

Figure 4-1. *Location of the experimental site ("pilot resin site") for the degassing borehole tests.*

Table 4-1. Degassing tests in boreholes conducted at Äspö HRL: Water saturated fracture transmissivity T_s, evolved gas content during the degassing test $\Delta\theta_g$, and observed relative transmissivity $T_{rel,obs}$, i.e., the ratio of the transmissivity before the degassing test and during/ after the degassing test.

Test hole(s) (and diameter ∅, mm)	Number of water bearing fractures	Test type[a]	T_s[b] (m^2/s)	$\Delta\theta_g$ (%vol)	$T_{rel,obs}$[d]
P2 (∅56)	2	SWT	$7 \cdot 10^{-9}$	2.4	0.89
P4 (∅56)	1	SWT	$4 \cdot 10^{-9}$	0.1	0.93
P4-P8	1	DT	$4 \cdot 10^{-9}$ [c]	13	0.53
KA2512A (∅85)	1	SWT	$8 \cdot 10^{-7}$	1	0.90

[a] SWT = single-well test; DT = dipole test.
[b] Estimated assuming radial flow conditions.
[c] Transmissivity of the fracture intersecting borehole P8.
[d] Calculated on basis of the slope of the borehole inflow – borehole drawdown relation, see Appendix B.

4.3.1 Single-well borehole tests at relatively low gas contents /Geller and Jarsjö, 1995; Jarsjö and Destouni, 1997a/

The single-well test sequence consisted of a series of constant pressure tests (CPTs) and pressure recovery tests (PRTs). During a CPT, the borehole pressure is kept approximately constant at a target pressure, using a back pressure controller, and the flowrate is monitored. During a subsequent PRT, the borehole is closed, such that the flowrate is equal to zero, and the borehole pressure is monitored as a function of time. The test sequence contained the following phases:

- Phase (1) – characterise the flow system for single-phase conditions by a series of tests at borehole pressures above the estimated bubble pressure.
- Phase (2) – allow two-phase flow conditions to develop by reducing the borehole pressure to, or below atmospheric pressure and measure the change in hydraulic conductivity.
- Phase (3) – repeat tests above the estimated bubble pressure to observe whether hysteresis effects occur in the resaturation of the system to single liquid phase conditions.

Results showed that there were no indications of significant hydraulic conductivity reductions due to degassing in the pilot hole test in borehole KA2512A /Geller and Jarsjö, 1995/. The observed flowrate – pressure drawdown relation was linear all the way down to atmospheric borehole pressure, demonstrating the lack of any influence on flowrates. As a result, the relative transmissivity (i.e., the ratio of the transmissivity before the degassing test and during/ after the degassing test) was close to unity (with a value of 0.9) as shown in Table 4-1. Besides the conclusions regarding degassing, the observed linearity thus also showed that the changes in stress conditions, due to the lowering of borehole pressures, did not influence flowrates (and hence effective conductivities) to any measurable degree. The local volumetric groundwater gas content, measured on-site during the testing, ranged between 0.5 and 1% (Table 4-1), which is relatively low.

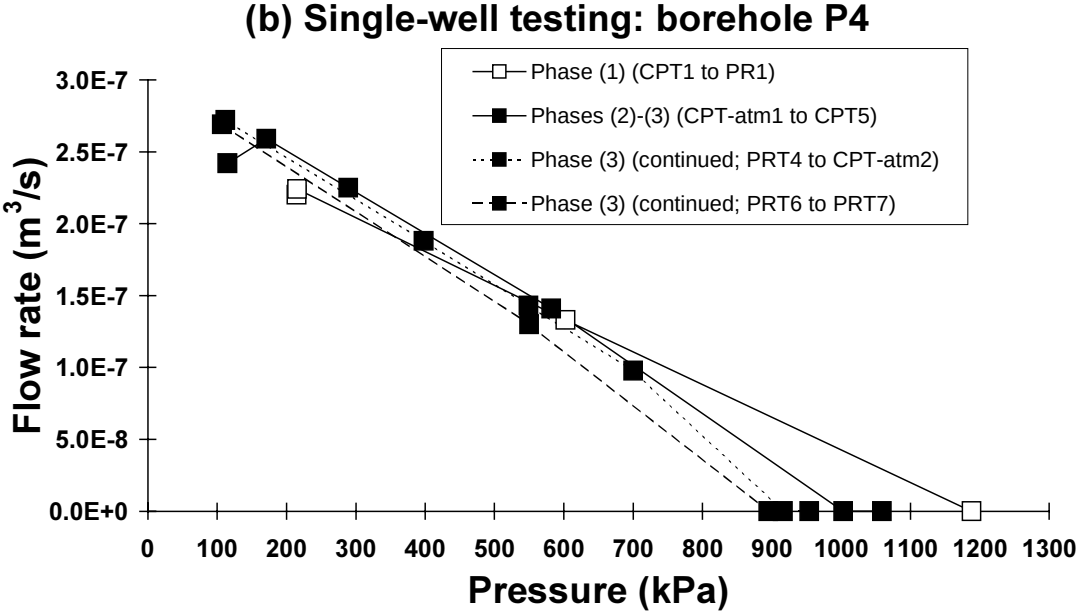

Figure 4-2. *The relation between flowrate and pressure observed during the single-well degassing test in borehole P4 /Jarsjö and Destouni, 1997a/.*

Two additional single-well tests were performed in boreholes P2 and P4 by Jarsjö and Destouni /1997a/. The gas content in the water was also during these tests relatively low, as shown in Table 4-1. In both tests, the borehole pressures exhibited a linear relation with the steady-state flowrates; Figure 4-2 shows the results obtained in borehole P4. Hence, no significant flow reduction due to degassing were observed in boreholes P2 and P4, and the relative transmissivities T_{rel} were approximately the same as during the pilot hole test in borehole KA2512A (Table 4-1). The pilot hole test and the two additional single-well tests in boreholes P2 and P4 thus indicate that, at these relatively low gas contents, degassing does not cause significant hydraulic conductivity reductions around boreholes.

4.3.2 The dipole borehole test at higher gas contents /Jarsjö and Destouni, 1997a/

The main differences between the single-well test sequences (see paragraph above) and the dipole degassing test sequence is that for the latter, the evolved gas content of the groundwater was elevated by injection of gas saturated water during the hydraulic testing. Gas saturated water was introduced to the fracture through a continuous injection in one borehole while performing hydraulic testing in a neighbouring borehole /see Jarsjö and Destouni, 1997a, and Jarsjö and Destouni, 2000, for details/. As a consequence, the gas content of the outflowing water during the entire dipole test was high (13%; Table 4-1).

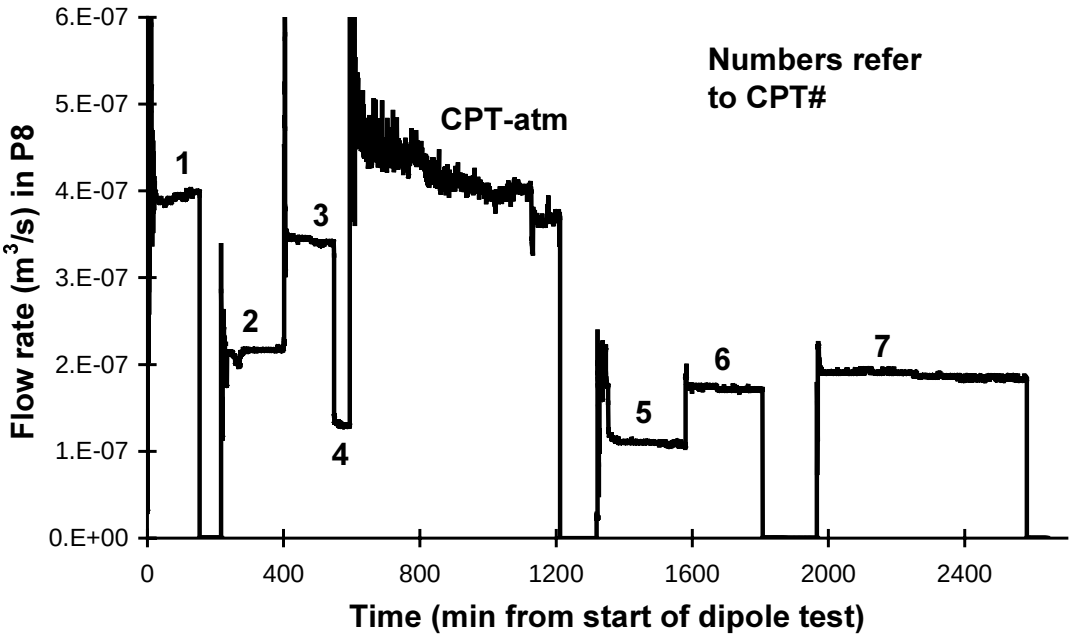

Figure 4-3. *The flowrate transients during the dipole testing in borehole P8 /data from Jarsjö and Destouni, 1997a/.*

Figure 4-3 illustrates the flowrate transients during the dipole testing in borehole P8; these flowrates are responses to the regulated borehole pressures of the (eight) CPTs. In addition, two PRTs were conducted during the dipole testing; the flowrate was then equal to zero as also seen in Figure 4-3. The figure furthermore shows that the flowrates in P8 decreased rapidly during the first minutes of the CPTs, and stabilised thereafter. The exception is the degassing test at atmospheric pressure (CPT-atm), which will be discussed in more detail below.

The relation between the steady-state flowrate and the borehole pressure in borehole P8 was approximately linear under single-phase flow conditions (phase (1), CPTs 1-4), as indicated by the white squares (numbered 1-4) in Figure 4-4. Linear regression showed that the coefficient of correlation R^2 between the single-phase CPTs and a straight line was as high as 0.99. Further, Figure 4-4 shows that the degassing test (CPT-atm; indicated by a black square) deviates from this linear relation. The inflow to the borehole was considerably lower than expected, resulting in a relative fracture transmissivity value of 0.53 (Table 4-1). Degassing is the most likely cause for this flowrate reduction. As shown in Section 6.4, there are no indications that turbulence or fracture deformation contributed to the reduction.

Figure 4-4 also shows that even though the borehole pressures were increased again during the phase (3) repeat tests (CPTs 5-7), the flowrates were still lower than during phase (1). The fact that the flow still was reduced during the last repeat CPT (CPT 7; Figure 4-3 and Figure 4-4) implies that the re-dissolution of the gas phase was slower

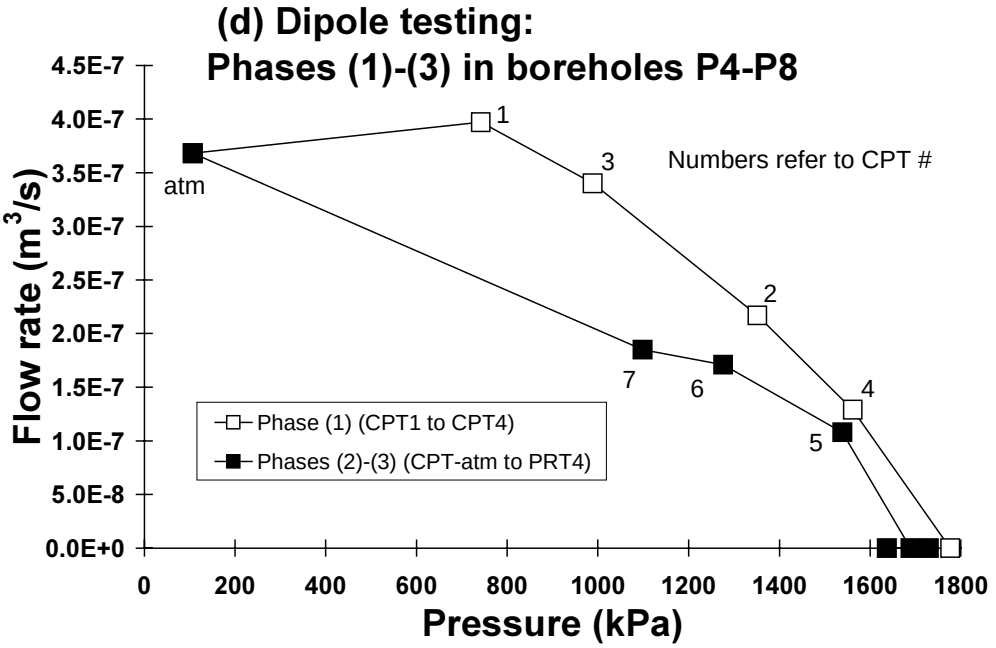

Figure 4-4. *The relation between flowrate and pressure observed during the dipole degassing test in boreholes P4 and P8 /Jarsjö and Destouni, 1997a/ at a gas content of about 13%.*

than the formation of the gas phase. As for the formation of the gas phase, the decreasing flowrates versus time for the degassing test CPT-atm in Figure 4-3 may reflect the accumulation of gas bubbles with time in the fracture, showing that the eduction in transmissivity due to degassing does not occur instantaneously as the orehole is opened.

As Figure 4-4 also suggests, the difference between the phase (3) flowrates and the phase (1) flowrates is smaller for high borehole pressures. This may be an effect of the considerable volume reduction of the gas phase, which can be expected as the water pressures increase. According to the ideal gas law, the volume of gas should be reduced to only 10% of the original volume as the borehole pressures increase from 100 kPa to 1000 kPa. The resulting degree of water saturation (volume of water per total pore volume) should then be increased correspondingly. Hence, the unsaturated hydraulic conductivity that can be evaluated for phase (2)–(3) represents an apparent conductivity value that is influenced by the variable degrees of water saturation during the different stages of phase (3).

5 Laboratory observations of degassing effects

In this chapter, we make a systematic summary of the performed laboratory degassing experiments. The data presented here are further evaluated in Chapter 6, Interpretation. In Chapter 6, references are made to the different fractures of this chapter through section number and fracture name, e.g., 5.1Äspö fracture for the Äspö fracture of Jarsjö and Geller /1996/, presented in Section 5.1, or 5.5 Äspö 1 fracture for the Äspö 1 fracture of Gale /1999/, presented in Section 5.5.

5.1 Radial flow experiments /Jarsjö and Geller, 1996/

The general objectives for these experiments were to investigate the effect of fracture geometry, boundary conditions and gas content on the flow reduction due to degassing. The specific objective was to investigate the effect of gas contents that are of similar, low range as observed in the pilot hole field test (see Section 4.3) on flow reductions due to groundwater degassing.

5.1.1 Experimental procedures

Degassing experiments in transparent epoxy replicas of actual rock fractures from the Stripa mine and the Äspö HRL were conducted in the laboratory with converging, radial flow /Jarsjö and Geller, 1996/. The aperture distribution of these variable aperture fractures was determined through light intensity measurements, using dyed water. This technique was previously used by Nicholl and Glass /1994/. The fractures were completely water saturated before gas (CO_2) saturated water was introduced into the fracture. At first, the water pressures were kept above the bubble pressure, which prevented a separate gas phase from developing. Then, the outlet pressures were lowered below the bubble pressure and gas started to develop in the fracture.

The transparent fracture replicas allowed direct observation of gas and liquid phase distributions during the experiments, a technique previously used by Nicholl et al. /1994/ and Persoff and Pruess /1995/. The steady-state gas saturation and relative transmissivity were measured for each experiment. A total of seven experiments were conducted in replicas of one Stripa fracture and one Äspö fracture /Jarsjö and Geller, 1996/. In the seventh and last experiment, the Äspö fracture replica was considerably deformed, implying that the results from this experiment are not comparable with the other Äspö fracture replica results. Therefore, this experiment is excluded from the following description. In some experiments, a separate gas phase evolved in the fracture annulus; this gas phase may have affected the overall flow reduction /see further Jarsjö and Geller, 1996/.

5.1.2 Fracture aperture distribution

For the Äspö fracture, the measured aperture distribution and the best fit of log-normal probability density functions for the fracture aperture is shown in Figure 5-1. This best match (R^2=0.96) was obtained for μ_{lna}=-2.44 (geometric mean aperture a^G=exp[μ_{lna}]= 0.087 mm) and σ_{lna} =0.88.

The match between the Stripa aperture distribution and the unimodal log-normal pdf (2-16) was poor. Therefore, we fitted a bimodal log-normal pdf which is a combination of two log-normal distributions, where distribution 1 is described by $f_{\ln}(x; \mu_{lnd1}, \sigma_{lnd1})$ and distribution 2 is described by $f_{\ln}(x; \mu_{lnd2}, \sigma_{lnd2})$ (see Appendix A). Figure 5-2 shows the best match between the experimental aperture data and the bimodal distribution. The R^2-value was 0.97, and μ_{lnd1} and σ_{lnd1} for log-normal distribution 1 were -1.85 and 0.460, respectively. For log-normal distribution 2, μ_{lnd2} and σ_{lnd2} were -1.35 and 0.195, respectively.

5.1.3 Boundary conditions, gas phase evolution and flow reduction

The experiments were performed with radial, converging, flow. The fracture diameter was 115 mm and the central outlet (or simulated borehole) was 3.2 mm in diameter. Table 5-1 summarises boundary conditions and the fracture transmissive properties for the Jarsjö and Geller /1996/ experiments.

Table 5-1. Degassing laboratory experiments conducted by Jarsjö and Geller /1996/. The outlet pressure p_{out} equalled the atmospheric pressure p_{atm}.

Experiment	$p_{in,end}$ (kPa)	p_b (kPa)	$\Delta\theta_g$ (%)	T_s (m^2/s)	T_{rel} (m^2/s)	$S_{g,end}$ (%)
Stripa-1%	0.2	1.3	1.3	$1.1\cdot10^{-6}$	1.0	2
Stripa-3%	3.6	3.8	3.5	$1.1\cdot10^{-6}$	0.07	13
Äspö-3%a	1.9	3.5	3.2	$1.4\cdot10^{-7}$	0.6*	5*
Äspö-3%b	3.0	3.8	3.5	$1.1\cdot10^{-7}$	0.4*	0*
Äspö-7%a	10	7.6	7.0	$0.93\cdot10^{-7}$	0.2	38
Äspö-15%a	4.0	16	15	$1.2\cdot10^{-7}$	0.2	38

$p_{in,end}$ = Fracture inlet pressure at the end of the experiment (in kPa above the outlet pressure $p_{out}=p_{atm}$).
p_b = Bubble pressure (in kPa above the outlet pressure $p_{out}=p_{atm}$), estimate based on the CO_2-water equilibrium pressure.
$\Delta\theta_g$ = Evolved gas content (% evolved gas from a unit volume of water), estimate based on p_b and p_{out}.
T_s = Saturated fracture transmissivity at test start (m^2/s).
T_{rel}= $T_{us}/T_{s,}$ where T_{us} is the transmissivity at unsaturated (degassing) conditions.
$S_{g,end}$ = Fracture gas saturation (volume % gas per total fracture volume) at the end of the experiment.

* Flow reduction caused by gas in the fracture annulus.

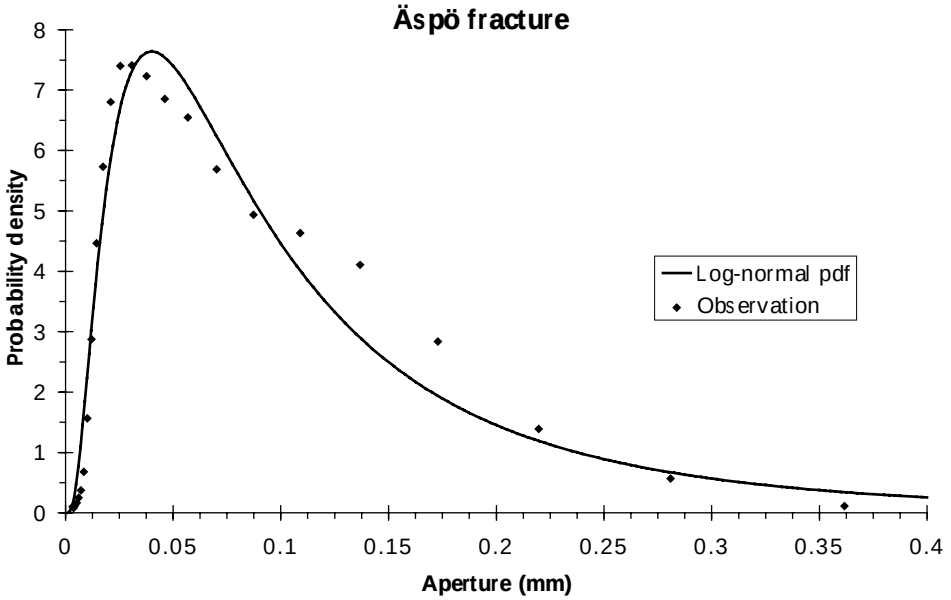

Figure 5-1. *Observed aperture distribution of the Äspö fracture compared with the best fitted log-normal pdf.*

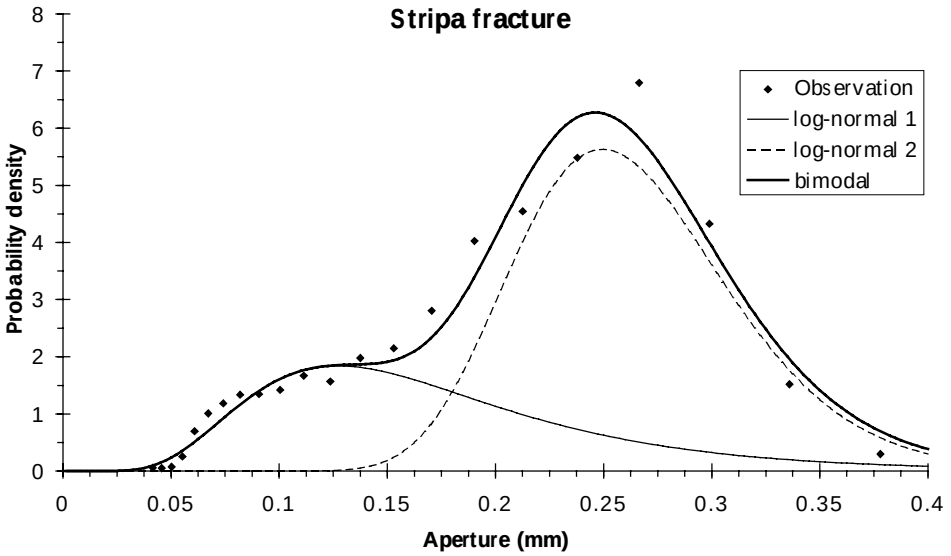

Figure 5-2. *Observed aperture distribution of the Stripa fracture compared with the best fitted bimodal pdf.*

Table 5-1 shows that between 1% and 15% gas evolved per unit volume of water in these experiments. As a consequence, fracture gas saturation degrees of up to 40% were observed. In some experiments where the fracture inlet pressure was lower than the bubble pressure, degassing and gas accumulation occurred in the fracture annulus (i.e., at the edge of the fracture). In most experiments, the transmissivity was considerably reduced, and consequently, the relative transmissivity value was lower than unity (Table 5-1).

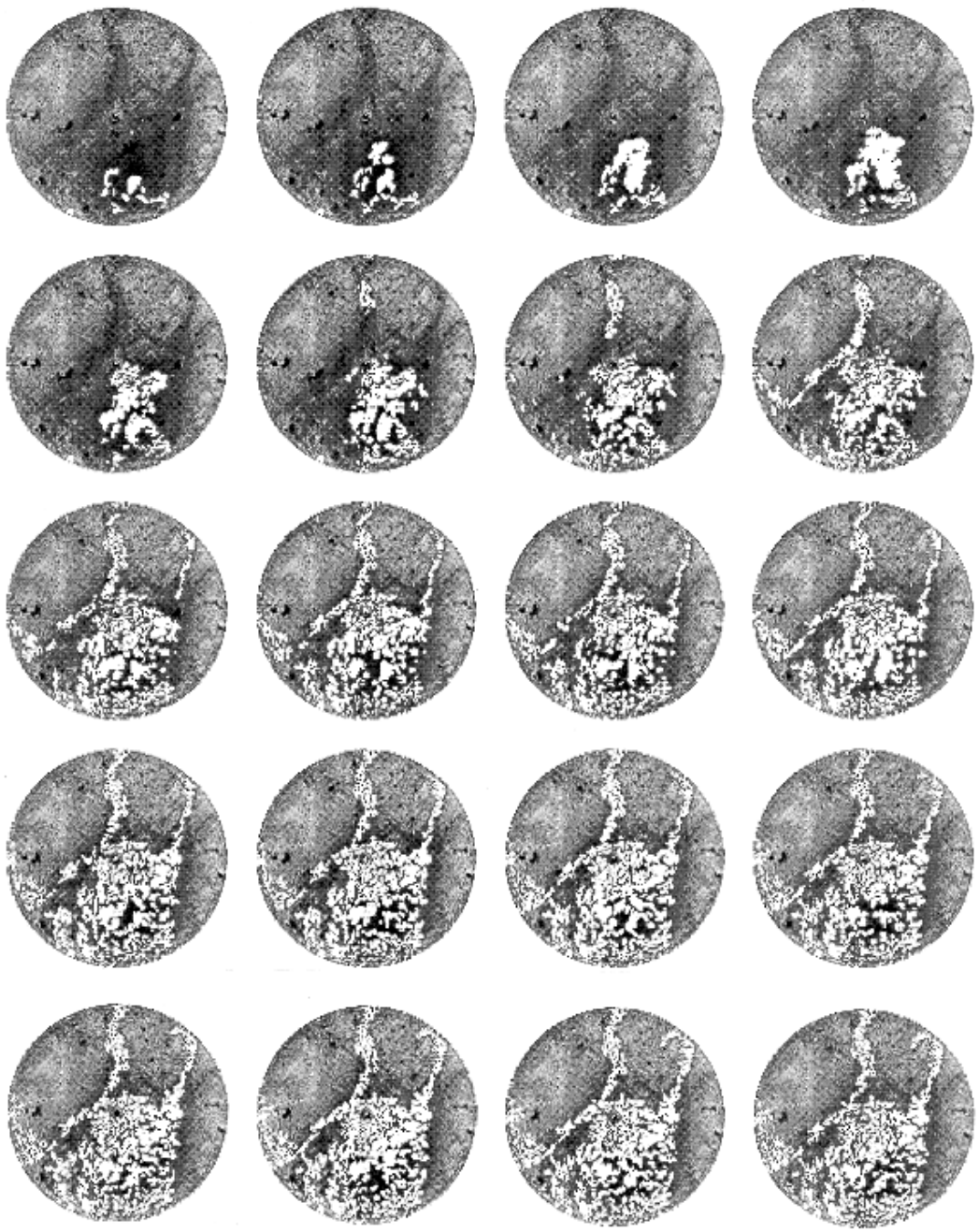

Figure 5-3. *Images of the gas phase evolution for the Äspö-7%a experiment.*

The transient gas phase evolution and accumulation processes leading to the above-mentioned approximately steady conditions are illustrated in Figure 5-3. The fracture plane is in the plane of the figure. Dark areas represent wider fracture aperture regions and lighter areas represent tighter regions. The central outlet can be seen as a dark spot in the centre of the fracture plane, and the white spots in the fracture plane correspond to gas bubbles. The time interval between each image is 1 to 2 hours. The evolution of the gas phase was similar in all experiments; Figure 5-3 shows the Äspö-7%a experiment. It can be seen that the location of the gas bubbles at steady-state (last image of Figure 5-3) agrees very well with the pattern of wider apertures (dark areas) and that no gas bubbles exist in the tightest regions. Furthermore, Figure 5-3 shows that although gas occupies only the wider apertures, it does not fully fill the wider pore space; there is also water between the gas bubbles. This condition was considered in the model development (see Figure 3-2, Section 3.1.3)

5.2 Linear flow experiments /Geller, 1998/

The linear flow experiments of Geller /1998/ were performed in the same fracture replicas as an initial set of linear experiments of Geller et al. /1995/. Two experiments were performed in a Dixie Valley fracture replica (DV97-1 and DV97-2) and one experiment was performed in a Stripa fracture replica (ST97). In the experiments of Geller et al. /1995/, degassing effects for relatively high evolved gas contents (6%–24%) were investigated, and it was shown that considerable flow reductions due to gas phase evolution occurred at these conditions. The outcome of the experiments of Geller et al. /1995/ furthermore indicated that the flow reduction was sensitive to physical characteristics of the fracture aperture.

The main objectives for the follow-up experiments /Geller, 1998/ were to:

- measure the effect of groundwater degassing on liquid flow rates for lower gas contents than the values used in Geller et al. /1995/,
- provide an extended data set for degassing models, and
- improve certainty of experimental gas contents.

5.2.1 Experimental procedures

The experimental procedures were similar to those described in Section 5.1.1. The main differences are that the endcap design was improved (see Section 5.2.3) and that the evolved gas content was measured using a gas trap. Further, the inlet pressure was kept at a constant value.

5.2.2 Fracture aperture distribution

Detailed aperture maps for the Dixie Valley and the Stripa fracture replica are shown in Geller /1998/, but the aperture distribution in terms of relative aperture frequencies is not available. The hydraulic fracture aperture (see Equation (2-7)) was 0.019 mm for DV97-1, 0.021 mm for DV97-2 and 0.016 for ST97.

5.2.3 Boundary conditions, gas phase evolution and flow reduction

The experiments were performed with linear flow across a 7.6×7.6 cm fracture plane. The inlet pressure was maintained constant throughout the experiments and was higher than the bubble pressure p_b in all experiments, in contrast to the experiments of Jarsjö and Geller /1996/ (Table 5-1). A certain amount of gas nevertheless evolved in the inlet tubing. However, the endcaps at the fracture inlet and outlet were designed to separate the gas and liquid phases, thereby eliminating the capillary barrier and ensuring that gas trapping in the inlet and outlet did not contribute to the inflow reductions. Table 5-2 shows that the relative transmissivity values were lower than unity under degassing conditions, implying that the flowrates were reduced due to groundwater degassing for all three experiments.

Table 5-2. Degassing laboratory experiments conducted by Geller /1998/.

Experiment	$p_{out,end}$ (kPa abs)	p_{in} (kPa abs)	p_b (kPa abs)	$\Delta\theta_{g,est}$ (%)	$\Delta\theta_{g,obs}$ (%)	T_s (m^2/s)	T_{rel} (m^2/s)
DV97-1	101.6	125.9	103.7	1.8	up to 3.4	$5.8 \cdot 10^{-9}$	0.73
DV97-2	103.3	126.5	106	2.5	up to 6.3	$7.9 \cdot 10^{-9}$	0.17*
ST97-1	101.6	126.8	106	4.1	6	$3.6 \cdot 10^{-9}$	0.23*

$p_{out,end}$ = Fracture outlet pressure in the end of the experiment (in kPa absolute).
p_{in} = Fracture inlet pressure (in kPa absolute).
p_b = Bubble pressure (in kPa absolute), estimate based on the CO_2-water equilibrium pressure.
$\Delta\theta_{g,est}$ = Evolved gas content (% evolved gas from a unit volume of water), estimate based on p_b and $p_{out,end}$.
$\Delta\theta_{g,obs}$ = Observed (measured) gas content. Higher than $\Delta\theta_{g,est}$ because of N_2-gas partitioning into the water at the p_{in}-equilibrium pressure value.
T_s = Saturated fracture transmissivity at test start (m^2/s).
T_{rel} = T_{us}/T_s where T_{us} is the transmissivity at unsaturated (degassing) conditions.

* Creep effects are believed to have influenced these tabulated values of T_{rel}; without these effects the values would presumably have been somewhat higher.

5.3 Large scale model experiments /Gale, 1999/

In the large scale physical model experiments of Gale /1999/, an artificial fracture surface with an area of approximately 3.5 square meters was used. The physical model was constructed from high strength concrete and the fracture plane was created by imprinting a geotextile fabric into the concrete surface between the two halves of the model. The resulting fracture plane was highly conductive and characterised by a uniform small scale roughness /Gale, 1999/ on which a large scale waviness was superimposed. A series of single phase experiments were first conducted on this fracture plane, followed by the injection of nitrogen gas at relatively high fixed flow rates (up to three times or more greater than the measured water flow rates, on a volume by volume basis), and at pressures just above the water pressure, into a selected number of manometer ports under convergent flow conditions. During these gas injection experiments, the borehole water discharge rates were reduced by as much as 80% to 90% of that measured during the single phase flow experiments when the gas was injected in all of the ports along one side of the physical model. At the higher gas flowrates, the water discharge pulsated indicating that it was being pushed by the gas as

temporary blockages were created. Adding between 3% to 5% nitrogen gas to the water injection at the model boundaries showed a marked decrease in discharge flowrates for the same applied boundary pressures. However, injection of a gas saturated water at pressures that were above the bubble pressure, followed by lowering of the fluid pressure at the discharge borehole under convergent flow conditions did not show a measurable reduction in the flowrate. This partly reflects the possibility that the bubbles were being swept out of the fracture plane before an effective blockage of the fracture pore space could be formed since gas bubbles were noted in the outlet tube. The degassing experiments on this large scale model were also constrained in the time required for the gas to evolve in the fracture plane by the high flowrates through the fracture plane and the relatively limited storage capacity (less than 400 litres) of the tanks that supplied the gas saturated water. The experiments clearly demonstrated the combined effects of changes in flow regime and two-phase flow on the observed transmissivity.

The parameter values that could be obtained from the large-scale model experiments were not compatible with the parameters needed for a more detailed interpretation using the relations of Jarsjö and Destouni /1998/. However, the same geotextile fabric that was used to create the fracture surface of the large scale model was also used to create the surface of the visualisation experiment fracture /Gale, 1999/, described below (Section 5.4). Similar gas sweeping effects were observed also in the visualisation experiments, and the experiments are further interpreted in Chapter 6 using the relations of Jarsjö and Destouni /1998/.

5.4 Visualisation experiments /Gale, 1999/

One of the main points of interest with these experiments was to confirm if the relatively uniform roughness of the fracture surface would affect the bubble trapping capacity of the fracture pore space at different hydraulic gradients as inferred for the large scale physical model experiments /Gale, 1999/.

5.4.1 Experimental procedures

The fracture surfaces were first created using a geotextile fabric to imprint the small scale roughness on the surfaces of two well mated concrete blocks by using the geotextile as a divider between two concrete pours in the same mold. After the concrete had cured, the concrete block was separated at the geotextile layer, the geotextile was removed and the blocks were fitted back together. The same geotextile fabric was also used in a similar fashion to create the surfaces on the large scale physical model experiments (see Section 5.3). Fracture replicas of these concrete surfaces were then cast at Sandia National Laboratories using transparent epoxy.

During the degassing experiments, CO_2-saturated water was introduced into the initially fully water-saturated fracture plane. The outlet valve was then opened gradually until the pressure inside the fracture was lower than the CO_2-saturation pressure. The inlet pressure was maintained above this CO_2-saturation pressure. During the experiments, pressure data from seven manometer ports in the fracture plane were recorded at five second intervals, and images were taken at one minute intervals. The aperture distribution was determined through light intensity measurements, using dyed water. This technique was previously used by Nicholl and Glass /1994/.

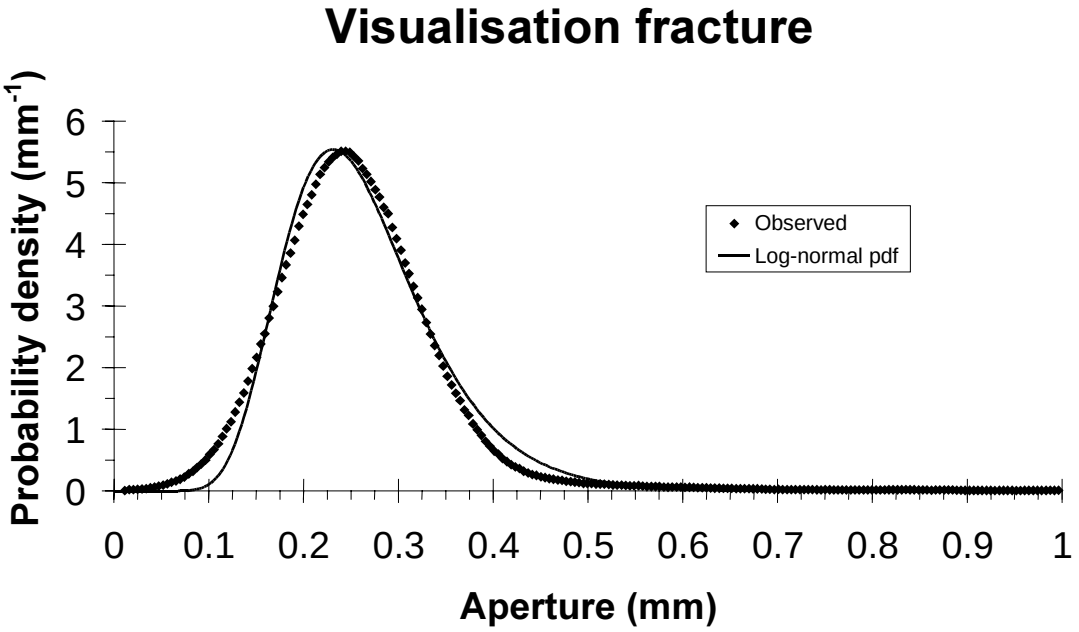

Figure 5-4. *Observed aperture distribution of the visualisation fracture compared with the best fitted log-normal pdf /Gale, 1999/.*

The high flowrate swept the water and small bubbles out of the fracture plane before the bubbles could accumulate and grow. In order to enhance the bubble nucleation, the inlet pressure was lowered by about 0.01 MPa, so that bubbles started to evolve also at the edge of the fracture.

5.4.2 Fracture aperture distribution

The measured fracture aperture distribution and the best fit of a log-normal probability density function is shown in Figure 5-4. The residual sum of squares (R^2) value was 0.99, the mean value of ln a (μ_{lna})of the fitted distribution was –1.38 (corresponding to a geometric mean aperture a^G=exp[μ_{lna}] of 0.25 mm) and the standard deviation of ln a (σ_{lna}) was 0.30.

5.4.3 Boundary conditions, gas phase evolution and flow reduction

The rectangular fracture plane measured 29.2×29.2 cm. In the linear flow experiment, the inlet and the outlet edges of the fracture plane extended throughout the full length of two opposite edges of the fracture. The other two fracture edges were sealed to provide no flow boundary conditions. During the linear flow experiment, the inlet pressure head was maintained at 2.3 meters, and the outlet pressure head was 0.2 meters in the end of the experiment. In the converging flow experiment, two inlets extended throughout the full length of two opposite edges of the fracture, whereas the outlet consisted of a central opening with radius of 2 mm. Also in this experiment, the other two fracture edges were sealed. During the radial flow experiment, the inlet pressure head was maintained at 12.3 metres, and the outlet pressure head was 0.53 metres in the end of the experiment. Further, the relative transmissivity (i.e., the ratio between the transmissivity

value at two-phase flow conditions and the one at single-phase flow conditions) was 0.78.

5.5 Linear flow experiments /Gale, 1999/

In this report, we further consider the linear flow experiments of Gale /1999/, conducted in samples of natural fractures in rock. These experiments are referred to as the small scale experiments in the report of Gale /1999/. A full suite of degassing experiments were conducted in two samples of a natural fracture, that were collected at the pilot resin site at Äspö HRL. These fractures are denoted as Äspö 1 and Äspö 2 in the following sections. A first series of experiments were conducted in the Äspö 1 fracture using carbon dioxide gas. However, steady, single-phase flow conditions did not establish initially in these experiments. Data are presented by Gale /1999/ for carbon dioxide degassing experiments at 2.0 MPa, 5.0 MPa, and 10 MPa of normal stress. These data show that the changes in fracture transmissivity, due to decreasing both the inlet and outlet pressures while maintaining the same overall hydraulic gradient, at 2.0 MPa of normal stress, were gradual. At 5.0 MPa of normal stress, the inlet and outlet pressures were increased an decreased systematically and corresponding increases and decreases in fracture transmissivity were recorded. At 10 MPa of normal stress the fracture transmissivities oscillated rapidly due to carbon dioxide degassing, over close to an order of magnitude, although the inlet pressures were maintained at or above the bubble pressure and the outlet pressure was reduced systematically. Therefore, the reduction of flowrates due to degassing and the development of two-phase flow conditions could not be determined precisely. By contrast, in a second series of experiments on the same Äspö 1 fracture plane, at 10 MPa of normal stress, using nitrogen gas saturated water, relatively stable single-phase flow conditions were successfully established initially, and clear decreases of about an half order of magnitude in the fracture transmissivity were observed as the outlet pressure decreased below the bubble pressure and nitrogen gas evolved in the fracture pore space due to degassing.

All of the experiments on the Äspö 2 sample were conducted using nitrogen gas saturated water and all of the experiments on this sample showed systematic and measurable changes in fracture transmissivity due to degassing with only minor fluctuations. In the following sections, we summarise and interpret this set of experiments that were conducted with nitrogen gas in more detail.

5.5.1 Experimental procedures

Two samples of natural fracture planes (Äspö 1 and Äspö 2) were recovered from the pilot resin site at Äspö HRL. In the laboratory, a shear-permeability apparatus /Gale et al., 1990/ was used to load the samples and simulate in-situ normal stress conditions by ensuring a fairly uniform loading over the fracture plane. The fractures were subject to confining pressures between self-weight and 10 MPa. The water was saturated with nitrogen gas at a (bubble) pressure corresponding to the water pressure at the fracture inlet. Initially, the fracture outlet pressure was kept as close as possible to the inlet pressure, in order to establish single-phase flow conditions by preventing water pressures from decreasing considerably below the gas bubble pressure. Then, the fracture outlet pressure was decreased stepwise, such that the water pressures in the fracture plane

decreased below the nitrogen bubble pressure and gas started to form in the fracture pore space. The flowrates were monitored throughout the test sequence.

After completion of the degassing experiments, resin was injected and profiles were cut both along the X and Y axes of the rectangular fracture. The profiles were viewed and photographed under a microscope. The resin thickness and fracture aperture were calculated on basis of the obtained images, see Gale /1999/ for further details.

5.5.2 Fracture aperture distribution

The measured fracture aperture distribution and the best fit of a log-normal probability density function is shown for the Äspö 1-fracture in Figure 5-5. The residual sum of squares (R^2) value was 0.98, the mean value of ln a (μ_{lna})of the fitted distribution was –1.91 (corresponding to a geometric mean aperture a^G=exp[μ_{lna}] of 0.15 mm) and the standard deviation of ln a (σ_{lna}) was 0.47.

Figure 5-6 shows the measured fracture aperture distribution and the best fit of a log-normal probability density function for the Äspö 2-fracture. The residual sum of squares (R^2) value was 0.99, the mean value of ln a (μ_{lna}) of the fitted distribution was –1.71 (corresponding to a geometric mean aperture a^G=exp[μ_{lna}] of 0.18 mm) and the standard deviation of ln a (σ_{lna}) was 0.57.

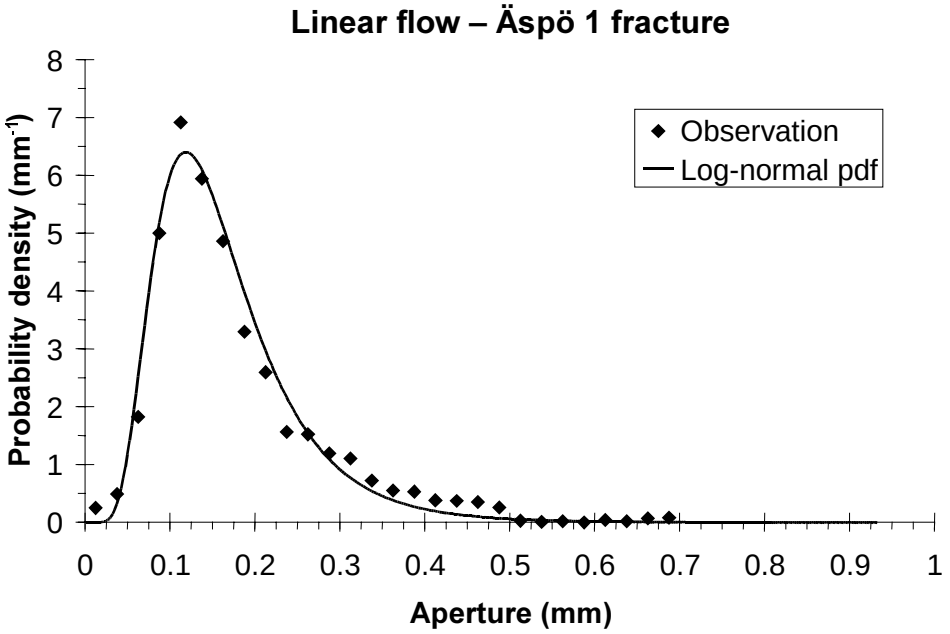

Figure 5-5. *Observed aperture distribution of the Äspö 1 fracture compared with the best fitted bimodal pdf.*

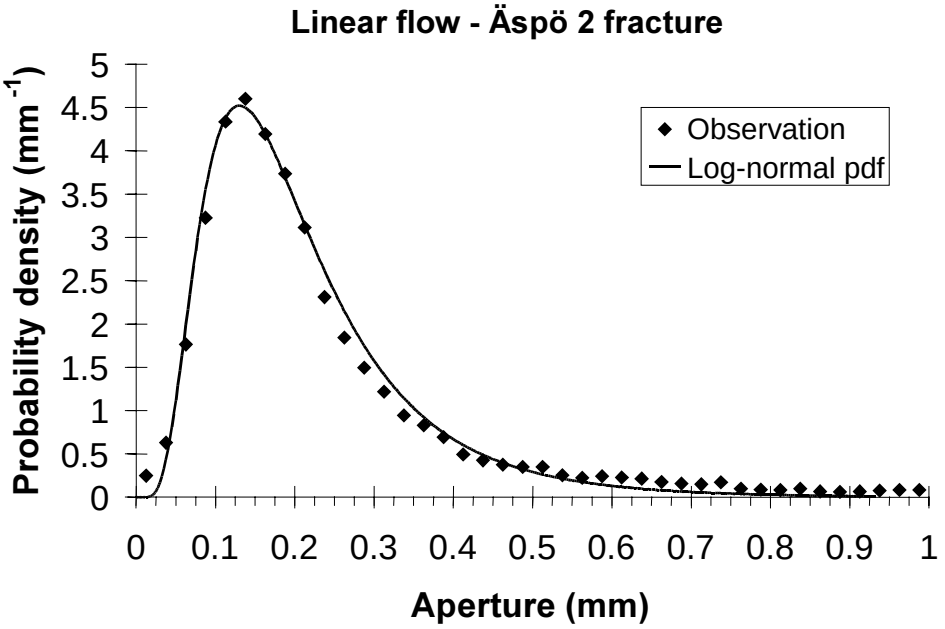

Figure 5-6. *Observed aperture distribution of the Äspö 2 fracture compared with the best fitted bimodal pdf.*

5.5.3 Boundary conditions, gas phase evolution and flow reduction

Figure 5-7 shows the boundary conditions during these linear flow degassing experiments. The length of the fracture, or distance between port 1 and 8 was 275 mm for Äspö sample 1, and 290 mm for Äspö sample 2. The width of the fracture was 185 mm for Äspö 1 and 180 mm for Äspö 2.

Table 5-3 summarises the conditions prevailing during the linear flow experiments of Gale /1999/, showing the fracture inlet pressure p_{in}, the fracture outlet pressure p_{out}, the bubble pressure p_b, the estimated evolved gas content $\Delta\theta_{g,est}$, the transmissivity T for each pressure step and the corresponding reduction relative to the initial pressure step 0, T_{step}/T_{step0}. The experiments were performed with water that was saturated with nitrogen at pressures corresponding to the tabulated bubble pressure values p_b. The fractures were subject to confining pressures between self-weight and 10 MPa, as also indicated in Table 5-3. As a result of the stepwise decrease of the outlet pressure (during steps 0 to 2 in Table 5-3), the transmissivity of the fracture decreased with time, as further illustrated in Figure 5-8.

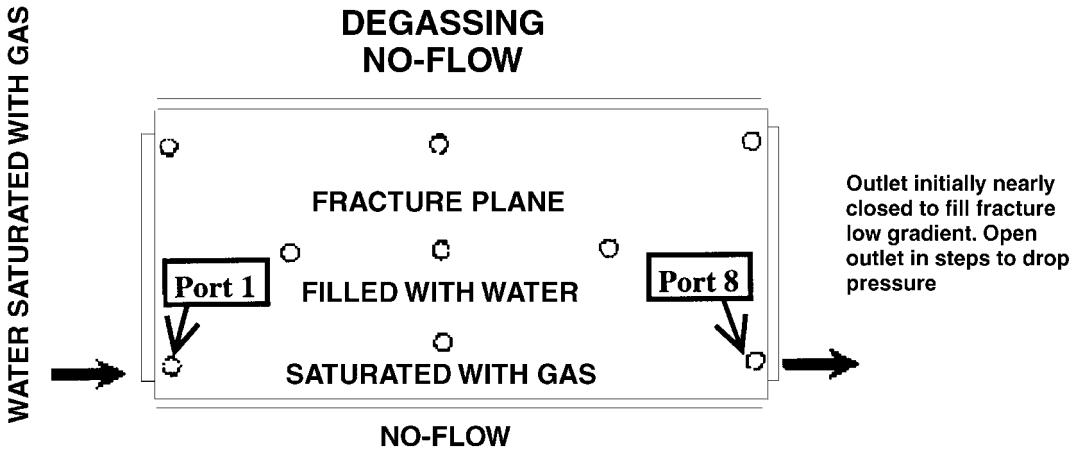

Figure 5-7. *Boundary conditions during the linear flow degassing experiments /after Gale, 1999/.*

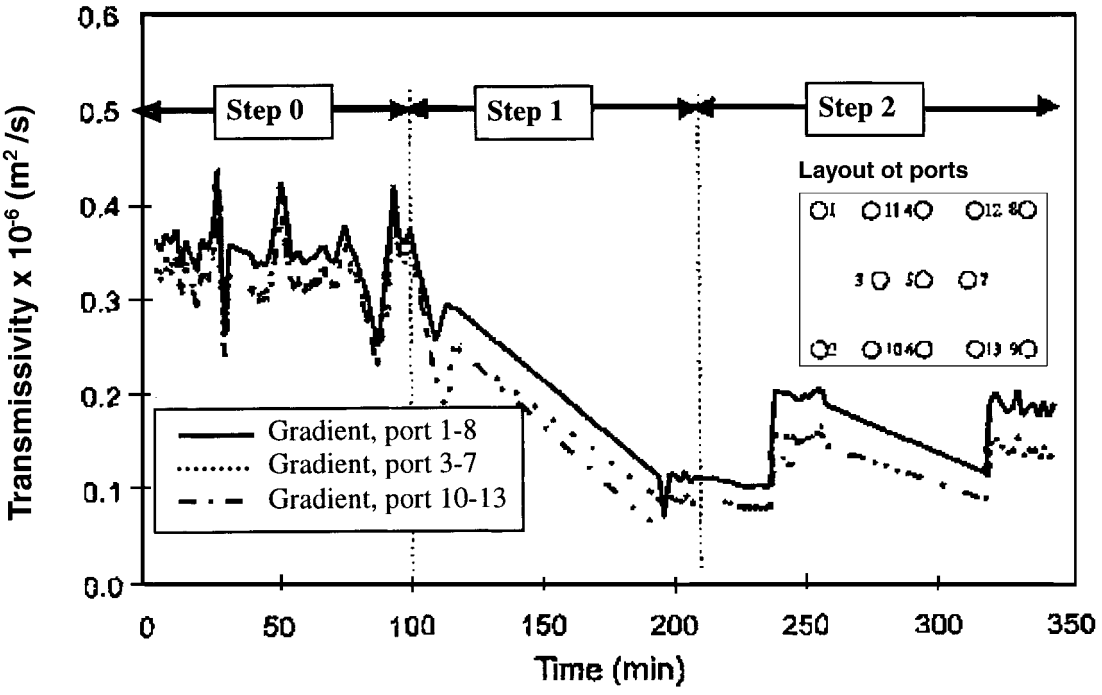

Figure 5-8. *Fracture transmissivity versus time in the Äspö 2 fracture for the experiment conducted with 10 MPa confining pressure /modified from Gale, 1999/.*

Table 5-3. Linear flow degassing experiments conducted with nitrogen gas of Gale /1999/.

Experiment fracture, confining pressure, step number)	p_{in} (kPa abs)	p_{out} (kPa abs)	p_b (kPa abs)	$\Delta\theta_{g,est}$ (%)	T_{step} (m^2/s)	T_{step}/T_{step0}
Äspö 1, 10 Mpa, step 0	420	401	420	0.09	$1.5 \cdot 10^{-7}$	1
Äspö 1, 10 Mpa, step 1	418	342	420	0.5	$1.0 \cdot 10^{-7}$	0.65
Äspö 1, 10 Mpa, step 2	399	230	420	1.6	$0.85 \cdot 10^{-7}$	0.55
Äspö 2, 1 MPa, step 0	412	410	412	0.01	$5.3 \cdot 10^{-6}$	1
Äspö 2, 1 MPa, step 1	376	367	412	0.02	$2.6 \cdot 10^{-6}$	0.49
Äspö 2, 1 MPa, step 2	322	312	412	0.06	$1.4 \cdot 10^{-6}$	0.26
Äspö 2, 5 MPa, step 0 *	400	384	373	0	$0.88 \cdot 10^{-6}$	1
Äspö 2, 5 MPa, step 1 *	392	368	373	0.03	$0.7 \cdot 10^{-6}$	0.80
Äspö 2, 5 MPa, step 2 *	388	137	373	3.4	$0.09 \cdot 10^{-6}$	0.10
Äspö 2, 10 MPa, step 0 *	419	343	353	0.06	$3.4 \cdot 10^{-7}$	1
Äspö 2, 10 MPa, step 1 *	420	252	353	0.8	$1.1 \cdot 10^{-7}$	0.30
Äspö 2, 10 MPa, step 2 *	409	145	353	2.9	$1.1 \cdot 10^{-7}$ to $2 \cdot 10^{-7}$	0.30 to 0.58

p_{in} = Fracture inlet pressure (in kPa absolute).
p_{out} = Fracture outlet pressure (in kPa absolute).
p_b = Bubble pressure (in kPa absolute), estimate based on the N_2 saturation tank pressure.
$\Delta\theta_{g,est}$ = Evolved gas content (% evolved gas from a unit volume of water), estimate based on p_b and p_{out}.
T_{step} = transmissivity value at the end of the pressure step; T_{step0} = value throughout step 0.

* in Gale /1999/ the steps 0 to 2 of these experiments are referred to as 1 to 3.

In two of the experiments (Äspö 2 at 1 MPa and 5 Mpa), both the outlet pressure p_{out} and the inlet pressure p_{in} were greater than p_b during step 0, implying that no gas should have evolved in the fracture at this initial stage. In the two other experiments, p_{out} was somewhat below p_b during stage 0, whereas p_{in} still was above or equal to p_b. Table 5-3 furthermore shows the transmissivity value for each pressure step (T_{step}) and the ratio between this transmissivity and the transmissivity during the initial pressure step 0 (T_{step}/T_{step0}). As shown in Gale /1999/ the transmissivities fluctuated somewhat within each pressure step. However, they typically exhibited a clear decreasing trend, reflecting the evolution of a gas phase in the fracture. The transmissivity values shown in Table 5-3 represent the transmissivities at the end of each pressure step. The exception is step 2 in the Äspö 2 fracture at 10 MPa, where the transmissivity fluctuated between the two tabulated values, as shown in Figure 5-8.

6 Interpretation

In this chapter, we consider the available degassing-related experimental observations and test various hypotheses underlying the developed degassing models (Chapter 3), interpreting the degassing observations made in the laboratory (Chapter 5), and in the field (Chapter 4). We furthermore use the degassing models for investigating the practical implications of degassing and two-phase flow in general for the hydraulic properties of deep bedrock.

The outline of the chapter is as follows. In Section 6.1, we first compare the values of parameters that are expected to be strongly related to the presence, or absence, of degassing effects with the actual outcome of the degassing experiments. This comparison is followed by a more detailed interpretation. The probability for bubble trapping and gas accumulation is predicted for different experiments in Section 6.2.1. Expressions for relative transmissivity and inflow reduction are compared with experimental data in Sections 6.2.2 and 6.3; these expressions are based on the underlying assumption that the bubble trapping probability is high and gas accumulates in the fracture. If these conditions are not fulfilled, the gas saturation in the fracture is expected to be low and flow reductions are expected to be small, since the formed gas bubbles would continuously be swept away by the flowing water. Section 6.3 also contains the above-mentioned investigation regarding the practical implications for the hydraulic bedrock properties.

6.1 Estimation of the relative low pressure zone extent

Flow reductions have been observed both in the field (see Chapter 4) and in laboratory tests (see Chapter 5) when the water pressure has been lowered to atmospheric pressure. There is also experimental evidence on the absence of flow reductions for corresponding water pressure lowerings. Provided that the observed behaviour can be explained by occurrence/ absence of groundwater degassing, then some degassing-related condition must have been favourable in the former experiments, and not so favourable in the latter experiments. As concluded in Section 3.1.1 on basis of the basic degassing relations (see Sections 2.1.1 and 2.1.2), the extent of the low-pressure zone, X_{low} in relation to the total fracture length L, should provide some indication on whether or not it is reasonable to expect degassing-related flow reductions. We will therefore in the following investigate whether or not there is a correlation between the relative extent of the low-pressure zone, X_{low}/L, and the actual outcome of degassing experiments and observations in the field and in the laboratory (in terms of the occurrence or absence of an observable flow reduction). More specifically, we will here consider all available experiments that were conducted either in natural rock fractures, or replicas of natural rock fractures. Experiments in artificial fractures are interpreted in Section 6.2.1.

Table 6-1 summarises the borehole pressures at no flow (p_0), the borehole pressures during the degassing tests (p_{bh}), the evolved gas contents $\Delta\theta_g$ and the bubble pressures (p_b) for the experiments and observations in the field and in the laboratory. In the field

experiments under natural conditions, where p_b can not be estimated on basis of gas saturation pressures (because they are not known), the measured $\Delta\theta_g$-values were used for estimation of p_b, through Equation (2-3).

Table 6-1. Borehole pressures at no flow (p_0), borehole pressures during the degassing test (p_{bh}), estimated, steady-state evolved gas content during the test ($\Delta\theta_g$), corresponding bubble pressures (p_b), and length of the fracture L, in addition to the estimated, steady-state relative extent of the low-pressure zone (X_{low}/L), assuming similar boundary conditions as those prevailing during the tests.

Test or observation	p_0 (kPa)	p_{bh} (kPa)	$\Delta\theta_g$ (%vol)	p_b (kPa)	L (m)	X_{low}/L	Reduced inflow?
Single-well test (SWT) in P2[a]	2000	36	2.4	160	150	$1.3\cdot10^{-4}$ [i]	no
SWT in P4[b]	1000	115	0.1	121	150	$1.3\cdot10^{-5}$ [i]	no
Dipole test (DT; P4-P8)[c]	1000	107	13	957	150	$\geq 2.6\cdot10^{-3}$ [j]	**yes**
Pilot hole test (PHT; single-well test)[d]	3000	120	1	167	150	$4.0\cdot10^{-5}$ [i]	no
Stripa Simulated drift experiment (SDE)[e]	2300	110	3	260	150	$5.3\cdot10^{-3}$	**yes**
Radial flow laboratory tests[f]	102–108	98–102	3–15	103–120	0.06	1	**yes**
Linear flow laboratory tests[g]	126–127	102–103	2–4	104–106	0.076	$8.6\cdot10^{-2}$–$1.7\cdot10^{-1}$	**yes**
Linear flow laboratory tests[h]	219–317	34–265	0.02–3	250–317	0.275& 0.290	$2.1\cdot10^{-1}$–1	**yes**

[a] This is one of the field experiments of Jarsjö and Destouni /1997a/, summarised in Section 4.3; the values regard the conditions during the degassing tests at atmospheric pressure.

[b] This is one of the field experiments of Jarsjö and Destouni /1997a/, summarised in Section 4.3; the values regard the conditions during the degassing tests below atmospheric pressure.

[c] This is one of the field experiments of Jarsjö and Destouni /1997a/, summarised in Section 4.3.

[d] This is the field experiment of Geller and Jarsjö /1995/, summarised in Section 4.3.

[e] This is the field experiment of Olsson /1992/, summarised in Section 4.2.

[f] These are the radial flow laboratory tests with CO_2-gas in replicas of natural rock fractures /Jarsjö and Geller, 1996/, summarised in Section 5.1.

[g] These are the linear flow laboratory tests with CO_2-gas in replicas of natural rock fractures /Geller, 1998/, summarised in Section 5.2.

[h] These are the linear flow laboratory tests with N_2-gas in natural rock fractures /Gale, 1999/, summarised in Section 5.4.

[i] calculated with H_0-H_w (of Equation (2-4)) equalling $(p_0-p_{bh})/(\rho g)$.

[j] calculated with a well pressure of 2600 kPa in P4 and 107 kPa in P8, and a separation distance of 1.1 m.

The estimates listed in Table 6-1 are based on simplified fracture geometry and boundary conditions, such that Equations (2-4) and (2-5) for radial flow, or corresponding equations for linear flow, are valid. For the field tests, the calculations are based on the assumption that r_0 (or L in Table 6-1) equals 150 metres in all cases. Note, however, that the conclusion we reach in the end of this section is the same assuming an r_0-value that is one order of magnitude greater, or smaller, than the presently assumed value. For the

dipole test, we used superposition to estimate the relative extent of the low-pressure zone around the withdrawal test hole in the direction of the injection hole. Since this is the direction of the highest pressure increase, the X_{low}/L-value may have been larger than that in other directions, as indicted by the "≥"-sign in Table 6-1. Specifically we estimated the hydraulic head distribution around the test (withdrawal) and injection holes, $\phi_t(r_t)$ and $\phi_i(r_i)$, respectively, by superimposing the Equation (2-4) solutions for the two boreholes over the distance of 1.1 metres (r_i-r_t=1.1) between them. By superimposing boundary conditions we arrived at the resulting hydraulic head $\phi_{TOT}(r_t)=\phi_t(r_t)+\phi_i(r_t=r_i\text{-}1.1)$ of 107 kPa at the wall of the withdrawal well ($r_t=r_w$), 2600 kPa at the injection well wall (r_t=1.5-r_w) and 1000 kPa at the outer boundary (equals the observed shut-in borehole pressure at no flow and no injection in borehole P4).

Table 6-1 shows that the relative low-pressure zone extent X_{low}/L was greater for the laboratory tests, the dipole field test and the Stripa drift observation, were flow reductions were observed, than for the three single-well tests, where no flow reductions were observed. Hence, in all experiments where degassing either did certainly cause the flow reduction (i.e., the laboratory tests), or was the most likely cause for the flow reduction (i.e., the dipole test), or was hypothesised to have caused observed inflow reductions (i.e., the Stripa observations), the value of X_{low}/L is greater than for the tests where degassing did not cause any significant inflow reductions. Considering the eight (sets of) experiments in Table 6-1, the probability for this X_{low}/L–outcome to occur randomly, i.e., to occur even if there is no correlation between observable flow reductions and the relative low-pressure zone extent X_{low}/L, is only 1.8%. We may hence conclude that such a correlation exists.

6.2 Interpretation of laboratory experiments

We use the degassing model described in Section 3 in the interpretation of the laboratory experiments. Since the model is based on a statistical description of the fracture aperture we will in the following consider those experiments where the fracture aperture distribution was measured (i.e., the 5.1 radial flow experiments, the 5.5 linear flow experiments and the 5.4 visualisation experiments), thereby considerably reducing uncertainties related to parameter estimation. This allows us to compare the model predictions and the experimental outcome, investigating various necessary assumptions regarding processes of expected importance for the understanding of degassing effects.

6.2.1 Bubble trapping probability – sweeping effects

In the following comparison we assume spatially uncorrelated fracture aperture values. We refer to Jarsjö and Destouni /1998/ for a quantitative comparison of model predictions assuming uncorrelated and correlated fracture apertures, respectively. As shown in Section 3.1.2, an estimate of the bubble trapping probability for uncorrelated fracture apertures may be obtained as the area below the pdf $f(L_b)$ between the minimum and maximum limits for physically possible bubble length (L_b)-values ($L_{b,min}$ and $L_{b,max}$). Taking the $L_{b,min}$-value as the mean aperture value ($\bar{a}$) of $1.1\cdot10^{-4}$ metres for the 5.1 Äspö fracture (indicated by the vertical line to the left of the shaded area in Figure 6-1), and the $L_{b,max}$-value as the low-pressure zone extent of 0.058 metres for the 5.1 Äspö fracture (outside the range of the graph of Figure 6-1), the bubble trapping probability for the 5.1 Äspö fracture is indicated by the shaded area of Figure 6-1.

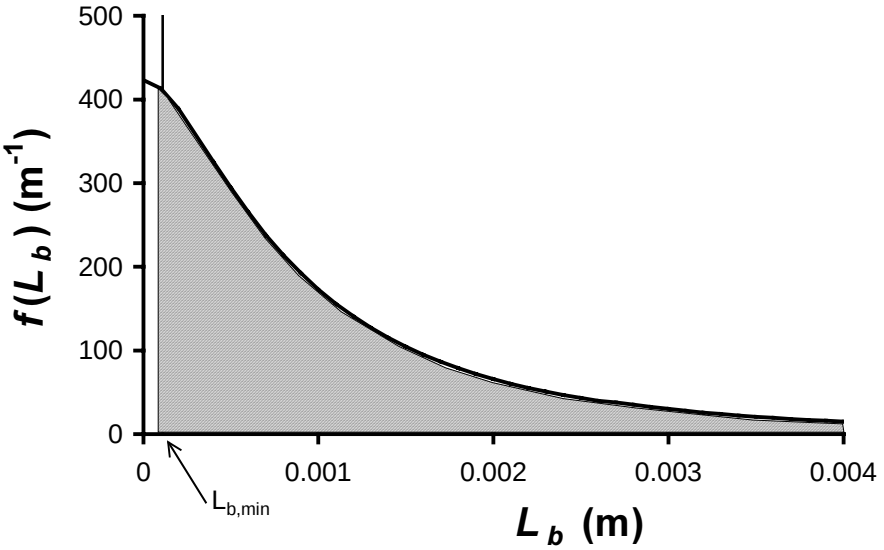

Figure 6-1. *Illustration of a relatively high bubble trapping probability (shaded area) for the 5.1 Äspö fracture. The pdf $f(L_b)$ was calculated using Equation (3-2) and the $L_{b,min}$-value (vertical line) corresponds to the measured mean aperture value of the 5.1 Äspö fracture.*

Figure 6-1 shows that the relevant area below $f(L_b)$ (i.e., the area between the physical limits) constitutes a large fraction of the total area below $f(L_b)$ for positive L_b, which implies that the bubble trapping probability should be high in this fracture. The figure illustrates the conditions in the vicinity of the fracture outlet, where the pressure gradients were high (about 180 m/m) due to the converging flow. Further away from the outlet, the pressure gradients were lower, which implies even higher bubble trapping probabilities than those illustrated in Figure 6-1. The high predicted bubble trapping probabilities are consistent with the experimental observations of an immobile gas phase development in the 5.1 Äspö fracture by Jarsjö and Geller /1996/, see Figure 5-3. Jarsjö and Destouni /1998/ considered also spatially correlated fracture apertures, and reached the same conclusion also in that case regarding bubble trapping in this 5.1 Äspö fracture.

Figure 6-2 illustrates the bubble trapping probability for the 5.1 Stripa fracture. This fracture was best described with a bimodal pdf and the corresponding pdf $f(L_b)$ in Figure 6-2 was calculated using Equation (A-2) in Appendix A. The bimodality is reflected in a slightly longer tail in the pdf for $f(L_b)$ in comparison with unimodal pdf's. Figure 6-2 shows that the trapping probability (shaded area) is lower in the 5.1 Stripa fracture than in the 5.1 Äspö fracture. However, the probability is still relatively high for the 5.1 Stripa fracture, particularly considering that Figure 6-2 (like Figure 6-1) shows the conditions in the vicinity of the fracture outlet, where bubble trapping probabilities are the lowest due to converging flow. This prediction is consistent with observations of trapped gas bubbles in the fracture during the Stripa-3% experiment (Table 5-1).

During the linear flow experiments in the 5.5 Äspö 2 fracture, considerable flow and transmissivity reductions were observed as a result of groundwater degassing. These observations are consistent with the calculated high bubble trapping probability for this experiment (Figure 6-3). The linear flow conditions imply that the pressure gradient and bubble trapping probability is approximately constant throughout the fracture. The conditions were similar in the experiments with the 5.5 Äspö 1 fracture, where transmissivity reductions due to groundwater degassing also were observed.

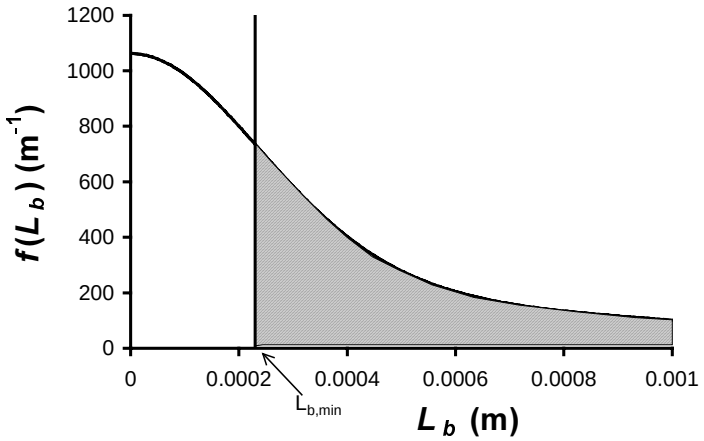

Figure 6-2. *Illustration of the bubble trapping probability (shaded area) for the 5.1 Stripa fracture. The pdf $f(L_b)$ was calculated using Equation (A-2) of Appendix A and the $L_{b,min}$-value (vertical line) corresponds to the measured mean aperture value of the 5.1 Stripa fracture.*

Whereas the 5.1 Äspö and Stripa fractures and the 5.5 Äspö 2 fracture were (replicas of) natural rock fractures, the 5.4 visualisation fracture was made artificially. In relation to the natural fractures discussed in this report, the aperture distribution was more uniform; the standard deviation (of ln*a*) was 0.3 in the 5.4 visualisation fracture, whereas it was 0.47 or higher (up to 0.88; Chapter 5) in the natural fractures. However, the value of 0.3 is realistic for natural fractures, since it is within the range of previously observed standard deviations in natural rock fractures /0.2 to 1.2; Hakami, 1995/.

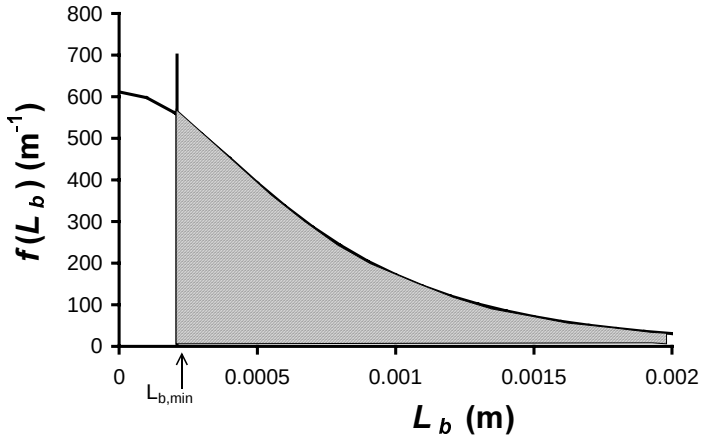

Figure 6-3. *Illustration of a relatively high bubble trapping probability (shaded area) for the 5.5 Äspö 2 fracture. The pdf $f(L_b)$ was calculated using Equation (3-2) and the $L_{b,min}$-value (vertical line) corresponds to the measured mean aperture value of the 5.5 Äspö 2 fracture. Conditions were similar also in the 5.5 Äspö 1 fracture.*

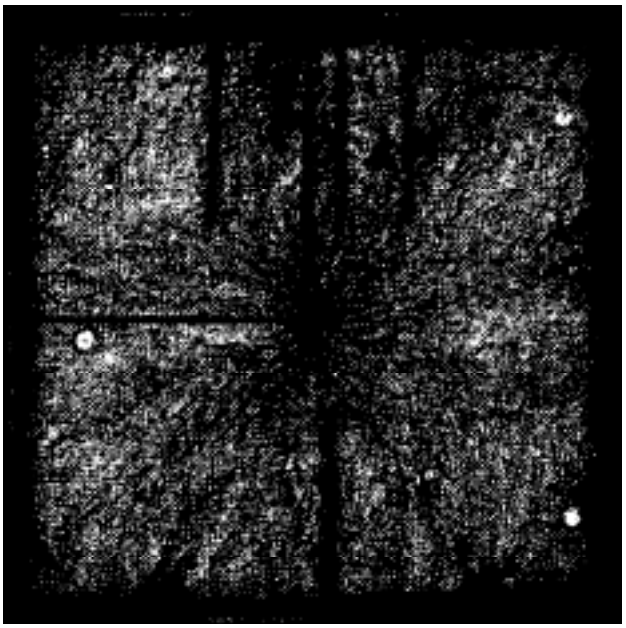

Figure 6-4. *Image illustrating the presence of trapped gas (grey regions) in the 29.2×29.2 cm fracture of the visualisation experiment. The black area in the centre of the image corresponds to the area swept clear of gas around the outlet/ central borehole.*

For the 5.4 visualisation fracture, the area around the outlet was swept clear of gas under converging flow conditions /Gale, 1999/. An image of the transparent 29.2×29.2 cm fracture during the two-phase flow experiment is shown in Figure 6-4. Areas that contain gas bubbles appear grey. The black, vertical lines are manometer ports that are visible through the transparent replica. The thinner, horizontal line to the left is the outlet tube from the central borehole. The central borehole, or outlet, is not visible, however it has the same diameter as the outlet tube. The black area in the centre of the image corresponds to the area swept clear of gas around the outlet/ central borehole. The distance between the borehole and the edge of this area is between 2 and 3 centimetres.

Figure 6-5 shows that the predicted bubble trapping probability for the 5.4 visualisation fracture is equal to zero in the vicinity of the outlet, for the measured average gradient of 810 m/m (measured between the outlet to the nearest port, 1.4 cm from the outlet). The consistency between the experimental observation of the bubble sweeping effect and the predicted low bubble trapping probability for bubbles longer than $L_{b,min}$ (Figure 6-5) clearly demonstrates the relevance of the assumption underlying the model that bubbles need to be larger than the critical length $L_{b,min}$, approximately equalling the mean aperture, in order to accumulate in the fracture.

Further away from the fracture outlet in the converging flow experiments, the gradients were considerably lower, with values equal to or less than the gradient observed in the linear flow experiments (7.9 m/m) conducted in the same fracture. For the linear experiments, the bubbles had a periodic stability, that is, they were trapped and slowly grew larger until they formed clusters and migrated rapidly in the direction of flow. As seen in Figure 6-6, the overall bubble trapping probability is high, considering bubble sizes larger than $L_{b,min}$. More specifically, the figure also shows that relatively small bubbles on the order of a millimetre have high bubble trapping probability densities, whereas the probability density is lower for longer bubbles on the order of a centimetre.

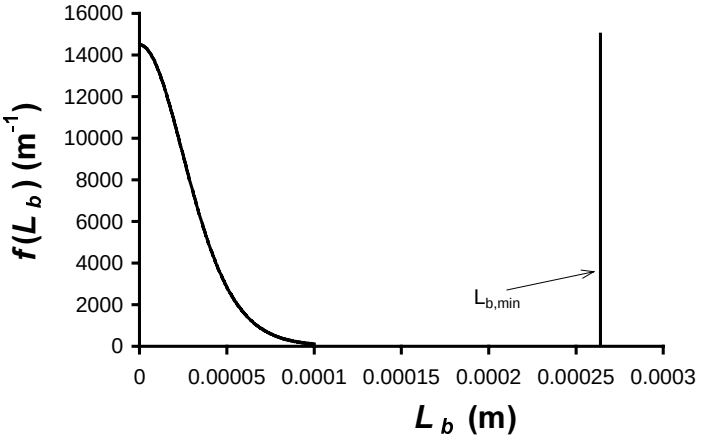

Figure 6-5. *Illustration of the low bubble trapping probability in the vicinity the fracture outlet for convergent flow in the 5.4 visualisation fracture. The pdf f(L_b) was calculated using Equation (3-2) and the $L_{b,min}$-value (vertical line) corresponds to the measured mean aperture value.*

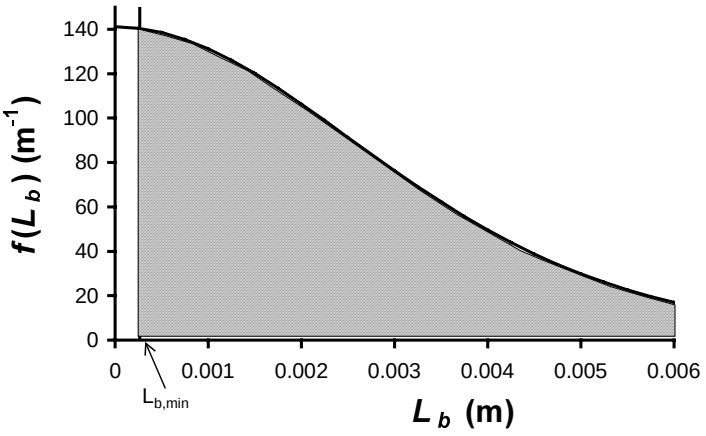

Figure 6-6. *Illustration of the high bubble trapping probability for linear flow in the 5.4 visualisation fracture. The pdf f(L_b) was calculated using Equation (3-2) and the $L_{b,min}$-value (vertical line) corresponds to the measured mean aperture value.*

6.2.2 Gas saturation and relative transmissivity

Figure 6-7 shows a comparison between observed gas saturations as a function of the bubble pressure in the laboratory experiments of Jarsjö and Geller /1996/, and modelled gas saturations, using expression (3-7) and the methodology described in more detail in Jarsjö and Destouni /1998/. As shown in Figure 6-7, the best agreement between predictions and observations was obtained assuming a water occupancy fraction α (see paragraph 3.1.3) between 0.2 and 0.4 in the wide aperture region.

Figure 6-8 shows a comparison between observed relative transmissivities as a function of the bubble pressure in the laboratory experiments of Jarsjö and Geller /1996/, and modelled relative transmissivities, using expression (3-8) and the methodology outlined in Jarsjö and Destouni /1998/. In Figure 6-8, arithmetic averaging of local transmissivity values was used to estimate an effective, relative transmissivity. For comparison, the prediction presented in Figure 6-9 was obtained using harmonic averaging. As discussed in Zimmerman and Bodvarsson /1996/, harmonic averaging of local transmissivity values yields the effective, macroscopic transmissivity only for the case where the aperture varies transverse to the flow direction, and arithmetic averaging yields the effective transmissivity only for aperture variation along the flow direction. Furthermore, harmonic averaging provides a lower bond to the actual, isotropic transmissivity, whereas arithmetic averaging provides an upper bond. In degassing problems, the separate gas phase will evolve in the vicinity of boreholes and drifts, where water pressures are low, implying that the zones of reduced transmissivity should be mainly transverse to the main flow direction. The match between experimental observations and modelled flow reduction is better in Figure 6-9 (harmonic averaging) than in Figure 6-8 (arithmetic averaging), suggesting that the effective, relative transmissivity is closer to the harmonic average of the local relative transmissivity values.

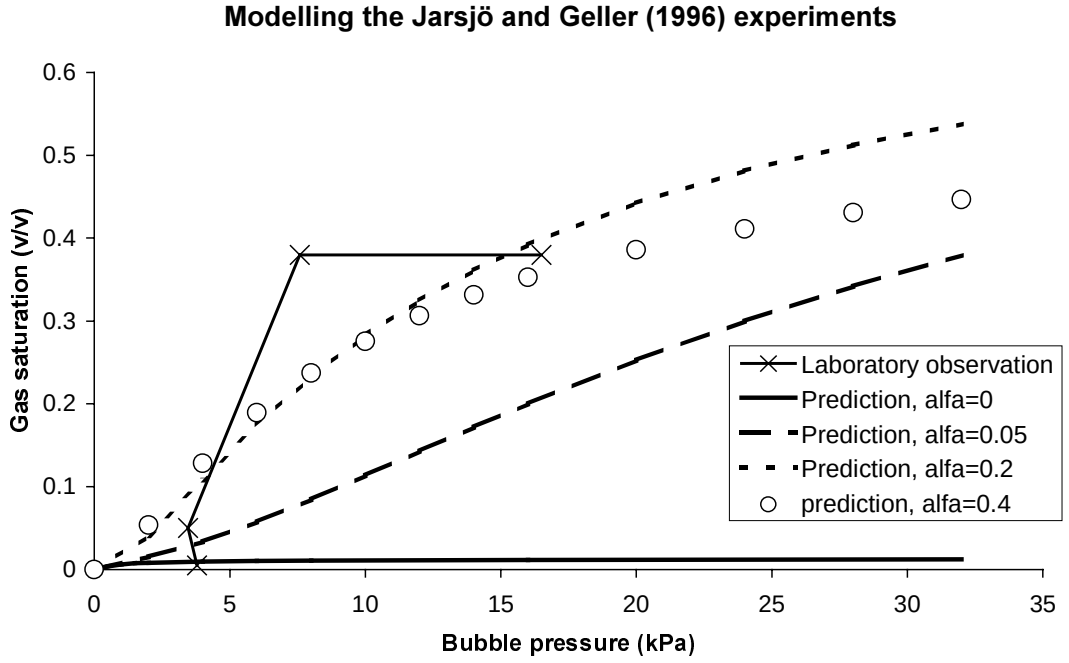

Figure 6-7. *Observed gas saturation degree in the 5.1 Äspö fracture /Jarsjö and Geller, 1996/, in comparison with predictions /from Jarsjö and Destouni, 1998/.*

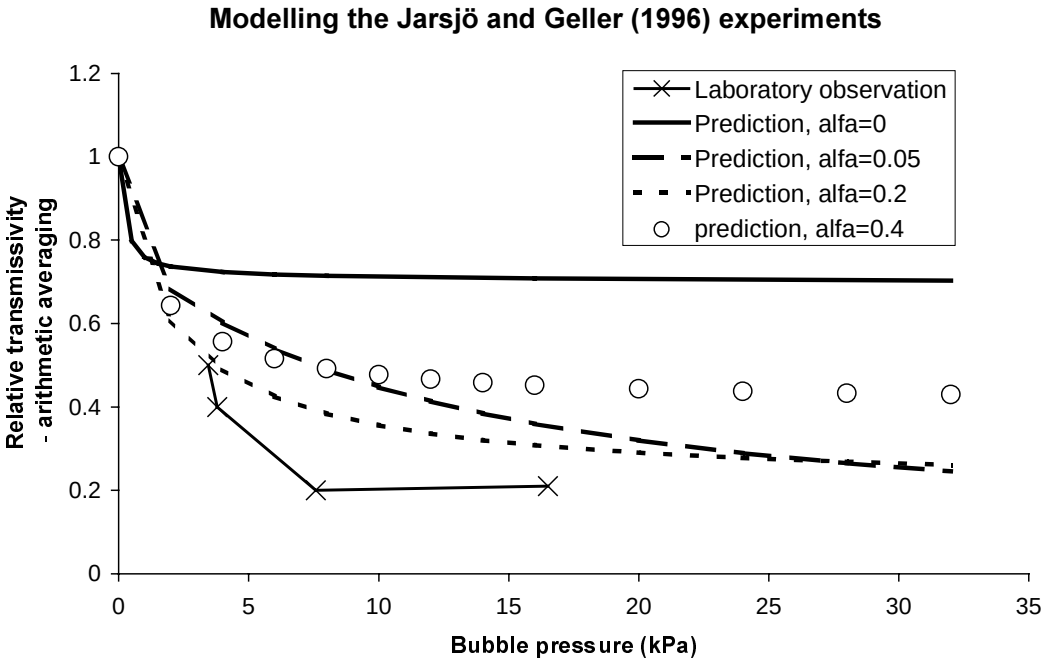

Figure 6-8. *Observed relative transmissivities in the 5.1 Äspö fracture (Jarsjö and Geller, 1996), in comparison with predictions (using arithmetic averaging of the local relative transmissivity values; from Jarsjö and Destouni, 1998).*

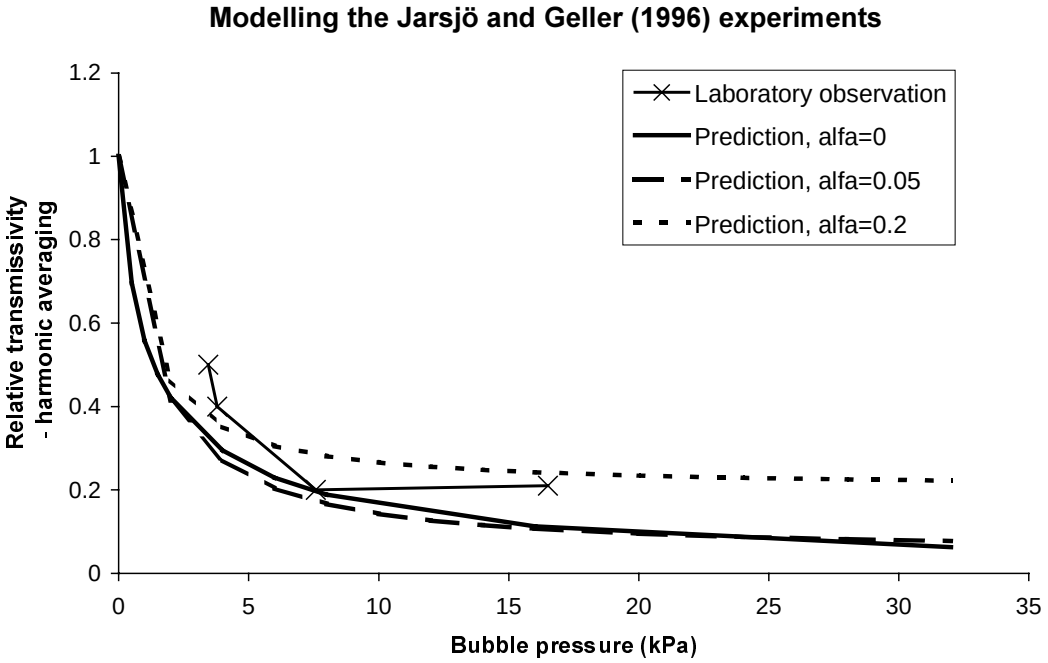

Figure 6-9. *Observed relative transmissivities in the 5.1 Äspö fracture /Jarsjö and Geller, 1996/, in comparison with predictions (using harmonic averaging of the local relative transmissivity values).*

Figure 6-9 suggests that the degassing predictions with harmonic averaging agree relatively well with experimental observations also for α=0. However, it is evident that the assumption of α=0 results in much lower predicted gas saturation degrees (Figure 6-7) than those observed. Also, α=0 results in a relatively large discrepancy between observed relative transmissivities and predictions with arithmetic averaging (Figure 6-8). The best overall agreement between observations and model predictions is obtained for α-values around 0.2 (Figure 6-7, Figure 6-8 and Figure 6-9), although the predictions are relatively insensitive to the actual value of α within the range 0.2 to 0.4.

Figure 6-10 shows a comparison between the observed and modelled (α=0.2) decrease in transmissivity for the 5.5 linear flow linear flow experiments. The y-axis shows the decrease in transmissivity between step 0 of the experiments, at relatively high water pressures, and steps 1 and 2, at which the fracture outlet pressure was lowered further to obtain more favourable conditions for degassing. The modelling was based on the fracture aperture distributions for the Äspö 1 and 2 fractures shown in Figure 5-5 and Figure 5-6, respectively, and the pressure conditions shown in Table 5-3.

In the Äspö 1–10 MPa experiment, the outlet pressure was about 20 kPa below the bubble pressure during the initial step 0 (see Table 5-3), implying that groundwater degassing may have influenced also this initial transmissivity value. Model results indicated a considerable transmissivity reduction due to groundwater degassing at this step (corresponding to a relative transmissivity value of 0.44 using harmonic averaging and 0.63 using arithmetic averaging). Since harmonic averaging already had predicted a larger reduction for step 0 than arithmetic, Figure 6-10 shows that it predicts a somewhat more modest further decrease for pressure step 1 and 2 in the Äspö 1–10 MPa experiment (grey bars) than arithmetic averaging do (white bars). This is in contrast to the other experiments shown in Figure 6-10, where the relative transmissivity during

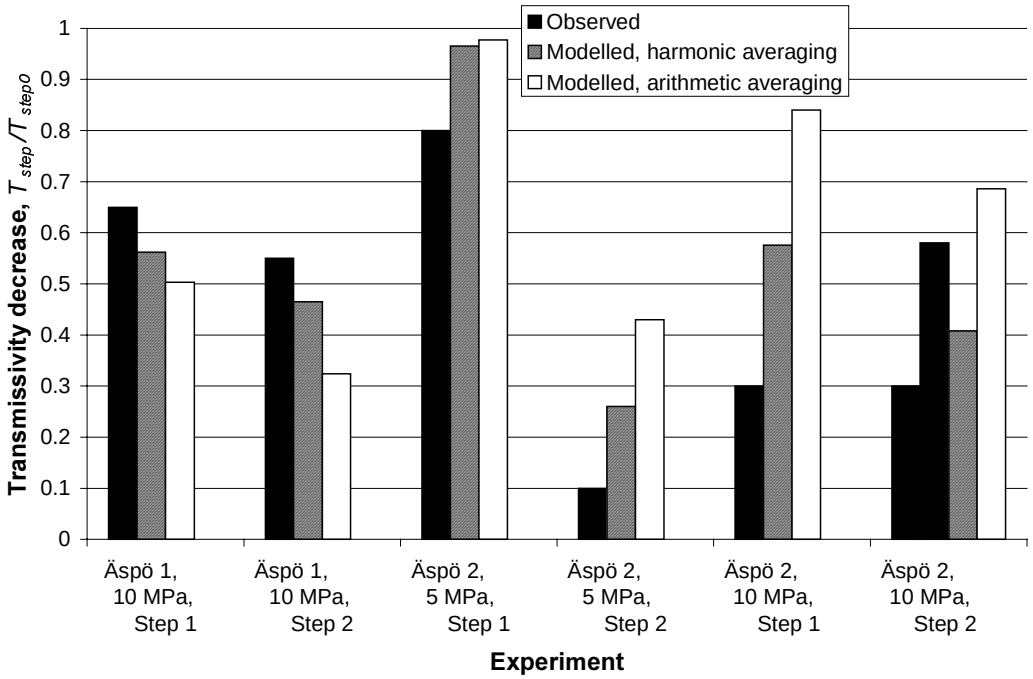

Figure 6-10. *Observed (black bars) and modelled transmissivity decrease using harmonic averaging (grey bars) and arithmetic averaging (white bars) for the 5.5 linear flow experiments of Gale /1999/.*

step 0 either was predicted to be equal to unity, or close to unity, such that harmonic averaging predicts the largest further decrease.

The model predictions of transmissivity decrease are in all cases closer to the observed decrease (black bars of Figure 6-10) using harmonic averaging (grey bars) rather than arithmetic averaging (white bars) of local relative transmissivity values. The same result was obtained for the 5.1 Äspö fracture experiments (see Figure 6-8 and Figure 6-9). Hence, the physically most relevant harmonic averaging did indeed also provide the best estimates in all cases. It was therefore used in the interpretation of the field experiments, Section 6.3.

6.3 Interpretation of field experiments

6.3.1 Inflow reduction in boreholes

Table 6-2 shows the parameter values used in the modelling of the degassing experiments in boreholes. We have assumed radial flow conditions, a radius of influence r_0 of 150 metres in all cases and fracture boundary pressures p_{bound} equalling the borehole pressures at no flow (p_0; measured in the experiment, see Table 6-1). The borehole pressures during the degassing test p_{bh} and the bubble pressures p_b of Table 6-2 equal the previously reported values for the different experiments (also summarised in Table 6-1). We assumed a standard deviation value of ln a ($\sigma_{\ln a}$, where a denotes the fracture aperture) of 0.8 in all cases. This is within the range of standard deviation values for rock fracture apertures previously reported by Hakami /1995/ – see Section 2.2. Furthermore, we estimated the mean value of ln a ($\mu_{\ln a}$) on basis of the statistical relation

$$\mu_{\ln a} = \ln \bar{a} - \sigma_{\ln a}^2/2 \qquad (6\text{-}1)$$

where the mean aperture $\bar{a}$ was assumed to equal the hydraulic aperture a_h times 1.4 (see further Section 2.2), and the hydraulic aperture a_h was obtained from the measured fracture transmissivity at water saturated conditions T, through Equation (2-8).

Table 6-2. Parameter values used in the modelling of the degassing experiments in boreholes (Figure 6-11).

Experiment	r_w (mm)	r_0 (m)	$\mu_{\ln a}$	$\sigma_{\ln a}$	p_{bound} (kPa)	p_b (kPa)	p_{bh} (kPa)
SWT/P2[a]	28	150	-3.8	0.8	2000	160	36
SWT/P4[b]	28	150	-4.0	0.8	1000	121	115
DT/P4-P8[c]	28	150	-4.0	0.8	1000	957	107
PHT[d]	42.5	150	-2.2	0.8	3000	167	120

[a] Single-well test in borehole P2 /Jarsjö and Destouni, 1997a/.
[b] Single-well test in borehole P4 /Jarsjö and Destouni, 1997a/.
[c] Dipole test – boreholes P4 and P8 /Jarsjö and Destouni, 1997a/.
[d] Pilot hole test in borehole KA2512A /Geller and Jarsjö, 1995/.

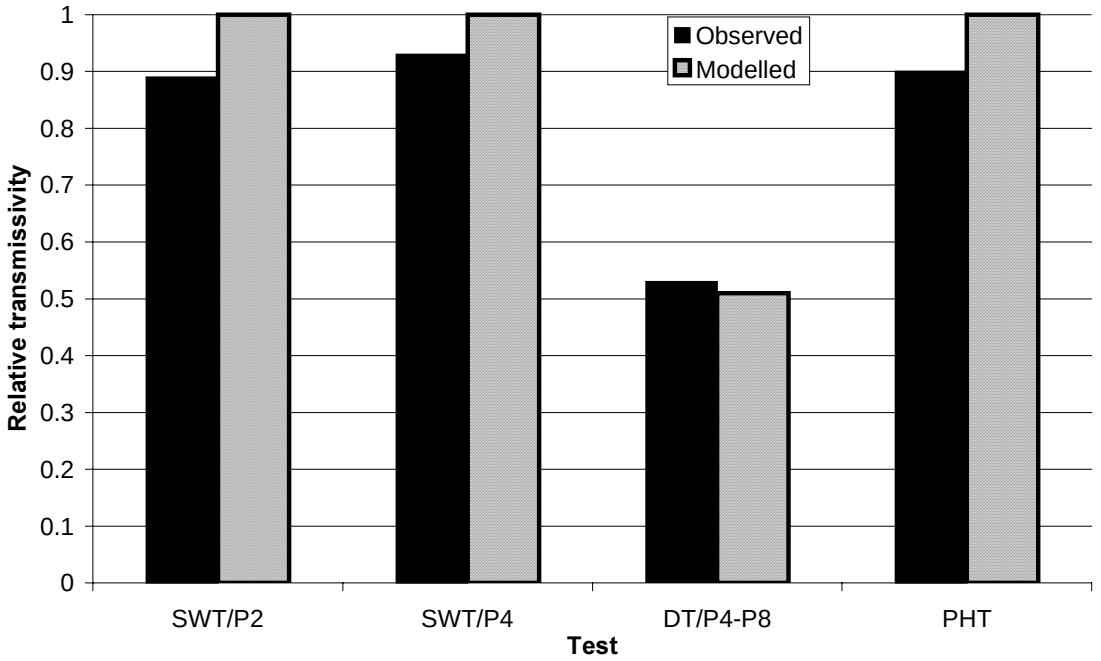

Figure 6-11. *Observed (black bars) and modelled (grey bars) relative transmissivities for the degassing experiments in boreholes.*

Figure 6-11 shows that the modelled relative transmissivity values T_{rel} (using relation (2-19) with $T_{rel}=T_w/T_s$ and the methodology described in Jarsjö and Destouni, 1998) agree well with the experimental observations in the different boreholes. In the modelling, we used harmonic averaging of the transmissivity values, which provided the best agreement between model predictions and laboratory observations (Section 6.2.2).

Some of the parameters used in the modelling of the relative transmissivity (Table 6-2) were based on rather rough and non site-specific estimates, such as the r_0-value and the $\sigma_{\ln a}$-value. With the aim to investigate whether or not the model results shown in Figure 6-11 are sensitive to the assumed values of these parameters, and whether or not more general conclusions can be drawn regarding degassing effects in the vicinity of boreholes, we will in the following show more generally how the modelled relative transmissivity is affected by different plausible parameter values (given in Table 6-3). We then consider a range of parameter values that are relevant for rock fractures intersecting boreholes at depths between 20 and 600 metres (Table 6-3). We have furthermore used the borehole pressure during the degassing test p_{bh} as a reference point at 0 kPa and, based on the findings in Section 6.2.2, assumed a value of 0.2 for the model parameter α. As previously shown in Figure 6-9, the model results are relatively insensitive to α. The results are furthermore not affected by the absolute values of the parameters r_w and r_0, but depend only on the ratio r_w/r_0.

Figure 6-12 shows the modelled relative transmissivity for the eight hypothetical cases listed in Table 6-3, as a function of the bubble pressure (normalised by the boundary pressure). The figure shows that the relative transmissivity curves are very similar for the different cases 1 to 8, which indicates that the model results are insensitive to the r_w/r_0, $\mu_{\ln a}$, $\sigma_{\ln a}$ and p_{bound} values within the considered ranges. This also implies that the model predictions of the borehole tests (Figure 6-11) are robust for these parameter ranges.

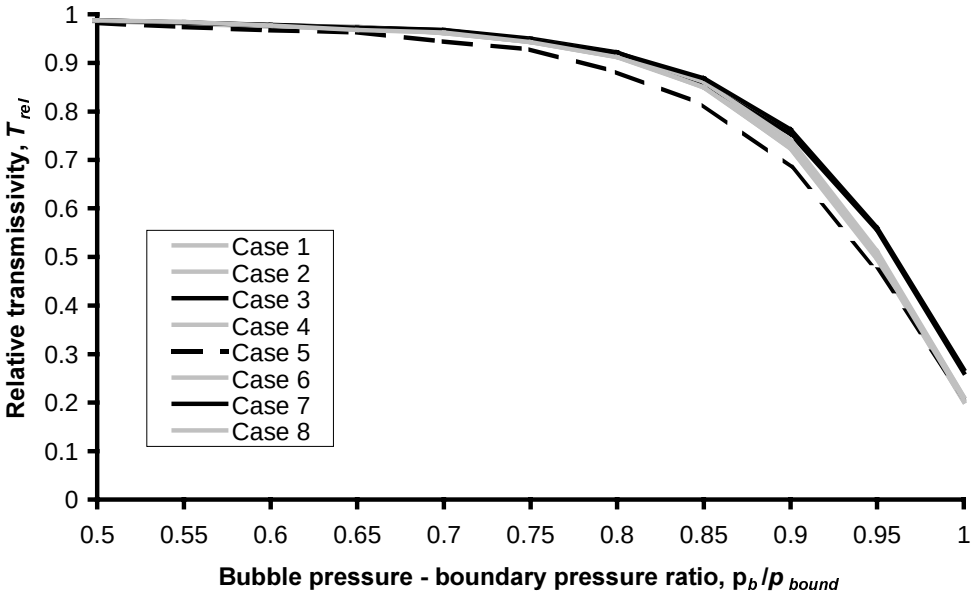

Figure 6-12. *Relative transmissivity as a function of the bubble pressure – boundary pressure ratio, for the different hypothetical fractures and boundary conditions listed in Table 6-3.*

Table 6-3. Parameters for the modelled cases in Figure 6-12. Numbers in bold indicate differences from Case 1.

Case	r_w/r_0	r_0 (m) for r_w=0.03m	μ_{lna}	σ_{lna}	p_{bound} (kPa)	p_b (kPa)
1	$2{\cdot}10^{-4}$	150	-4	0.8	2000	0 to 2000
2	$2{\cdot}10^{-4}$	150	**-1**	0.8	2000	0 to 2000
3	$2{\cdot}10^{-4}$	150	-4	**0.2**	2000	0 to 2000
4	$2{\cdot}10^{-4}$	150	**-1**	**0.2**	2000	0 to 2000
5	$\mathbf{2{\cdot}10^{-3}}$	**15**	-4	0.8	2000	0 to 2000
6	$\mathbf{2{\cdot}10^{-5}}$	**1500**	-4	0.8	2000	0 to 2000
7	$2{\cdot}10^{-4}$	150	-4	0.8	**200**	**0 to 200**
8	$2{\cdot}10^{-4}$	150	-4	0.8	**6000**	**0 to 6000**

As Figure 6-12 furthermore shows, the p_b/p_{bound} ratio (on the x-axis) considerably influences the relative transmissivity, but only if the ratio is relatively large (more than about 0.8). For values below 0.8, T_{rel} is close to unity and flow reductions due to groundwater degassing are negligible. Under natural conditions at the Äspö HRL, the gas contents at atmospheric pressure are relatively low, around 3% (sometimes even considerably lower, see Section 4.1). The gas consists mainly of nitrogen, implying bubble pressure values of about 260 kPa for a gas content of 3%. At 200 metres depth, the borehole pressure at no flow (or boundary pressure p_{bound}) is approximately equal to the hydrostatic water pressure of 2000 kPa. The above-mentioned p_b/p_{bound} ratio is hence around 0.13, which is far below the value of 0.8. Hence, based on both the borehole test observations and the consistent model predictions, we conclude more generally that groundwater degassing will not cause considerable inflow reductions in fractures intersecting open boreholes, under natural conditions.

6.3.2 Inflow reduction in drifts

The relatively large inflow reductions observed during the Stripa simulated drift experiment (SDE; see Section 4.2) were possibly a result of groundwater degassing, although there were also other possible causes for the observed flow reductions. The gas content in the water was about 3% and the hydrostatic water pressure was 2300 kPa, implying a bubble pressure p_b of 260 kPa and a relatively low p_b/p_{bound} ratio (see previous section) of 0.11. Both experimental and model results show that degassing would not cause considerable transmissivity or flow reductions around boreholes for such a low ratio. In this section, we consider the different conditions that may prevail around drifts, and model the outcome of the Stripa SDE.

Drifts and tunnels intersect more fractures per unit length than boreholes. The hydraulic conditions in the vicinity of drifts and tunnels may be quite complex, with considerable variability in the hydraulic properties. Furthermore, as shown in Figure 2-3, the water pressures around drifts are typically significantly lower than those around open boreholes at the same radial distances. This implies that for a given bubble pressure, the extent of the low-pressure zone X_{low} (where degassing can occur; defined as the zone where the water pressure is lower than the gas bubble pressure) is considerably larger around drifts than around boreholes. Table 6-1 shows that the relative low-pressure zone X_{low}/L was indeed much larger for the Stripa SDE (with a value of $5.3 \cdot 10^{-3}$) than for the three single-well (borehole) tests (SWTs) at natural gas contents (with values between $1.3 \cdot 10^{-5}$ and $1.3 \cdot 10^{-4}$ for the SWTs in P2 and P4 and the PHT). In this comparison, the length L of the fractures were assumed to be the same (150 metres) in all experiments. However, the conclusion that the X_{low}/L-value was larger around the Stripa drift than around the boreholes will remain unchanged even under the "unfavourable" assumption that L for the drift case was 1500 metres, or 10 times higher than L for the borehole cases. The fact that a developed gas-containing zone is likely to be larger around drifts than around boreholes may also affect the local conditions within that zone. For instance, a larger gas containing zone extent implies that less flowing volume of water is available per unit volume of gas, such that gas re-dissolution may take longer time as the pressures increase above the bubble pressure again.

Considering the above-mentioned differences between drifts and boreholes, we investigated

- *the effect of increased variability in the transmissive properties* (considering that the larger drift may be intersected by a larger number of hydraulically different fractures), and

- *the effect of slow gas re-dissolution* (considering that the ratio between the gas-water interfacial area and the gas volume may decrease as the scale and the total gas volume increase for drifts),

in the modelling of degassing around drifts.

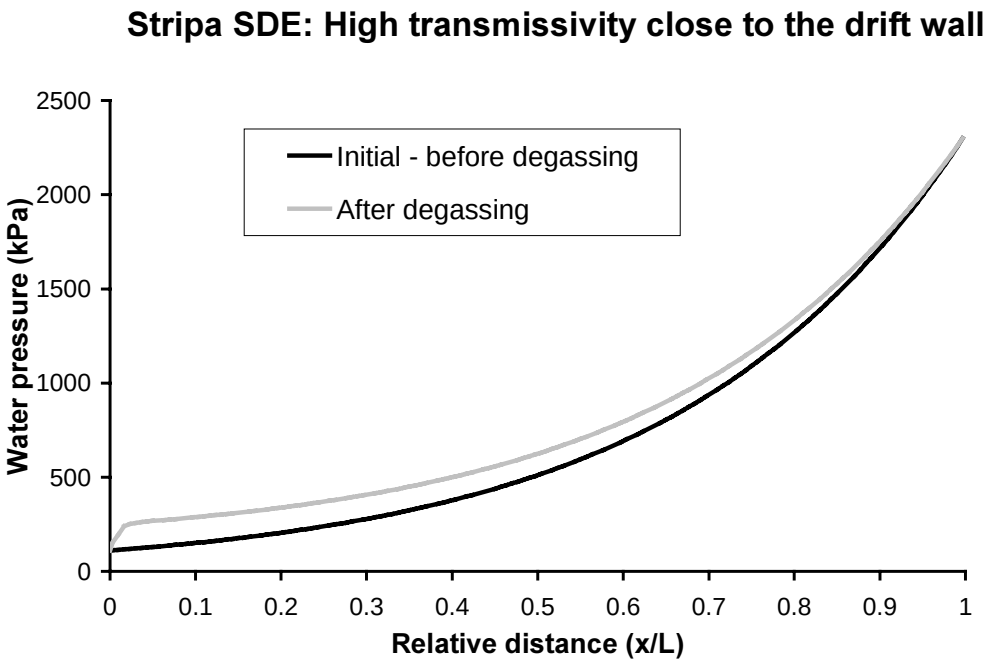

Figure 6-13. *Water pressures before groundwater degassing (black line) and after (grey line) as a function of the relative distance from the drift wall, located at x/L=0. The modelled relative transmissivity was close to unity (0.94).*

We modelled the Stripa SDE, first assuming that the spatially variable transmissivity was higher close to the drift wall than further away from the drift wall. We further assumed a fracture boundary pressure p_{bound} equalling the p_0-value of Table 6-1 (2300 kPa), a borehole pressure during the degassing test p_{bh} equalling the atmospheric pressure (110 kPa) and a bubble pressure p_b of 260 kPa (Table 6-1). For this case, Figure 6-13 shows the modelled water pressures before groundwater degassing (black line) and after (grey line). The x-axis shows the relative distance x/L from the drift wall, located at $x/L=0$; L is the distance to the outer boundary, at which water pressures no longer are influenced by the drawdown in the drift. The grey line indicates that the water pressure gradient is much steeper close to the drift wall after degassing. The reason is that the transmissivities are reduced locally close to the wall, due to the presence of a gas phase, for water pressures that are lower than the bubble pressure (of 260 kPa). Because of this steepness, the zone of reduced transmissivities is small ($x/L<0.033$; Figure 6-13) and the effective, relative transmissivity T_{rel} for the whole domain ($0<x/L<1$) is close to unity (0.94). The transmissivity reduction caused by degassing is hence negligible in this case.

Figure 6-14 shows the modelled water pressures before and after groundwater degassing considering opposite conditions than those of Figure 6-13, namely that the transmissivity is lowest closest to the drift wall. Although the water pressures as a function of x/L differ between Figure 6-14 and Figure 6-13, the results in terms of the effective, relative transmissivity T_{rel} are similar; the value of T_{rel} is 0.96 in Figure 6-14. We conclude that the predicted relative transmissivities are insensitive to variability in the fracture transmissive properties. Further, the results of small transmissivity reductions (T_{rel} values close to unity) are in contrast to the Stripa SDE observations of considerable transmissivity reductions.

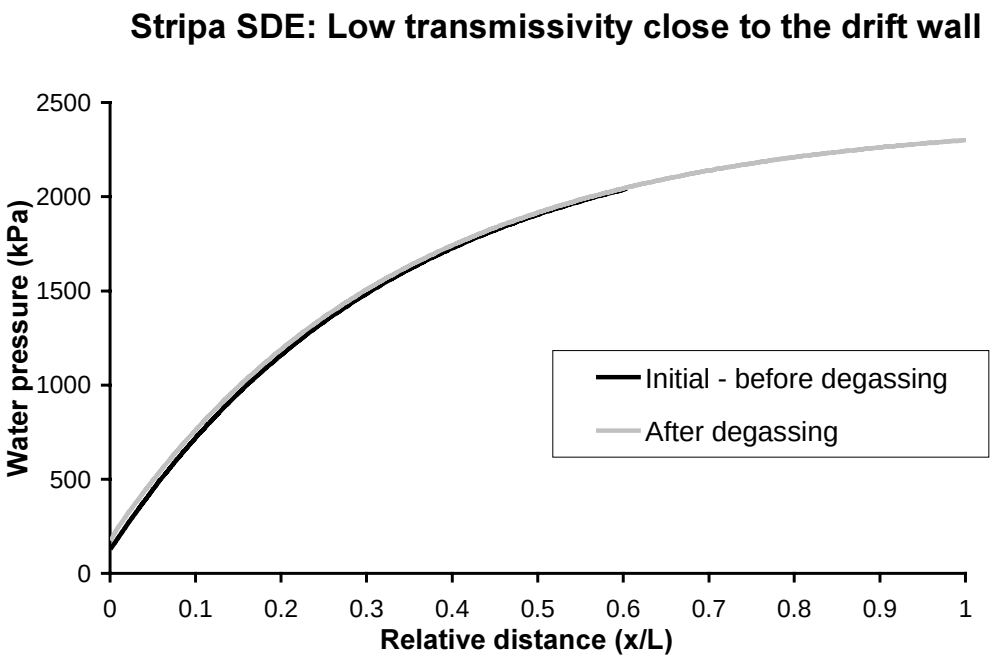

Figure 6-14. *Water pressures before groundwater degassing (black line) and after (grey line) as a function of the relative distance from the drift wall, located at x/L=0. The modelled relative transmissivity was close to unity (0.96).*

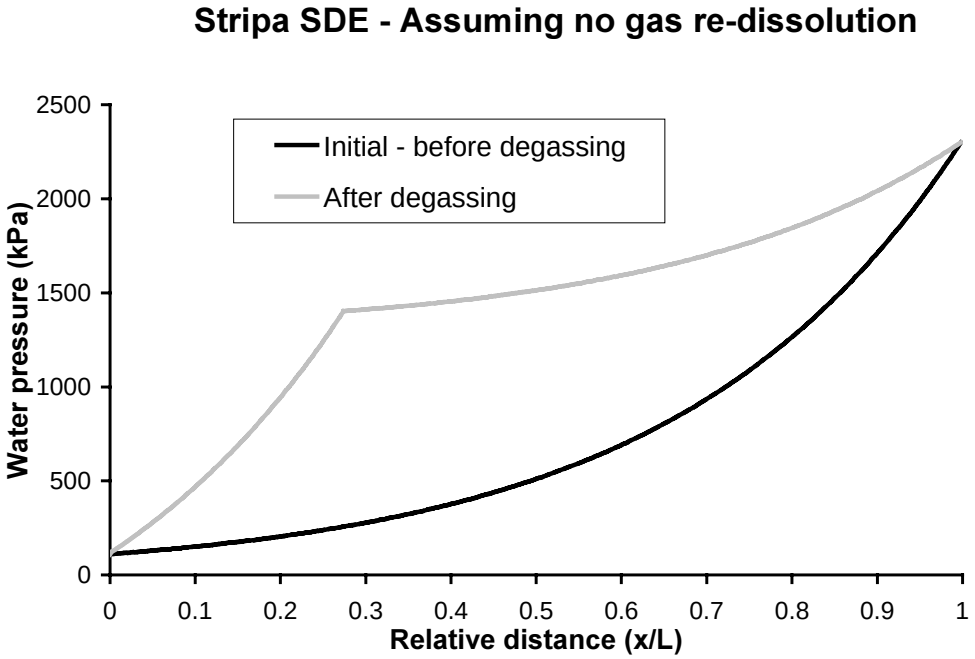

Figure 6-15. *Water pressures before groundwater degassing (black line) and after (grey line) as a function of the relative distance from the drift wall, located at x/L=0. Conditions are the same as in Figure 6-13, except for an assumption of no gas re-dissolution. The modelled relative transmissivity is in this case 0.44.*

We now modified the degassing model to account for the possible effect of a relatively slow gas re-dissolution around drifts (see discussion above). We assumed, as we also did in the previous modelling, that gas initially forms where the water pressure is lower than the bubble pressure. For the example shown in Figure 6-15, with a bubble pressure p_b of 260 kPa, gas then forms in the zone where the initial pressure (black line) is lower than $p_{b,}$ i.e., for $x/L<0.28$. As a result of this gas phase formation, the transmissivity is reduced along the distance $x/L<0.28$, resulting in increased pressure gradients. Assuming now that no gas is re-dissolved due to this local pressure increase, the pressure at degassing conditions is indicated by the grey line in Figure 6-15. The resulting relative transmissivity T_{rel} is then 0.44, indicating considerably reduced flowrates.

The modelled conditions are exactly the same in Figure 6-13 as in Figure 6-15, except that in Figure 6-13, the gas is assumed to re-dissolve as soon as the local pressure increases above the bubble pressure, resulting in a considerably smaller zone of reduced transmissivities. Whereas the model assumption used in Figure 6-13 resulted in consistent results between degassing model predictions and borehole and laboratory observations, the model does not reproduce the observations of the Stripa simulated drift experiment, unless relatively slow gas re-dissolution is assumed; Figure 6-15 shows the limiting case that the gas is not re-dissolved at all.

In summary, consistent results between laboratory observations and borehole test observations on the one hand, and model predictions on the other hand, were obtained using the model assumption that the gas re-dissolves as the water pressure increases above the bubble pressure. Based on both observations and model predictions, we conclude more generally that groundwater degassing will not cause considerable inflow reductions in fractures intersecting open boreholes, under natural conditions. The only plausible degassing-based explanation for the observed inflow reductions during the Stripa simulated drift experiment is that the gas re-dissolution was relatively slow, once the gas phase had formed.

6.4 Alternative explanations

In this section, we investigate possible alternative explanations to the inflow reductions that were observed during the dipole degassing test at Äspö HRL (see Section 4.3.2).

6.4.1 Turbulence effects

Turbulence effects may occur for higher values of Reynolds number (Re); the critical Re-value for which turbulence effects start to evolve differs from medium to medium (see Section 3.2 for details). Table 6-4 summarises the values of r_w, Q, and Re_{max} for the degassing borehole tests that have been conducted in the field. Also, single-phase flow experiments that were a part of the laboratory degassing tests in rock fracture replicas /Jarsjö and Geller, 1996/ are included in Table 6-4. The highest flowrates occurred during the pilot hole test, resulting also in the highest value of Re_{max} of 1400. However, the relation between borehole pressure and flowrate was found to be linear, indicating that turbulence effects were absent or negligible in the pilot hole test. In contrast, during the dipole test, where a non-linear pressure-flowrate relation was observed, the values of Re_{max} were only between 1.1 and 4.5, which is about the same range as for the P4 test and below the range for the P2 test; the pressure–flowrate relation was linear in both P4

and P2. Furthermore, in both the laboratory experiments of Jarsjö and Geller /1996/ and the experiments summarised by Romm /1966/, laminar flow conditions were observed for higher, or considerably higher, values of Re than those prevailing during the dipole test. Hence, the Re value evaluation yields no indications of turbulence being a factor contributing to the observed flowrate reductions during the dipole degassing test.

Table 6-4. Estimates of the maximum values of Reynolds number (Re_{max}).

Borehole test	r_w (mm)	Range of tested Q (m^3/s)	Range of Re_{max} $\left(=\frac{Q}{\pi r_w \upsilon}\right)$	Linear p-Q relation for tested Q-range?
Single-well test (SWT) in P2	28	$5.3 \cdot 10^{-7}$ – $1.3 \cdot 10^{-6}$	6.0–15	yes
SWT in P4	28	$9.8 \cdot 10^{-8}$ – $2.8 \cdot 10^{-7}$	1.1–3.1	yes
Dipole test (DT; P4-P8)	28	$1.1 \cdot 10^{-7}$ – $4.0 \cdot 10^{-7}$	1.1–4.5	**no**
Pilot hole test (PHT; single-well test)	42.5	$1.0 \cdot 10^{-4}$ – $1.9 \cdot 10^{-4}$	750–1400	yes
Laboratory tests	1.6	$8.3 \cdot 10^{-9}$ – $8.3 \cdot 10^{-8}$	1.7–17	yes

6.4.2 Fracture deformation

An alternative phenomenon that may in principle lead to measurable hydraulic conductivity reductions is stress-induced fracture deformation caused by increased effective stresses when lowering the borehole pressure to atmospheric pressure. However, such effects are not believed to have contributed to the observed flow reductions in the field (during the dipole test in borehole P8, see Section 4.3) for the following reasons:
(i) Laboratory experiments /e.g., Barton et al., 1992/ have shown that non-elastic, irreversible rock fracture deformation is much higher during the first loading-unloading cycle than during the subsequent cycles. The test hole (P8) pressure had been lowered to atmospheric pressures several times before the start of the dipole test, implying that the main part of any irreversible deformation of the fracture intersecting P8 should have occurred at these occasions and not during the degassing test. (ii) The E-modulus for the Äspö rock is sufficiently high /69±5 GPa; Xiangchun and Shaoquan, 1997/ not to cause any considerable changes in fracture aperture, given the actual water pressure change of $6 \cdot 10^{-4}$ GPa during the dipole degassing test (Figure 4-4) and assuming linear elastic behaviour of the fracture asperities. (iii) The observed linear relations between flowrate and borehole pressure measured in the fractures intersecting boreholes P2 and P4 show that the changes of the in-situ rock stresses due to a water pressure lowering down to atmospheric pressure did not at all influence the transmissivity of these neighbouring fractures at the Äspö HRL degassing test site (see Figure 4-2).

7 Summary and conclusions

In this report, the achievements within the SKB degassing and two-phase flow programme are summarised and systematically interpreted. The achievements include both original development of predictive models, as well as testing of these models and actual use of them for investigating the practical implications of degassing and two-phase flow in general for the hydraulic properties of deep bedrock. ►In the following, our main contributions in terms of novel model development are indicated with grey arrows and grey lines in the margin.◄ ►Moreover, the main conclusions related to process understanding and the use of these models for implication assessment are indicated with black arrows and black lines in the margin.◄

Groundwater degassing can under certain conditions contribute to the development of a local, unsaturated zone around boreholes and drifts in a regionally saturated rock mass. Other possible sources of two-phase flow conditions in the vicinity of a deep repository include air entry in connection with tunnel ventilation and gas generation in the repository due to corrosion or biological processes. In order to address all the above two-phase flow problems, quantitative models are needed. Generally, constitutive relations between capillary pressure, (gas/water) saturation degree and relative permeability provide an important basis in quantitative two-phase flow modelling. However, traditional constitutive relations for unsaturated flow in porous media /e.g., Brooks and Corey, 1964; and van Genuchten, 1980/ are based on parameters that can readily be estimated in soil, but are difficult or impossible to determine independently in fractured rock. Therefore, the predictive capability of such typical soil constitutive relations is limited for rock fractures under field conditions, although several studies have indicated that they can be calibrated to reproduce observed unsaturated fracture flow behaviour.

►In this report, we present an alternative, fracture aperture based, relation for two-phase flow.◄ The relation is based on properties (the mean aperture and the aperture standard deviation), for which undisturbed field estimates can be obtained through the resin injection technique. Since there are no previous comparative studies for this alternative fractured rock relation, we compared it with the widely used van Genuchten relation for unsaturated flow in porous media. The results showed that both relations yield the same kind of unsaturated flow behaviour, given a wide range of (realistic) parameter values. As discussed above, the van Genuchten relation has been proven useful for calibrated reproduction of unsaturated fracture flow. ►The consistent result of the comparison presented here implies that the novel fractured rock relation is at least equally capable of calibrated reproduction of unsaturated fracture flow as the van Genuchten relation. Moreover, due to the fact that it is based on parameters that are physically relevant and independently measurable in rock fractures, it has the potential of independent prediction capabilities, which is not the case with the porous medium relations.◄ For the special case of groundwater degassing, we therefore developed this fractured rock relation further, and directly compared the predictions of the developed relations with the actual outcome of both laboratory and field experiments.

Whereas groundwater degassing is primarily expected to occur relatively close to open boreholes and drifts, where detailed information on fracture aperture properties in principle can be obtained, other multiphase processes that can potentially affect the

performance of deep repositories may take place at much larger scales. For instance, for the scenario of gas generation in the repository and subsequent transport through the fractured rock, the relevant scale can be on the order of a kilometre. On this scale, the hydrologic conditions cannot be known in detail throughout the domain. Rather, detailed information will be available in a finite number of sampling locations. This point information then needs to be interpreted in some way that is relevant for the large-scale problem. On basis of the Leverett-scaling procedure for characteristic curves in porous media, we therefore developed a corresponding procedure for the fracture aperture based characteristic curves, and investigated the applicability of this procedure. ▶More specifically, we investigated the relevance of using a characteristic curve obtained in a subregion of the model domain (through detailed measurements), and scale this curve based on "soft" data, i.e., some information on the fracture transmissivity distribution in other subregions, in order to obtain characteristic curves for the latter subregions. The results showed that the errors associated with the proposed scaling procedure were small for fractures of different mean apertures, as long as the aperture standard deviations were similar.◀ The method was furthermore exact for fractures with different mean apertures and the same aperture standard deviation.

The main objectives for the degassing-related part of the two-phase flow project were to show if degassing of groundwater at low pressures has significant effects on measurements of hydraulic properties in boreholes and drifts, and to show under what conditions two-phase flow will occur and be significant. In this report, we considered all available laboratory and field investigations that have been conducted within the SKB degassing and two-phase flow programme. We used this data set for testing various hypotheses underlying the developed degassing models. The model results, in combination with the experimental data, are then used for addressing the above mentioned objectives of the degassing project.

There are at least two factors that may contribute to a considerable hydraulic conductivity reduction due to degassing. First, the occurrence of bubble trapping implies that gas may accumulate in the fracture, such that that the local degree of fracture gas saturation (i.e., gas volume per total fracture volume) is considerably greater than the evolving volumetric gas content $\Delta\theta_g$. Second, the non-linear relative hydraulic conductivity functions for unsaturated flow imply that hydraulic conductivity decreases considerably with increasing degree of gas saturation. However, none of these two factors can possibly contribute to hydraulic conductivity reduction unless a separate gas phase forms within the fracture pore space. Further, the size of the fracture zone where gas forms and the local hydraulic conductivity changes needs to be sufficiently large in relation to the total fracture size; otherwise, if the developed gas phase occupies only a very small part of the water-bearing fracture, the effective hydraulic conductivity of the entire fracture will remain essentially unchanged.

A general restriction for the local occurrence of groundwater degassing is that the bubble pressure of the gas dissolved in the water needs to be higher than the local water pressure; otherwise the gas will not come out of solution, which prevents the evolution of a separate gas phase within the fracture pore space. Water pressures are often decreased down to atmospheric pressure when water is withdrawn from deep boreholes and drifts in the bedrock, for example, during hydraulic and tracer testing. Field data from different sites in the deep bedrock in Sweden suggest that the bubble pressures indeed can be higher than the atmospheric pressure, since up to 5 volumetric percent gas have been observed to evolve when lowering borehole pressures from formation pressure down to atmospheric pressure. At Äspö HRL, between 0.1% and 5% gas has been

observed evolving at 350–400 metres depth. At Laxemar, the gas contents ranged between 2% and 5% and 1000 metres depth, and at the Stripa mine, the gas content ranged between 2% and 4% at 385 metres depth. At all the above-referenced sites, nitrogen is the dominating gas, occupying approximately 80% of the total gas volume. At the Wellenberg site in Switzerland, a change in gas composition and content with depth has been observed, with the more shallow groundwater being dominated by nitrogen and the deeper groundwater being dominated by methane. At 300–400 metres depth, the formation water is generally close to fully saturated with methane at formation pressure (with local existences of a free gas phase), implying even higher volumetric gas contents at atmospheric pressure conditions than for corresponding depths at the Swedish sites.

►Hence, the gas content data suggest that the natural conditions are such that degassing is plausible in Swedish bedrock.◄ Furthermore, degassing was hypothesised to have caused an observed inflow reduction during a hydraulic and tracer test series in the Stripa mine in Sweden. Then, the inflow to the drift was a factor eight smaller than the inflow measured at the same location before the drift excavation, in six boreholes forming a ring. As opposed to the drift case, water pressures around the boreholes were considerably above atmospheric pressure due to borehole pressure regulation, thus preventing degassing to occur around the boreholes. The potential occurrence and impact of degassing, relative to other phenomena that may have contributed to the observed inflow reduction in Stripa (such as changes in the rock stress conditions), could not be quantified based on available data. Without providing any conclusive answers, the Stripa observations thus raised important questions about whether or not and to what extent groundwater degassing may be expected to affect hydraulic property values that are determined from drift inflow measurements at large depths below the groundwater table, or from hydraulic tests in boreholes.

To address the potential degassing problem, the focus of an experimental field programme was directed towards borehole tests, because they are easier to control and may be conducted at much lower costs than drift experiments. The main objective was to investigate whether the lowering of pressures down to atmospheric pressures in a borehole intersecting a water bearing fracture would lead to degassing, unsaturated zone formation and, as a consequence, changes in the fracture hydraulic properties. During the pilot hole degassing test, there were no indications of considerable flow reductions due to degassing /Geller and Jarsjö, 1995/. The same result was obtained for two additional single-well tests /Jarsjö and Destouni, 1997a/. The gas contents during all these three tests were relatively low; 2.4% and less. Therefore, a dipole test was conducted /Jarsjö and Destouni, 1997a/ where the gas content in the test hole was raised to 13% through continuous injection of gas (N_2) saturated water in a nearby borehole. The results for the dipole test showed that the inflow was considerably reduced under these conditions; the flowrates at the end of the test were approximately 50% of the ones that were expected for single-phase conditions. ►The field tests hence indicate that considerable degassing effects may occur in boreholes only under certain conditions.◄

►Through a series of laboratory experiments, degassing effects were further observed under a wide range of different conditions (e.g., different fracture aperture distribution, gas content, flow geometry and boundary pressure), showing that the magnitude of flow reductions due to degassing indeed differed considerably between the considered set-ups.◄ For instance, radial and linear flow experiments in transparent epoxy replicas of natural rock fractures (sampled at the Äspö HRL and in the Stripa mine) showed that evolved gas contents between 3% and 15% can cause fracture gas saturations of up to

40 volumetric percent, and considerable reductions in flowrates as compared with corresponding single-phase conditions. For linear flow experiments /Gale, 1999/ in actual rock fractures that were re-assembled in the laboratory, considerable fracture transmissivity reductions were observed at lower evolved gas contents than for the radial flow experiments. Visualisation experiments in transparent, artificial fractures, indicated that there are instances where gas bubbles do not accumulate in the fracture (as in the above-mentioned experiments) but are swept away by the (converging) flow. As a result, the relative flowrate reductions were not so great, even though gas bubbles formed within the fracture pore space.

In order to interpret and predict the occurrence of groundwater degassing, there is a need to identify governing parameters and conditions. Provided that the different behaviours observed in the laboratory and in the field (i.e., occurrence or absence of flow reductions) can be explained by occurrence or absence of groundwater degassing, then some degassing-related condition must have been favourable in the cases where flowrate reductions were observed, and not so favourable in the other experiments. Basic degassing relations show that the extent of the low-pressure zone, X_{low}, in relation to the total fracture length dimension, L, should provide some indication on whether or not it is reasonable to expect degassing-related flow reductions. We therefore investigated whether or not there is a correlation between the relative extent of the low-pressure zone, X_{low}/L, and the actual outcome of degassing experiments and observations in the field and in the laboratory (in terms of the occurrence or absence of an observable flow reduction). More specifically, we considered all available experiments that were conducted either in natural rock fractures, or in replicas of natural rock fractures.

The results of this comparison showed that in all experiments where degassing either certainly did cause the flow reduction, or was a likely cause for the flow reduction, the value of X_{low}/L was greater than for the tests where degassing did not cause any significant inflow reductions. Considering that in total eight (sets of) experiments where accounted for in this analysis, the probability for this X_{low}/L–outcome to occur randomly, i.e., to occur even if there were no correlation between X_{low}/L and observed flow reductions, is only 1.8%. This clearly supports that the observed flow reductions are degassing-related.

►Even though the extent of the low-pressure zone is relatively large and a separate gas phase evolves in the fracture pore space, gas will not accumulate in the fracture unless the gas bubbles are trapped by the rough fracture surfaces. Because the gas contents in the field generally are 5% or less in Sweden, we do not expect high local degrees of gas saturation or measurable transmissivity reduction unless bubbles are trapped. In all laboratory observations in transparent rock fracture replicas, where direct observation of the gas phase was possible, bubbles were trapped (to different extents) in the fracture pore space.◄ In contrast, in an artificial fracture, characterised by smaller but realistic (for natural rock fractures) aperture standard deviation values, parts of the fracture were swept clear from bubbles by the converging flow /Gale, 1999/. These observations were compared with predictions of the bubble trapping probability, using the relation of Jarsjö and Destouni /1998/. This relation had previously only been compared with a very limited data set. The present, extended comparison with four different sets of experiments shows that the expression predicts trapping probability close to zero for the experiment where considerable gas sweeping effects were observed, whereas relatively high trapping probabilities were predicted for the three other experiments, where gas was observed to accumulate in the fracture. The relation is based on the mean fracture

aperture and aperture standard deviation value (and for the correlated cases, the aperture correlation length), which can be measured independently and in situ through resin injection techniques. ►This implies that the developed relation for estimation of bubble trapping probability can be applied for site specific conditions in order to investigate whether or not gas is at all likely to accumulate in the fracture and affect the water flow.◄

►Fracture aperture based degassing expressions for gas saturation degree and relative transmissivity were developed for the condition that gas will accumulate in the fracture, i.e., that the bubble trapping probabilities are high.◄ This condition can be checked using the above-mentioned expression for bubble trapping probability. Since low bubble trapping probabilities imply lower gas saturations and lower flow reductions, the developed gas saturation and relative transmissivity expressions constitute limiting cases. Note, however, that the experimental results on bubble trapping indicated high bubble trapping probabilities in natural fractures, implying that these limiting cases often apply for the observed natural conditions.

The above-mentioned fracture aperture based degassing relations were developed through combining a constraint for the existence of a free gas phase with the implications of capillary effects in the fracture pore space. More specifically, this was done by relating the gas content dissolved in the water phase (or corresponding bubble pressure) to a critical aperture, below which gas is no longer assumed to exist as a separate phase. The physical motivation for this assumption is that the phase pressure would be too high (i.e., higher than the bubble pressure) for the gas to exist under equilibrium conditions in apertures smaller than this critical aperture, due to capillary effects. The assumption that there is such a critical aperture was confirmed by experimental observations under degassing conditions in transparent epoxy replicas of rock fractures, where water was observed to fully occupy the tighter aperture regions. The same experiments furthermore showed that water and gas co-existed in the wider aperture regions (with apertures greater than the critical aperture). This condition was considered in the model relations, through the parameter α, which quantifies the fraction of water in the wide aperture region; hence $(1-\alpha)$ quantifies the fraction filled with gas in this region. A comparison between model predictions and experimental observations for both gas saturation degree and transmissivity reduction showed that a value of α of 0.2 yielded the best predictions. This value was therefore used in the modelling of the field results. However, for α-values between 0.2 and 0.4 the model results were relatively insensitive to the actual value of this parameter, indicating that the exact α-value is not a critical parameter within this range.

We furthermore addressed the question whether arithmetic or harmonic averaging of local transmissivity values will generally yield the best estimate for degassing based relative transmissivities in heterogeneous fractures. As discussed in Zimmerman and Bodvarsson /1996/, harmonic averaging of local transmissivity values yields the effective, macroscopic transmissivity only for the case where the aperture varies transverse to the flow direction, and arithmetic averaging yields the effective transmissivity only for aperture variation along the flow direction. Furthermore, harmonic averaging provides a lower bond to the actual, isotropic transmissivity, whereas arithmetic averaging provides an upper bond. In degassing problems, the separate gas phase will evolve in the vicinity of boreholes and drifts, where water pressures are low, implying that the zones of reduced transmissivity should be mainly transverse to the main flow direction. Hence, the harmonic averaging of local transmissivities should be

the most physically relevant procedure for degassing problems. ►In this report, we compared model predictions using both harmonic and arithmetic averaging with the actual outcome of ten laboratory experiments at various gas contents in natural rock fractures, and replicas of natural rock fractures. The results showed that the physically most relevant harmonic averaging did indeed also provide the best estimates in all cases. It was therefore used in the interpretation of the field experiments.◄

►We used the derived expression for relative transmissivity to predict the outcome of the conducted field borehole tests. In three of these borehole tests (the single-well tests), the transmissivity reduction was negligible, whereas a considerable, 50% reduction was observed in the dipole test. This experimental result was reproduced using the developed degassing-based expression for relative transmissivity.◄ However, some of the parameters used in this expression were based on more general, non site-specific estimates, such as the radius of influence (R)-value and the aperture standard deviation (σ_{lna})-value. With the aim to investigate whether or not the previously discussed model results were sensitive to the assumed values of these parameters, and whether or not more general conclusions can be drawn regarding degassing effects in the vicinity of boreholes, we investigated how the modelled relative transmissivity is affected by different plausible parameter values.

In this investigation, we considered a range of parameter values that are relevant for rock fractures intersecting boreholes at depths between 20 and 600 metres. ►The investigation showed that the model results were robust, i.e., insensitive to the ratio between well radius and radius of influence (r_w/R), the mean aperture μ_{lna}, the aperture standard deviation σ_{lna} and the boundary pressure p_{bound} values within the considered ranges. This robustness further implies that the model predictions of field borehole tests are also robust for these realistic parameter ranges.◄

►We furthermore identified a single, dominant parameter for degassing effects in boreholes, namely the ratio between the bubble pressure and the boundary pressure (p_b/p_{bound}). Considering radial borehole inflow, we showed that this parameter considerably influences the modelled relative transmissivity, particularly for relatively large ratios (more than about 0.8).◄ For values below 0.8, the modelled relative transmissivity T_{rel} was close to unity, implying that flow reductions due to groundwater degassing are negligible. Under natural conditions at the Äspö HRL, the gas (mainly nitrogen) contents at atmospheric pressure are relatively low, around 3% (sometimes even considerably lower). This corresponds to a nitrogen bubble pressure of about 260 kPa. At 200 metres depth, the borehole pressure at no flow (or boundary pressure p_{bound}) is approximately equal to the hydrostatic water pressure of 2000 kPa. The above-mentioned p_b/p_{bound} ratio is thus around 0.13, which is far below the value of 0.8. ►Hence, based on both the borehole test observations and the consistent model predictions, we conclude more generally that groundwater degassing will not cause considerable inflow reductions in fractures intersecting open boreholes under conditions normal for Swedish granitic bedrock.◄

The relatively large inflow reductions observed during the Stripa simulated drift experiment (SDE) were possibly a result of groundwater degassing, although there were also other possible causes for the observed flow reductions. The hydrostatic water pressure was 2300 kPa and the gas content in the water was about 3%, implying a bubble pressure p_b of 260 kPa and a relatively low p_b/p_{bound} ratio of 0.11. Both experimental and model results show that degassing would not cause considerable transmissivity or flow reductions around boreholes for such a low ratio. Considering the

difference in size between a borehole and a drift, we investigated the possible influence of scale effects for ambient conditions relevant in the SDE. The considered effects included spatial variability in the fracture aperture statistics (i.e., considering that the larger drift may be intersected by a larger number of hydraulically different fractures), and slow gas re-dissolution (i.e., considering that the ratio between the gas-water interfacial area and the gas volume may decrease as the scale and the total gas volume increase). The predicted relative transmissivities were found to be relatively insensitive to spatial variability in the fracture aperture statistics. In contrast, the relative transmissivity predictions were considerably different under the assumption that the gas will not re-dissolve once it has formed in the fracture pore space (even though local pressures increase above the gas bubble pressure as a consequence of the local transmissivity reduction due to the gas formation). Under this assumption, a considerable transmissivity reduction was predicted for the SDE, which is consistent with the experimental observations.

We conclude that the Stripa SDE cannot be reproduced by the degassing model unless relatively slow gas re-dissolution is assumed; we considered the limiting case that the gas could not re-dissolve at all once it had formed. This implies non-equilibrium conditions between the separate, evolved, gas phase and the gas dissolved in the water phase. The modelling of numerous laboratory experiments and boreholes tests, however, clearly showed that at these experimental scales, it is appropriate to assume that equilibrium conditions will be reached after some time. ▶Whereas slow gas re-dissolution provides the only possible degassing-based explanation for the reduced inflows observed during the Stripa SDE, there are also alternative explanations for these reductions, such as stress-induced fracture deformation. With regard to the observed inflow reduction in the dipole degassing (borehole) test, however, neither fracture deformation nor turbulence constitute likely explanations for the observations. Further, the large number of experimental observations of groundwater degassing at the laboratory scale and the boreholes field scale, in conjunction with consistent model predictions, imply that the degassing processes at these relatively small experimental scales are well understood and that the corresponding conclusions are empirically well founded.◀

8 List of symbols

a	Fracture aperture
$\bar{a}$	Arithmetic mean aperture value
a_1	Fracture aperture at location $l=l_1$ (upstream end of the considered bubble; Figure 3-1)
a_2	Fracture aperture at location $l=l_2$ (downstream end of the considered bubble; Figure 3-1)
a_c	Cut-off fracture aperture, above which gas may exist under equilibrium conditions
a_{Fi} $(i=1\text{-}4)$	Aperture of hypothetical fracture F*i*, characterised by the probability density function $f_{\ln}(a_{Fi};\ \mu_{\ln aFi},\sigma_{\ln aFi})$
a^G	Geometric mean of fracture aperture (=exp[$\mu_{\ln a}$])
a_h	Hydraulic fracture aperture, defined through equation (2-8)
A_{low}	Area of the low pressure zone, i.e., the area of the zone where $p_w<p_b$ under water saturated conditions. Measure of the size of the region where degassing can possibly occur
C	An assumed exponential and isotropic auto-correlation function, equal to $\sigma_{lnx}^2 \cdot \exp(-\lambda/h)$, where $h=l_2-l_1$
C_g	Molar concentration of gas dissolved in the liquid
D	Hydraulic diameter
f	Probability density function (pdf)
$f_{bi,\ln}$	One-variable, bimodal, log-normal probability density function
f_j	Joint two-variable, unimodal, log-normal probability density function
$f_{\ln}$	One-variable, unimodal, log-normal probability density function
g	Gravitational constant
h	Pressure head, equal to $-p_c/\rho g$; Separation distance along the mean flow direction, equal to l_2-l_1
H	Henry's constant in $kPa \cdot m^3 \cdot mol^{-1}$
H_0	Hydraulic head at $r=r_0$
h_b	Bubble pressure head, or air entry pressure head, in the Brooks-Corey model
H_w	Hydraulic head at $r=r_w$
k	Permeability
K	Hydraulic conductivity
K_{rel}	Relative conductivity, defined as the ratio between a phase conductivity $K(h=-p_c/\rho g)$ in a two-phase system (e.g. water and gas) and the phase conductivity under single-phase conditions, K_s.
K_s	Saturated (single-phase) hydraulic conductivity
l	Spatial coordinate along the mean flow direction
L	"Full" fracture extent, i.e., extent influenced by considered pressure head changes (For radial flow, this extent corresponds to the radius of influence, r_0)
l_1	Coordinate for the upstream end of the considered bubble (Figure 3-1)
l_2	Coordinate for the downstream end of the considered bubble (Figure 3-1)

L_b	Length (along the mean flow direction) of a trapped bubble (Figure 3-1)
$L_{b,max}$	Maximum length of a trapped bubble (physical constraint)
$L_{b,min}$	Minimum length of a trapped bubble (physical constraint)
m	Fitting parameter of the van Genuchten model
M	Slope of the steady borehole inflow – borehole drawdown relation ($m^3/(Pa \cdot s)$)
n	Soil parameter related to the width of the pore size distribution of the van Genuchten model
N	Flow geometry; N=1 implies linear flow, N=2 radial flow and N=3 spherical flow
n_m	Porosity of the medium
p	Pressure
p_0	Borehole pressure at no flow
p_b	Bubble pressure, equal to HC_g under equilibrium conditions
p_{bh}	Borehole pressure
p_{bound}	Pressure at the outer boundary of the fracture
p_c	Capillary pressure, equal to p_g-p_w
p_g	Non-wetting (gas phase) pressure
p_{in}	Fracture inlet pressure (laboratory experiments)
p_{out}	Fracture outlet pressure (laboratory experiments)
p_w	Wetting (water phase) pressure
Q	Flowrate
r	Radial distance from the well centre ($r_w \leq r \leq r_0$); Radius of a cylindrical pore
R	The gas constant
R^2	Coefficient of correlation
r_0	Radius of influence
Re	Reynolds number
r_w	Well radius
S	Liquid saturation degree, i.e., the fracture (pore) volume filled with the liquid divided by the total fracture (pore) volume
S_e	Effective wetting phase (here water) saturation, defined through equation (2-12)
S_g	Gas saturation degree
S_w	Water saturation degree
$S_{w,r}$	Residual, or irreducable, water saturation degree
T	Transmissivity ($=K \cdot a$)
T_{abs}	Absolute temperature (K)
T_{rel}	Relative transmissivity, defined as the ratio between a phase conductivity $T(p_c)$ in a two-phase system (e.g. water and gas) and the phase conductivity under single-phase conditions, T_s.
$T_{rel,obs}$	Experimentally observed T_{rel}
T_s	Saturated (single-phase) transmissivity
T_w	Transmissivity with respect to water
v	Pore water velocity

V_w	Total volume of water; Total volume of water in a fracture
V_{total}	Total fracture volume
w	Fracture width, measured perpendicular to the (mean) flow direction
X_{low}	Low pressure zone extent, i.e., the extent of the zone where $p_w<p_b$ under water saturated conditions. Measure of the size of the region where degassing can possibly occur
X_{gc}	Extent of the developed gas-containing zone. Is less than or equal to X_{low}, see Figure 2-4
α	Assumed water occupancy fraction in fracture regions where $a>a_c$; corresponding gas occupancy is (1-α)
δ	Soil parameter inversely related to the air entry pressure head value of the van Genuchten model
$\Delta\theta_g$	Evolved, volumetric gas content
ΔV_g	Total volume of evolved gas
ϕ	Hydraulic head
λ	Soil pore size distribution related parameter in the Brooks-Corey model; Aperture correlation length
$\mu_{\ln a}$	Mean value of ln a
μ	Fluid viscosity, dynamic
ν	Fluid viscosity, kinematic; Weight factor in the bimodal log-normal pdf (Appendix A)
Θ	Angle between horizontal plane and fracture plane (Figure 2-1)
θ	Contact angle between fluid interface and pore wall
ρ	Fluid density
σ	Interfacial tension between fluids
$\sigma_{\ln a}$	Standard deviation of ln a
σ_w	Surface tension of water (=the interfacial tension between water and air)
ξ	Integration variable

9 References

Bandurraga T M, Bodvarsson G S, 1999. Calibrating hydrogeologic parameters for the 3-D site-scale unsaturated zone model of Yucca Mountain, Nevada. J. Contam. Hydrol., 38, 25–46.

Banwart S, Wikberg P, Olsson O, 1997. A testbed for underground nuclear repository design. Environmental Science and Technology, 31, 510A–514A.

Barton N, Makurat A, Monsen K, Vik G, Tunbridge L, 1992. Rock mechanics characterization and modelling of the disturbed zone phenomena at Stripa. SKB TR 92-12, Stripa Project, Swedish Nuclear Fuel and Waste Management Co.

Bear J, 1972. Dynamics of Fluids in Porous Media. Dover Publications Inc., New York.

Bear J, 1979. Hydraulics of Groundwater. McGraw-Hill International Book Company, 567 pp.

Billsten M, Svensson U, 2000. Air bubbles – a potential explanation of the unusual pressure behaviour of the core at WAC Bennett Dam. In: Proceedings of the 20ième Congres des Grands Barrages, Commission Internationale des Grands Barrages, Beijing, 2000.

Birgersson L, Moreno L, Neretnieks I, Widén H, Ågren T, 1993. A Tracer experiment in a small fracture zone in granite. Water Resour. Res., 29, 3867–3878.

Birkholzer J, Tsang C-F, 1997. Flow channeling in unsaturated heterogeneous soil. Water Resour. Res., 33, 2221–2238.

Birkholzer J, Li G, Tsang C-F, Tsang Y, 1999. Modeling studies and analysis of seepage into drifts at Yucca mountain. J. Contam. Hydrol., 38, 349–384.

Brooks R H, Corey A T, 1964. Hydraulic properties of porous media. Hydrol. Pap. 3, Colorado State University, Fort Collins.

Demond A H, Roberts P V, 1993. Estimation of two-phase relative permeability relationships for organic liquid contaminants. Water Resour. Res. 29, 1081–1090.

Durner W, 1994. Hydraulic conductivity estimation for soils with heterogeneous pore structure. Water Resour. Res. 30, 211–223.

Emsley S, Olsson O, Stenberg L, Alheid H-J, Falls S, 1997. ZEDEX – A study of damage and disturbance from tunnel excavation by blasting and tunnel boring, SKB TR 97-30, Swedish Nuclear Fuel and Waste Management Co.

Finsterle S, Pruess K, 1995. Solving the estimation-identification problem in two-phase flow modeling. Water Resour. Res., 31, 913–924.

Fischer U, Kulli B, Flühler H, 1998. Constitutive relationships and pore structure of undisturbed fracture zone samples with cohesionless fault gouge layers. Water Resour. Res., 34, 1695–1701.

Fourar M, Bories S, Lenormand R, Persoff P, 1993. Two-phase flow in smooth and rough fractures: Measurement and correlation by porous-medium and pipe flow models. Water Resour. Res., 29, 3699–3708.

Gale J, 1999. Impact of flow geometry, flow regime, two-phase flow and degassing on the transmissivity of rough fractures. SKB PR IPR-99-08, Swedish Nuclear Fuel and Waste Management Co.

Gale J, MacLeod R, LeMessurier P, 1990. Site characterization and validation – Measurement of flowrate, solute velocities and aperture variation in natural fractures as a function of normal and shear stress, Stage 3. SKB Stripa project TR 90-11, Swedish Nuclear Fuel and Waste Management Company.

Gardescu I I, 1956. Behaviour of gas bubbles in capillary spaces. Trans. Am. Inst. Min. and Met. Eng., 86, 351–370.

Geller J T, 1998. Laboratory studies of groundwater degassing in replicas of natural fractured rock for linear flow geometry. SKB PR HRL-98-18, Swedish Nuclear Fuel and Waste Management Co.

Geller J T, Jarsjö J, 1995. Groundwater degassing and two-phase flow: Pilot hole test report. SKB ICR 95-03, Swedish Nuclear Fuel and Waste Management Co.

Geller J T, Doughty C, Long J C S, Glass R J, 1995. Disturbed zone effects: two phase flow in regionally water-saturated fractured rock, FY94 annual report, Rep. LBL-36848, Lawrence Berkeley Laboratory, Berkeley, California.

Gentier S, 1990. Morphological analysis of a natural fracture. International association of hydrogeologists, vol. 1, 315–326.

Hakami E, 1988. Water flow in single rock joints. Licentiatie thesis, Luleå University of Technology, Luleå.

Hakami E, 1995. Aperture distribution of rock fractures. Ph. D. thesis, Royal Institute of Technology, Department of Civil and Environmental Engineering, Division of Engineering Geology, Stockholm.

Hakami E, Stephansson O, 1993. Experimental technique for aperture studies of intersecting joints. Proceedings of the ISRM International Symposium Eurock ’93, Safety and Environmental Issues in Rock Engineering, Lisbon, Portugal, 301–308.

Iwano M, Einstein H H, 1993. Stochastic analysis of surface roughness, aperture and flow in a single fracture. Proceedings of the ISRM International Symposium Eurock ’93, Safety and Environmental Issues in Rock Engineering, Lisbon, Portugal, 135–141.

Jarsjö J, 1998. Hydraulic conductivity relations in soil and fractured rock: Fluid component and phase interaction effects. PhD thesis, Royal Institute of Technology, Div. of Water Resources Engineering, Stockholm.

Jarsjö J, Destouni G, 1997a. Groundwater degassing: Pilot injection – withdrawal field tests with gas saturated water. SKB PR HRL-97-02, Swedish Nuclear Fuel and Waste Management Co.

Jarsjö J, Destouni G, 1997b. Conditions for fracture transmissivity reduction due to degassing of groundwater: analytical expressions, numerical simulations and analysis of laboratory and field data. SKB PR HRL-97-03, Swedish Nuclear Fuel and Waste Management Co.

Jarsjö J, Destouni G, 1998. Groundwater degassing in fractured rock: Modelling and data comparison. SKB TR 98-17, Swedish Nuclear Fuel and Waste Management Co.

Jarsjö J, Destouni G, 2000. Degassing of deep groundwater in fractured rock around boreholes and drifts, Water Resour. Res., 36, 2477–2492.

Jarsjö J, Geller J T, 1996. Groundwater degassing: Laboratory experiments in rock fracture replicas with radial flow. SKB P R HRL-96-12, Swedish Nuclear Fuel and Waste Management Co.

Jouanna P, 1993. A summary of field test methods in fractured rocks. In: Bear, J., Tsang, C.-F. and de Marsily, G. (Eds.), Flow and contaminant transport in fractured rock, Academic Press Inc., San Diego, CA, 1993, pp 437–543.

Khaleel R, Relyea J F, 1995. Evaluation of van Genuchten – Mualem relationships to estimate hydraulic conductivity at low water contents. Water Resour. Res. 31, 2659–2668.

Kotelnikova S, Pedersen K, 1997. Evidence for methanogenic Archaea and homoacetogenic Bacteria in deep granitic rock aquifers. FEMS Microbiology Reviews, 20, 339–349.

Lanaro F, 1999. A random field model for aperture and roughness of rock fractures. Licentiate thesis, Royal Institute of Technology (KTH), Department of Civil and Environmental Engineering, Division of Engineering Geology, Stockholm, Sweden.

McDonald M G, Harbaugh A W, 1988. A modular three-dimensional finite-difference ground-water flow model. Techniques of Water-Resources Investigations of the United States Geological Survey, Book 6. Scientific Software Group, Washington, D.C.

Moreno L, Tsang C-F, 1991. Multiple peak response to tracer injection tests in single fractures: A numerical study. Water Resour. Res., 27, 2143–2150.

Moreno L, Tsang C-F, 1994. Flow channeling in strongly heterogeneous porous media: A numerical study. Water Resour. Res., 30, 1421–1430.

Mualem Y, 1976. A new model for predicting the hydraulic conductivity of unsaturated porous media. Water Resour. Res., 12, 513–522.

Murphy J R, Thomson N R, 1993. Two-phase flow in a variable aperture fracture. Water Resour. Res., 29, 3453–3476.

NAGRA, 1997. Geosynthese Wellenberg 1996. Ergebnisse der Untersuchungsphasen I und II. NAGRA Technical Report NTB 96-01 (in German), Nationale Genossenschaft für die Lagerung Radioaktiver Abfälle, Wettingen.

Nicholl M J, Glass R J, 1994. Wetting phase permeability in a partially saturated horizontal fracture. In Proceedings of the Fifth International High-Level Radioactive Waste Management Conference, Las Vegas, May 22-26, pp. 2007–2019, Am. Nucl. Soc., La Grange, Illinois.

Nicholl M J, Glass R J, Wheatcraft S W, 1994. Gravity-driven infiltration instability in initially dry nonhorizontal fractures. Water Resour. Res., 30, 2533–2546.

Nilsson A-C, 1997. Water and gas analyses of groundwater sampled in the borehole KZ0027A. SKB PR HRL-97-15, Swedish Nuclear Fuel and Waste Management Co.

Olsson O (Editor), 1992. Site characterisation and validation – Final Report. SKB Stripa Project TR 92-22, Swedish Nuclear Fuel and Waste Management Co.

Parlar M, Yortsos Y C, 1989. Bubble growth in porous media: I. Low supersaturations. Paper presented at Annual fall meeting, Soc. Pet. Eng., San Antonio, Texas.

Pedersen K, 1997. Investigations of subterranean microorganisms and their importance for performance assessment of radioactive waste disposal. Results and conclusions achieved during the period 1995 to 1997. SKB TR 97-22, Swedish Nuclear Fuel and Waste Management Co.

Persoff P, Pruess K, 1995. Two-phase flow visualization and relative permeability measurement in natural rough-walled fractures. Water Resour. Res., 31, 1173–1186.

Pruess K, Faybishenko B, Bodvarsson G S, 1999. Alternative concepts and approaches for modeling flow and transport in thick unsaturated zones of fractured rocks. J. Contam. Hydrol., 38, 281–322.

Pruess K, Tsang Y W, 1990. On two-phase relative permeability and capillary pressure of rough-walled fractures. Water Resour. Res., 26, 1915–1926.

Pruess K, Wang J S Y, Tsang Y W, 1990. On thermohydrologic conditions near high-level nuclear wastes emplaced in partially saturated fractured tuff. 1. Simulation studies with explicit consideration of fracture effects. Water Resour. Res., 26, 1235–1248.

Rajaram H, Ferrand L A, Celia M A, 1997. Prediction of relative permeabilities for unconsolidated soils using pore-scale network models. Water Resour. Res. 33, 43–52.

Reitsma S, Kueper B H, 1994. Laboratory measurement of capillary pressure-saturation relationships in a rock fracture. Water Resour. Res., 30, 865–878.

Romm E S, 1966. Fluid Flow in Fractured Rocks (in Russian). Nedra Publishing House, Moscow. (Engl. transl., W. R. Blake, Bartlesville, Okla., 1972.)

Smith L, Schwartz F W, 1993. Solute transport through fracture networks. In: Bear, J., Tsang, C.-F. and de Marsily, G. (Eds.), Flow and contaminant transport in fractured rock, Academic Press Inc., San Diego, CA, 1993, pp 129–167.

Walton J C, 1994. Influence of evaporation on waste package environment and radionuclide release from a tuff repository. Water Resour. Res., 30, 3479–3487.

van Genuchten M Th, 1980. A closed-form equation for predicting the hydraulic conductivity of unsaturated soils. Soil Sci. Soc. Am. J., 44, 892–898.

Witherspoon P A, Wang J S Y, Iwai K, Gale J E, 1980. Validity of cubic law for fluid flow in a deformable rock fracture. Water Resour. Res., 16, 1016–1024.

Xiangchun T, Shaoquan K, 1997. Report on indentation experiments and crack discrimination for calibrating cracks caused by TBM in Äspö. SKB PR HRL-98-03, Swedish Nuclear Fuel and Waste Management Co.

Zimmerman R W, Bodvarsson G S, 1996. Hydraulic conductivity of rock fractures. Transport in Porous Media, 23, 1-30.

Appendix A: Bimodal aperture pdf and corresponding bubble trapping probability pdf

The bimodal log-normal pdf is given by:

$$f_{bi,\ln}(a;\mu_{\ln d1},\sigma_{\ln d1},\mu_{\ln d2},\sigma_{\ln d2},\upsilon)=\upsilon f_{\ln}(a;\mu_{\ln d1},\sigma_{\ln d1})+(1-\upsilon)\,f_{\ln}(a;\mu_{\ln d2},\sigma_{\ln d2}) \tag{A-1}$$

where $f_{\ln}$ is the unimodal log-normal pdf, given by Equation (2-16). The distribution $f_{bi,\ln}$ is hence a combination of two log-normal distributions 1 and 2, where the coefficient υ of Equation (A-1) satisfies $0<\upsilon<1$ and represents the weight of distribution 1; the weight of distribution 2 is hence $(1-\upsilon)$. The pdf for L_b (3-2) was derived assuming unimodal log-normal pdfs for the fracture apertures a_1 and a_2 (see Figure 3-1). Given instead bimodal log-normal pdfs (A-1) for a_1 and a_2, the corresponding pdf for L_b is (note that these pdf's for a_1 and a_2 are identical and fully determined by $\mu_{\ln d1}$, $\sigma_{\ln d1}$, $\mu_{\ln d2}$ and $\sigma_{\ln d2}$, since we consider statistically stationary and uncorrelated aperture values):

$$\begin{aligned}f(L_b)=\frac{(dp/dl)}{2\sigma_w}\Bigg(&\upsilon^2\int_{-\infty}^{0} f_{\ln}(-\xi;-\mu_{\ln d1},\sigma_{\ln d1})\cdot f_{\ln}\left(\frac{L_b(dp/dl)}{2\sigma_w}-\xi;-\mu_{\ln d1},\sigma_{\ln d1}\right)d\xi+\\&+\upsilon(1-\upsilon)\int_{-\infty}^{0} f_{\ln}(-\xi;-\mu_{\ln d1},\sigma_{\ln d1})\cdot f_{\ln}\left(\frac{L_b(dp/dl)}{2\sigma_w}-\xi;-\mu_{\ln d2},\sigma_{\ln d2}\right)d\xi+\\&+\upsilon(1-\upsilon)\int_{-\infty}^{0} f_{\ln}(-\xi;-\mu_{\ln d2},\sigma_{\ln d2})\cdot f_{\ln}\left(\frac{L_b(dp/dl)}{2\sigma_w}-\xi;-\mu_{\ln d1},\sigma_{\ln d1}\right)d\xi+\\&+(1-\upsilon)^2\int_{-\infty}^{0} f_{\ln}(-\xi;-\mu_{\ln d2},\sigma_{\ln d2})\cdot f_{\ln}\left(\frac{L_b(dp/dl)}{2\sigma_w}-\xi;-\mu_{\ln d2},\sigma_{\ln d2}\right)d\xi\Bigg)\end{aligned} \tag{A-2}$$

with $f_{\ln}$ as in Equation (2-16).

Appendix B: Hydraulic conductivity and relative transmissivity estimation

The following analysis of field experiments is relevant for the case that steady conditions are established. The presence of constant pressure boundaries in the field implies that steady conditions will be reached after some time. For instance, the degassing site at Äspö HRL is located below an island, where the surrounding sea provides an approxmately constant pressure boundary. An evaluation of the conducted PRTs and CPTs showed that these tests were carried out for a sufficient period of time to reach steady conditions.

The fracture hydraulic conductivity (K) can be determined from the steady-state borehole inflow rate – borehole drawdown relation according to:

$$K = M\frac{\rho g L}{2A} \qquad \text{for } N=1 \qquad \text{(B-1)}$$

$$K = M\frac{\rho g}{2\pi a}\ln\left(\frac{r_w}{r_0}\right) \qquad \text{for } N=2 \qquad \text{(B-2)}$$

$$K = M\frac{\rho g}{4\pi}\frac{1}{r_w} \qquad \text{for } N=3 \text{ and } r << r_0 \qquad \text{(B-3)}$$

where N is the flow geometry (N=1 implies linear flow, N=2 radial flow and N=3 spherical flow), ρ is the fluid (water) density, g is the gravitational constant, r_w is the well (borehole) radius, L and r_0 are the length/ radius of influence (i.e. the distance from the well to the outer boundary where the pressures are not influenced by the opening of the borehole), A is the cross sectional area equalling the length of the borehole times a, the aperture width, and M is the slope of the steady borehole inflow – borehole drawdown relation ($m^3/(Pa\cdot s)$), with the drawdown being defined as the difference between the steady-state borehole pressure at no flow conditions (i.e., at the end of a pressure recovery test, PRT) and the borehole pressure during withdrawal (during a constant pressure test, CPT). For N=1, the fracture plane is assumed to be parallel to the borehole, for N=2 the fracture plane is assumed to be perpendicular to the borehole and for N=3 the borehole is represented by a sphere of radius r. For r = 28 mm (that is, the radius of the test holes P2, P4 and P8; Table 4-1), the approximate Equation (B-3) yields a K value that deviates less than 0.2% from the exact solution, given an r_0 equal to (or greater than) 25 metres.

Equations (B-1) and (B-2) implies that the fracture transmissivity $T=K\cdot a$ ($N\leq 2$). is proportional to M, the slope of the steady-state borehole inflow – borehole pressure relation. Given a specific value of M, the flow geometry needs to be determined in order to determine the absolute value of T, since the flow geometry determines the proportionality constant between T and M. However, the steady-state analysis aims at determining the relative decrease in T due to degassing and, assuming that N is the same before and after degassing conditions, the ratio of T values after (during test phases 2

and 3, see Section 4.3.1) and before (during test phase 1) the degassing test will be equal to the ratio of *M* values after and before the degassing test, regardless of the *N* value. This implies that the relative transmissivity can be obtained on basis of the experimental observations as:

$$T_{rel,obs} = \frac{T}{T_s} = \frac{T_{phase\,2-3}}{T_{phase\,1}} = \frac{M_{phase\,2-3}}{M_{phase\,1}} \qquad \text{(B-4)}$$